MARTIN MARIETTA ENERGY SYSTEMS LIBRARIES
3 4456 0361368 6

CENTRAL RESEARCH LIBRARY
DOCUMENT COLLECTION

4

ORNL-2718
Physics and Mathematics
TID-4500 (14th ed.)

PHYSICS DIVISION

ANNUAL PROGRESS REPORT

FOR PERIOD ENDING MARCH 10, 1959

OAK RIDGE NATIONAL LABORATORY
operated by
UNION CARBIDE CORPORATION
for the
U.S. ATOMIC ENERGY COMMISSION

CENTRAL RESEARCH LIBRARY
DOCUMENT COLLECTION
LIBRARY LOAN COPY
DO NOT TRANSFER TO ANOTHER PERSON
If you wish someone else to see this document, send in name with document and the library will arrange a loan.

Printed in USA. Price $2.25. Available from the

Office of Technical Services
Department of Commerce
Washington 25, D.C.

LEGAL NOTICE

This report was prepared as an account of Government sponsored work. Neither the United States, nor the Commission, nor any person acting on behalf of the Commission:

A. Makes any warranty or representation, expressed or implied, with respect to the accuracy, completeness, or usefulness of the information contained in this report, or that the use of any information, apparatus, method, or process disclosed in this report may not infringe privately owned rights; or

B. Assumes any liabilities with respect to the use of, or for damages resulting from the use of any information, apparatus, method, or process disclosed in this report.

As used in the above, "person acting on behalf of the Commission" includes any employee or contractor of the Commission, or employee of such contractor, to the extent that such employee or contractor of the Commission, or employee of such contractor prepares, disseminates, or provides access to, any information pursuant to his employment or contract with the Commission, or his employment with such contractor.

ORNL-2718
Physics and Mathematics
TID-4500 (14th ed.)

Contract No. W-7405-eng-26

PHYSICS DIVISION

ANNUAL PROGRESS REPORT

for Period Ending March 10, 1959

J. L. Fowler, Director
E. O. Wollan, Associate Director

DATE ISSUED

MAY 25 1959

OAK RIDGE NATIONAL LABORATORY
Oak Ridge, Tennessee
operated by
UNION CARBIDE CORPORATION
for the
U.S. ATOMIC ENERGY COMMISSION

MARTIN MARIETTA ENERGY SYSTEMS LIBRARIES

3 4456 0361368 6

FOREWORD

This issue marks the beginning of a change in policy with regard to Physics Division progress reports. For some time these reports have been issued on a semiannual basis, whereas they will now be published annually.

There has also been some change in the nature of the reporting. In those cases in which a paper has been written up for publication, has been submitted to a journal, or has appeared in a journal, only the abstract will appear in the progress report. In such cases preprints of the original articles will be available. The reports of research in progress are given as previously when preliminary results are available.

For the present report year reference should also be made to the Physics Division semiannual progress report for the period ending September 20, 1958 (ORNL-2610).

TABLE OF CONTENTS AND SUMMARY

POLARIZATION OF INTERNAL CONVERSION FOLLOWING BETA DECAY

R. L. Becker and M. E. Rose 1

Abstract of paper to be submitted for publication.

s-WAVE DETECTOR OF DEUTERON POLARIZATION AND 14-Mev POLARIZED-NEUTRON SOURCE

A. Galonsky, H. B. Willard, and T. A. Welton 1

A discussion is given of a new method for analysis of the polarization of a deuteron beam.

LONGITUDINAL POLARIZATION OF P^{32} BETA RAYS

A. R. Brosi, A. Galonsky, B. H. Ketelle, and H. B. Willard 4

The longitudinal polarization of P^{32} beta rays has been measured to an accuracy of about 2% by the method of Mott scattering from gold. The result is consistent with $-v/c$, the value predicted by the recent V-A theory of beta decay.

RECOIL MOMENTUM SPECTRA FOR THE BETA DECAY OF He^6

C. H. Johnson, F. Pleasonton, and A. H. Snell 5

The observed momentum spectrum of singly charged Li^6 recoils from the decay of He^6 shows that the Gamow-Teller interaction is predominantly axial-vector. Comparison of intensities of the singly and doubly charged ions at the peaks of the distributions yields an abundance ratio, charge 2/charge $(1 + 2) = (9.5 \pm 0.5)\%$.

POLARIZATION OF GAMMA RAYS IN Pb^{207}

P. H. Stelson, W. G. Smith, and F. K. McGowan 7

Abstract of paper to be submitted to the *Physical Review.*

COULOMB EXCITATION OF STATES IN Pt^{195}

F. K. McGowan and P. H. Stelson 8

Abstract of paper to appear in *Proceedings of the International Congress on Nuclear Physics*, Paris, France, July 1958, and to be submitted to the *Physical Review.*

DECAYS OF Rh^{106} AND Ag^{106}

R. L. Robinson, F. K. McGowan, and W. G. Smith 8

The gamma-ray spectra of Rh^{106} and Ag^{106} have been investigated with scintillation spectrometers. Levels and transitions in Pd^{106} have been proposed.

DECAY OF $I^{130} \rightarrow Xe^{130}$

W. G. Smith, P. H. Stelson, and F. K. McGowan 12

Abstract of paper submitted to the *Physical Review.*

PRECISION MEASUREMENT OF THE $Be^9(\gamma,n)$ CROSS SECTION

J. H. Gibbons, R. L. Macklin, J. B. Marion, and H. W. Schmitt 12

Abstract of paper submitted to the *Physical Review.*

TOTAL NEUTRON YIELDS FROM LIGHT ELEMENTS UNDER PROTON AND ALPHA BOMBARDMENT

J. H. Gibbons and R. L. Macklin 13

Abstract of paper submitted to the *Physical Review.*

NEUTRON RADIATIVE CAPTURE CROSS SECTIONS FROM 10 TO 150 kev
J. H. Neiler, R. L. Macklin, J. H. Gibbons, and P. D. Miller 13

Measurements of neutron radiative capture cross sections in the kev region have been made by a new method involving fast (millimicrosecond) time-of-flight techniques and a large liquid scintillator tank.

NEUTRON SCATTERING FROM BERYLLIUM
J. L. Fowler and H. O. Cohn 16

The total neutron cross section of beryllium, remeasured between 1.9 and 4.5 Mev, is in agreement with published data, provided that in-scattering corrections based on recent differential measurements are applied to all data.

NEUTRON-INDUCED FISSION FRAGMENT ANGULAR DISTRIBUTION FOR U^{234} AND U^{235}
R. W. Lamphere 18

The angular distribution of fragments from the fast-neutron-induced fission of U^{235} has been measured for neutron energies between 420 and 3700 kev.

NEUTRON ABSORPTION CROSS SECTIONS AT 27 kev
H. W. Schmitt, J. H. Gibbons, and C. N. Inskeep 20

The absolute neutron absorption cross sections of a number of elements have been measured at 27 kev by use of a spherical-shell transmission method. Elements measured were copper, zinc, silver, antimony, gold, and lead.

NEUTRON ACTIVATION AT 195 kev
W. S. Lyon and R. L. Macklin 22

Abstract of paper submitted to the *Physical Review*.

TOTAL CROSS SECTIONS IN THE KILOVOLT RANGE
P. D. Miller, J. H. Gibbons, W. M. Good, and J. H. Neiler 22

Total cross sections of elements in the range of A from 35 to 76 were measured in the energy range from 3 to 30 kev. Resonance parameters were extracted and strength functions calculated.

TOTAL NEUTRON CROSS SECTION OF Xe^{135} AS A FUNCTION OF ENERGY
E. C. Smith, G. S. Pawlicki, P. E. F. Thurlow, G. W. Parker, W. J. Martin, G. E. Creek, and P. M. Lantz 26

Abstract of paper submitted to the *Physical Review*.

FAST-CHOPPER TIME-OF-FLIGHT NEUTRON SPECTROMETER
R. C. Block, G. G. Slaughter, and J. A. Harvey 26

Fast-chopper time-of-flight spectrometer studies have been made on enriched samples of I^{129}, U^{233}, U^{234}, U^{235}, Pu^{240}, Lu^{175}, Lu^{176}, Ta^{180}, and La^{138}, on natural-abundance samples of Ta and La, and on samples of Am^{241}. The resonances observed were analyzed and compared with theoretical predictions of level spacings.

FUNDAMENTAL-MODE NEUTRON DISTRIBUTION IN PULSED COMPOSITE SYSTEMS
E. C. Campbell 31

General properties are derived for fundamental-mode thermal-neutron distributions in heterogeneous pulsed systems.

ATOMIC-BEAM SPECTROSCOPY
J. E. Sherwood and S. J. Ovenshine 32

The nuclear spins of I^{130} and I^{132} have been measured by means of the atomic-beam magnetic-resonance technique. The values obtained were 5 and 4, respectively.

DISSOCIATION OF C_6H_5T FOLLOWING BETA DECAY
T. A. Carlson, F. Pleasonton, and A. H. Snell 33

Abstract of paper to be submitted to the *Journal of Chemical Physics.*

EXTENSION OF THE ATOMIC ENERGY LEVEL CLASSIFICATION SCHEME FOR SINGLY IONIZED DYSPROSIUM (Dy II)
J. R. McNally, Jr. 33

Zeeman data of Blank and wavelength data of Gatterer and Junkes on the spectra of dysprosium have been used with IBM-605 calculated wave numbers on the Edlén scale to couple two of the energy-level doublets reported by Paulson and Blank.

INFRARED SPECTRA OF SOLID AMMONIA AND SOLID PHOSPHINE
P. A. Staats and H. W. Morgan 34

Infrared spectra obtained for the stable cubic phase, and two metastable phases, of NH_3 and ND_3 are discussed.

PRELIMINARY CLASSIFICATION OF THE SINGLY IONIZED PLUTONIUM ATOM (Pu II)
J. R. McNally, Jr., and P. M. Griffin 35

Abstract of paper published in the *Journal of the Optical Society of America.*

APPLICATION OF A DIGITAL COMPUTER TO THE ZEEMAN METHOD IN ATOMIC SPECTROSCOPY
K. L. Vander Sluis 36

Abstract of paper to be submitted to the *Journal of the Optical Society of America.*

ANTIFERROMAGNETISM IN $CrCl_3$ AND $FeCl_3$
J. W. Cable, M. K. Wilkinson, and E. O. Wollan 36

The results of single-crystal neutron diffraction investigations of the antiferromagnetic structures of $CrCl_3$ and $FeCl_3$ are presented.

NEUTRON DIFFRACTION INVESTIGATIONS OF THE FERROMAGNETIC ORDERING IN HoN
M. K. Wilkinson, H. R. Child, E. O. Wollan, and J. W. Cable 41

Preliminary observations on HoN at low temperatures indicate that this compound becomes ferromagnetic below about 20°K and that the Ho^{+++} ions in the magnetic lattice have an ordered magnetic moment of 8.0 $\pm$1.0 Bohr magnetons.

NEUTRON DIFFRACTION INVESTIGATIONS OF METALLIC CERIUM AT LOW TEMPERATURES
M. K. Wilkinson, H. R. Child, and E. O. Wollan 43

The diffuse neutron scattering from metallic cerium indicates that there is one magnetic electron in the $4f^1(^2F_{5/2})$ electronic state in both the normal fcc and hcp phases and that this electron is transferred to an electronic state in the collapsed fcc phase which has no atomic magnetic moment. Antiferromagnetic ordering is observed in the hcp phase below about 12.5°K.

NEUTRON DIFFRACTION INVESTIGATIONS OF ANTIFERROMAGNETISM IN CrF_2 AND $CrCl_2$
M. K. Wilkinson, J. W. Cable, and E. O. Wollan 48

Preliminary observations on CrF_2 and $CrCl_2$ at low temperatures show Néel transitions at about 51 and 20°K, respectively. Although the crystal structures of these compounds are very similar, different antiferromagnetic structures are indicated.

A DUO-PLASMATRON ION SOURCE FOR USE IN ACCELERATORS
C. D. Moak, H. E. Banta, J. N. Thurston, J. W. Johnson, and R. F. King 50

Abstract of paper to be submitted to the *Review of Scientific Instruments.*

LOW-TEMPERATURE HELIUM-VAPOR PULSE IONIZATION CHAMBER
J. W. T. Dabbs, S. H. Hanauer, and L. D. Roberts 51

Helium is shown to be a fairly satisfactory filling gas for low-temperature ionization chambers.

BROAD-AREA GERMANIUM SURFACE BARRIER COUNTERS
F. J. Walter, J. W. T. Dabbs, L. D. Roberts, and H. W. Wright 53

A theoretical and experimental study of germanium surface barrier counters at low temperatures indicates very satisfactory characteristics.

A 60° DEFLECTION, DOUBLE FOCUSING, UNIFORM FIELD, REACTION PRODUCT MAGNET
H. B. Willard and J. K. Bair 62

A double focusing, uniform field magnet has been designed and constructed for the analysis of charged particles from nuclear reactions.

LARGE-OUTPUT TIME-TO-VOLTAGE CONVERTER FOR HIGH COUNTING RATES
D. G. Maeder 65

A new time-of-flight measuring apparatus is described which differs from conventional time-to-pulse-amplitude converters in that it produces a d-c output large enough to be fed directly into a multichannel sorting device.

PHYSICS DIVISION ANNUAL PROGRESS REPORT

POLARIZATION OF INTERNAL CONVERSION FOLLOWING BETA DECAY[1]

R. L. Becker M. E. Rose

Beta decay provides a means of obtaining a nucleus in an oriented excited state. This orientation is manifested in the angular distribution, polarization, and higher tensor moments of the subsequent radiations. The polarization of internal conversion resulting from odd-rank orientations (e.g., polarization) of the daughter nucleus was investigated previously.[2] This polarization lies in the plane of the two measured directions. The transverse component was appreciable, and measurement of this transverse component offers some experimental advantages over measurement of the circular polarization of the competing gamma ray. In addition, there is a transverse polarization perpendicular to the plane of the two measured directions. This results from the even-rank orientations (i.e., alignment), and these appear only in forbidden beta transitions. This transverse polarization will vanish in the limits $Z \to 0$ or conversion energy $\to \infty$, or in the nonrelativistic limit. Thus, as could be expected, the polarization is greatest for low-energy conversion electrons and high Z. Its angular dependence is different from that of either of the other components and from the angular correlation without polarization. This polarization is analogous to the linear polarization of gamma rays observed in coincidence with a preceding radiation.

This paper contains details of a fully relativistic calculation for K-shell conversion by a point nucleus. Results are evaluated for first-, second-, and third-rank nuclear orientations, which are sufficient to cover the cases of allowed and first-forbidden beta decay. Polarization components are expressed in the customary form for angular correlations, in terms of geometrical factors and "particle" parameters. Results of extensive numerical evaluation of the conversion electron polarization parameters are included for mixed as well as pure multipole transitions. Some particular cases involving first-forbidden unique beta transitions are considered in detail.

[1] Abstract of writeup covering entire problem, including recent work, to be submitted for publication.

[2] M. E. Rose and R. L. Becker, *Phys. Rev. Letters* 1, 116 (1958); Program of the Conference on Weak Interactions, Gatlinburg, Tennessee, 1958, p 20–22.

---

s-WAVE DETECTOR OF DEUTERON POLARIZATION AND 14-Mev POLARIZED-NEUTRON SOURCE

A. Galonsky H. B. Willard T. A. Welton

Recently a great deal of interest[1] has been expressed in the development of polarizing ion sources for use in accelerators. In this connection a convenient analyzer for the resulting polarized beams would be most useful. It is well known that in both scattering and reactions induced by polarized s-wave protons the angular distribution of the scattered protons, or of any reaction product, is isotropic[2] just as it would be for unpolarized s-wave protons.[3] The purpose here is to point out that since isotropy does not necessarily follow for a reaction induced by polarized s-wave *deuterons*,[4] the $H^3(d,n)He^4$ reaction, for example, can be used as a sensitive detector of the polarization of a deuteron beam. This reaction will then also serve as a source of polarized, 14-Mev neutrons.

The different results obtained for proton and deuteron beams may be ascribed to the fact that

[1] G. Clausnitzer, R. Fleischmann, and H. Schopper, *Z. Physik* 144, 336 (1956); E. K. Zavoiskii, *J. Exptl. Theoret. Phys. (U.S.S.R.)* 5, 338, 603 (1957); R. L. Garwin, *Rev. Sci. Instr.* 27, 374 (1958).

[2] L. Wolfenstein, *Phys. Rev.* 75, 1664 (1949).

[3] E. Eisner, R. G. Sachs, and L. Wolfenstein, *Phys. Rev.* 72, 680 (1947) and 73, 528 (1947); C. N. Yang, *Phys. Rev.* 74, 764 (1948).

[4] It has already been shown independently that polarized s-wave deuterons may lead to anisotropy; L. J. B. Goldfarb, *Nuclear Phys.* 7, 622 (1958).

the spin projection has only two possible values for the proton, but three for the deuteron. The partial cross sections[5] for the d-H^3 resonance (E_{max} = 107 kev, $l_d = 0$, $J = 3/2^+$, $l_n = 2$) (ref 6) are the following:

$$\left(\frac{d\sigma}{d\Omega}\right)^{+1}_{3/2,1/2} = \left(\frac{d\sigma}{d\Omega}\right)^{+1}_{1/2,-1/2} = \left(\frac{d\sigma}{d\Omega}\right)^{-1}_{-3/2,-1/2}$$

$$= \left(\frac{d\sigma}{d\Omega}\right)^{-1}_{-1/2,1/2} = \frac{1}{2}\left(\frac{d\sigma}{d\Omega}\right)^{0}_{1/2,-1/2}$$

$$= \frac{1}{2}\left(\frac{d\sigma}{d\Omega}\right)^{0}_{-1/2,1/2} = 3K \sin^2\theta \cos^2\theta \ ,$$

$$\left(\frac{d\sigma}{d\Omega}\right)^{+1}_{3/2,-1/2} = \left(\frac{d\sigma}{d\Omega}\right)^{-1}_{-3/2,1/2} = 3K \sin^4\theta \ ,$$

$$\left(\frac{d\sigma}{d\Omega}\right)^{+1}_{1/2,1/2} = \left(\frac{d\sigma}{d\Omega}\right)^{-1}_{-1/2,-1/2}$$

$$= \frac{1}{2}\left(\frac{d\sigma}{d\Omega}\right)^{0}_{1/2,1/2} = \frac{1}{2}\left(\frac{d\sigma}{d\Omega}\right)^{0}_{-1/2,-1/2}$$

$$= \frac{K}{3}(9\cos^4\theta - 6\cos^2\theta + 1) \ ,$$

where $K = |\mathcal{U}|^2/16k^2$ is independent of angle, $\mathcal{U}$ is the relevant element of the collision matrix, and k is the deuteron wave number. The superscripts on the cross sections are the magnetic quantum numbers of the deuterons; the subscripts are those of the channel spins referred to the beam axis,[7] the first subscript for the d-H^3 channel (channel spin 1/2 does not contribute to this resonance reaction since $J = 3/2$ and $l_d = 0$) and the other for the n-He^4 channel. The cross section for a deuteron beam polarized with $m_d = +1$ is

$$\sum_{a,b}\left(\frac{d\sigma}{d\Omega}\right)^{+1}_{a,b} = \frac{2K}{3}(3\sin^2\theta + 2) \ ;$$

if $m_d = -1$ we get the same result, but if $m_d = 0$ we get $(4K/3)(3\cos^2\theta + 1)$. The differential cross section for an unpolarized beam, which is the average of the above three cross sections, is $8K/3$ – isotropic, as it must be.[3] The equality of the $m_d = \pm 1$ cross sections is a consequence of reflection invariance of the nuclear interaction. Similarly, for a proton beam, $m_p = +1/2$ and $-1/2$ give equal cross sections. These are isotropic for s waves, since an unpolarized beam, which can be represented as an equal mixture of $m_p = \pm 1/2$, gives isotropy.[3]

Thus we see that the angular distribution of the neutrons or alpha particles in the d-H^3 reaction is determined by the alignment (mean value of m_d^2) rather than by the polarization (mean value of m_d). If one were attempting experimentally to produce a pure $m_d = +1$ beam, for example, the major impurity would most likely be $m_d = 0$. Then the alignment and polarization would be equal. Figure 1 is a set of angular distributions resulting from various mixtures of $m_d = +1$ and 0 in the deuteron beam.

The main advantage of attempting to produce beams of polarized deuterons rather than polarized protons is that s waves, and therefore low voltages, are sufficient to produce anisotropy. In our $H^3(d,n)He^4$ example the cross section has its maximum at only 107 kev. In addition, this cross section at the maximum is very large (5 barns for an unpolarized beam), and the width is 140 kev. This scheme obviates the need for a pressurized electrostatic generator. With a low-voltage, open-air accelerator there need be no limitation on the size of the polarizing apparatus, and the easy accessibility of such apparatus has many obvious advantages. If convenient, the polarity of the accelerator may even be reversed so that the polarizer and ion source are at ground potential.

---

[5] R. G. Sachs, *Nuclear Theory*, chap. 10, esp Eqs. (10-12) and (10-54), Addison-Wesley, Cambridge, 1953.

[6] F. Ajzenberg and T. Lauritsen, *Revs. Modern Phys.* **27**, 77, esp 78–79 (1955).

[7] Because this reaction picks out of the deuteron beam only the s-wave part, which has no preferred direction, the angular dependences of the partial cross sections are really referred to the alignment axis, chosen here to coincide with the beam axis. For a different alignment axis the results may be obtained by rotating the angular distributions presented above through the angle between the two axes. In this case the differential cross sections will depend on both the polar and azimuthal angles. If the polarization state of the deuteron beam is too complex to be described solely in terms of one alignment axis, then the calculation must be altered.

As an example of how rapidly the polarization can be determined, consider the following conditions for a pure $m_d = +1$ beam, where the neutrons from a thick Zr-H^3 target are detected at 90°: deuteron energy = 200 kev, deuteron current = 1 mμa, detector solid angle = 1% of sphere (half angle = 12°), and detector efficiency = 20%. The resulting count rate is ~300 per second.

Reference to the partial cross sections listed above shows that the 14-Mev neutrons produced in the d-H^3 reaction are, in general, polarized. The $m_d = \pm 1$ deuterons produce equal and opposite neutron polarizations and the $m_d = 0$ deuterons no polarization. Figure 2 shows the polarization of the neutrons at 90° as a function of the contamination of an $m_d = +1$ beam by $m_d = 0$. The direction of polarization is opposite to the beam direction in the scattering plane and therefore transverse to the neutron direction. It is, of course, essential to the use of the neutrons in a subsequent nuclear process that the neutron polarization be transverse. By examination of the neutron angular distribution and polarization, it therefore appears that the complete polarization state of the deuteron beam can be determined.

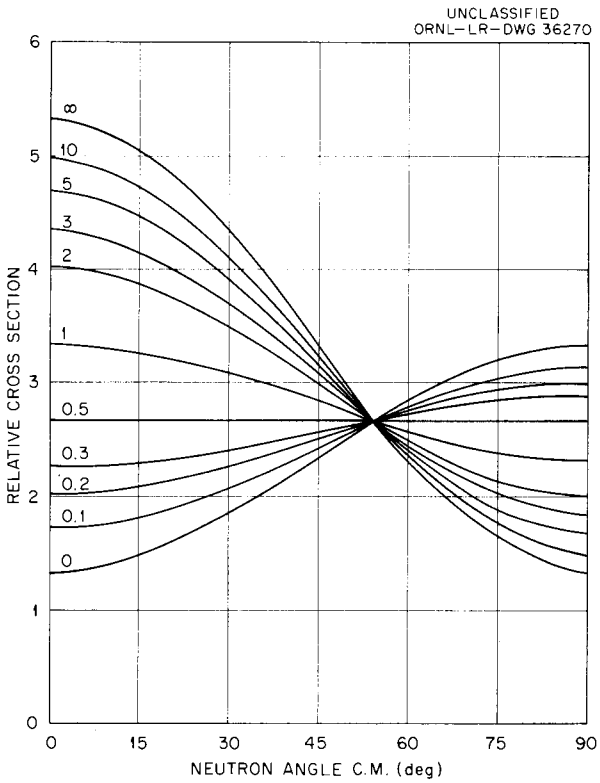

Fig. 1. Angular Distributions of Neutrons from the $H^3(d,n)He^4$ Resonance Reaction for Polarized Beams of Deuterons Containing a Mixture of $m_d = +1$ and 0. The label on each curve is the ratio of the $m_d = 0$ component to the $m_d = +1$ component.

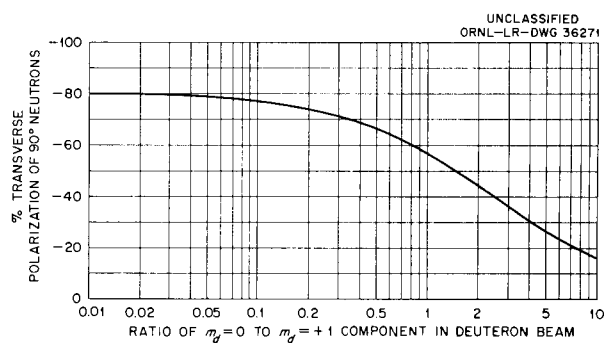

Fig. 2. Polarization of Neutrons Produced at 90° in the $H^3(d,n)He^4$ Resonance Reaction by a Polarized Deuteron Beam. The direction of polarization is opposite to the beam direction in the scattering plane and hence is transverse to the neutron direction.

LONGITUDINAL POLARIZATION OF P^{32} BETA RAYS

A. R. Brosi[1] A. Galonsky B. H. Ketelle[1] H. B. Willard

The two-component neutrino theory with no Fierz interference predicts that the longitudinal polarization of beta rays in an allowed transition is exactly v/c (ref 2), where v is the beta-ray speed and c is the speed of light. In order to check this theory we have measured the longitudinal polarization of P^{32} beta rays at 624 kev ($v/c = 0.893$) by observing the asymmetry in Mott scattering[3] of the beta rays by gold.

Between the P^{32} source and the gold scattering foil is a spherical electrostatic spin rotator[4] which selects the beta-ray energy to ±2% (±0.3% in v/c) and precesses its spin so that an initially longitudinal electron acquires a predominantly transverse orientation. Electrons scattered through 135 ± 8° are counted by two azimuthally opposing anthracene scintillation spectrometers. The ratio of the counting rates in the two spectrometers, designated up/down, is $(1 - PeS)/(1 + PeS)$, where Pe is the beta-ray polarization transverse to the scattering plane and S is the polarization produced by scattering through 135° unpolarized electrons from gold. The most reliable value of S is that interpolated from the calculations of Sherman,[5] in which, however, no account is taken of screening of the nucleus by the atomic electrons or of inelastic scattering.

From numerical computations and subsidiary experiments we have evaluated corrections of the order of 1% for each of the following: angular widths of the incident beam (and concurrently the spin direction) and of the scattering angle, depolarization in the source, scattering of beta rays from the condenser plates of the spin rotator, asymmetries from geometric misalignments, and counting of electrons scattered from the walls of the scattering chamber and "beam" catcher. Wherever feasible, the design of the apparatus and the preparation of the sources were executed so as to minimize these corrections.

As there is always multiple scattering, and consequently a "washing-out" of the asymmetry, in any polyatomic scattering foil, it is very difficult to measure the true asymmetry with high statistical accuracy. The procedure adopted was to measure the asymmetry as a function of thickness of scattering foil and then extrapolate to zero thickness. The open points of Fig. 1 were obtained with a 1.2-curie source less than 2 mm in diameter and about 4 mg/cm^2 thick. The straight line through the points is a least-squares fit that extrapolates to an up-down ratio very close to that expected for a beta-ray polarization of $-v/c$. Although the standard error of the extrapolated value is only 1/2%, errors from the effects mentioned in the previous paragraph bring the total uncertainty in the

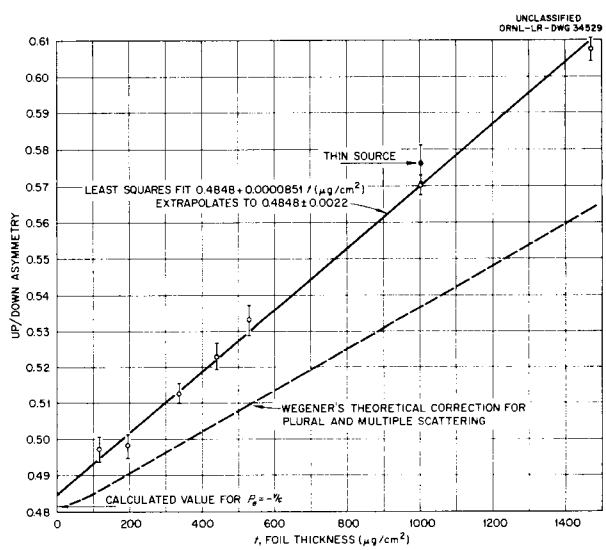

Fig. 1. Asymmetry Dependence on Thickness of Gold Scatterer. A straight line fitted by the least-squares method to the data obtained with a thick, strong source (open points) extrapolates to a value very close to that calculated for $Pe = -v/c$. The solid point, obtained with a thin, weak source, shows that there is little, if any, depolarization in the thick, strong source. The dashed curve, from an approximate calculation by H. Wegener [*Z. Physik* 151, 252 (1958)], has the proper linear dependence, but it obviously underestimates the size of the effect.

---

[1]Chemistry Division.

[2]J. D. Jackson, S. B. Treiman, and H. D. Wyld, *Phys. Rev.* **106**, 517 (1957).

[3]H. A. Tolhoek, *Revs. Modern Phys.* **28**, 277 (1956).

[4]H. B. Willard *et al.*, *Phys. Semiann. Prog. Rep. March 10, 1958*, ORNL-2501, p 68; A. Galonsky *et al.*, *Bull. Am. Phys. Soc.* **3**, 305 (1958); B. H. Ketelle *et al.*, *Bull. Am. Phys. Soc.* **4**, 76 (1959).

[5]N. Sherman, *Phys. Rev.* 103, 1601 (1956).

polarization to about 2%, the value of the polarization being consistent with $-v/c$. A final evaluation of corrections and errors is not complete.

It should be mentioned that if we accept the two-component neutrino theory with a left-handed neutrino and use our result to test the validity of the recent vector, axial-vector (V-A) theory of beta decay,[6] a 2% deviation of polarization from $-v/c$ allows C_T/C_A to be 10%.

[6]R. P. Feynman and M. Gell-Mann, *Phys. Rev.* **109**, 193 (1958); E. C. G. Sudarshan and R. E. Marshak, *Phys. Rev.* **109**, 1860 (1958).

RECOIL MOMENTUM SPECTRA FOR THE BETA DECAY OF He^6

C. H. Johnson F. Pleasonton A. H. Snell[1]

Recoil experiments in beta decay determine the angular correlation between the emitted beta particle and neutrino and thus give a measure of the relative strengths of the coupling constants in beta decay. A He^6 recoil experiment can give rather definite results because it involves a pure allowed Gamow-Teller transition with one final state. In the last year the He^6 recoil experiment assumed particular prominence because early results,[2] which contradicted recent parity experiments, were found to be in error.[3]

For the decay of He^6 the asymmetry parameter for the correlation between the electron and antineutrino is

$$a = -\frac{1}{3}\,\frac{1-(|C_T|^2+|C_T'|^2)/(|C_A|^2+|C_A'|^2)}{1+(|C_T|^2+|C_T'|^2)/(|C_A|^2+|C_A'|^2)},$$

where the C's are the usual tensor and axial-vector coupling constants. For the tensor interaction ($a = +\frac{1}{3}$) the leptons are emitted preferentially in the same direction, so that the Li^6 recoils have relatively large momentum, whereas for the axial-vector interaction ($a = -\frac{1}{3}$) the leptons are emitted preferentially in opposite directions, giving the recoil relatively less momentum. Kofoed-Hansen[4] and Rose[5] have given expressions for the spectrum as a function of a.

The recoil spectra of both the singly charged and the doubly charged Li^6 ions are being studied with the spectrometer which is shown schematically in Fig. 1 and which was used for an earlier investigation[6] of A^{37}. The He^6 is generated by the $Be^9(n,\alpha)He^6$ reaction in a box containing BeO at the pool-side facility of the ORR. Water vapor carries the He^6 through 80 ft of tubing to the laboratory, where the vapor is removed by a series of three cold traps containing ice, dry ice, and liquid nitrogen. Water was chosen because it is readily condensable to a liquid, noncorrosive, and not readily dissociated in the flux of the reactor. A hot Cu-CuO trap was inserted to remove dissociation products which do occur. The portion of He^6 which has not decayed in transit is left to decay in the field-free conical source volume, and is monitored by a beta- and gamma-sensitive proportional counter.

Recoils are analyzed by the spectrometer which subtends a small solid angle at the end of the source volume. The spectrometer uses both magnetic and electrostatic deflectors, in series, thus eliminating simultaneous observation of singly and doubly charged Li^6 ions. The magnetic analyzer defines the momentum resolution to 1%. Absolute calibration of the magnet and mutual alignment of the magnetic and electrostatic deflectors are accomplished with a normal-helium ion source whose potential is measured relative to a standard cell. Ions are detected by an Allen-type electron multiplier. Three stages of differential pumping enable one to count with a signal-to-background ratio of 4 at the peak of the charge 1 spectrum.

[1]Director's Division.

[2]B. M. Rustad and S. L. Ruby, *Phys. Rev.* **97**, 991 (1955).

[3]B. M. Rustad, post-deadline paper at the Annual Meeting of the American Physical Society (1958).

[4]O. Kofoed-Hansen, *Phys. Rev.* **74**, 1785 (1948).

[5]M. E. Rose, *The Beta-Decay Interaction and the Analysis of Recoil Experiments*, ORNL-1593 (Sept. 15, 1953).

[6]A. H. Snell and F. Pleasonton, *Phys. Rev.* **100**, 1396 (1955).

UNCLASSIFIED
ORNL-LR-DWG 34660R

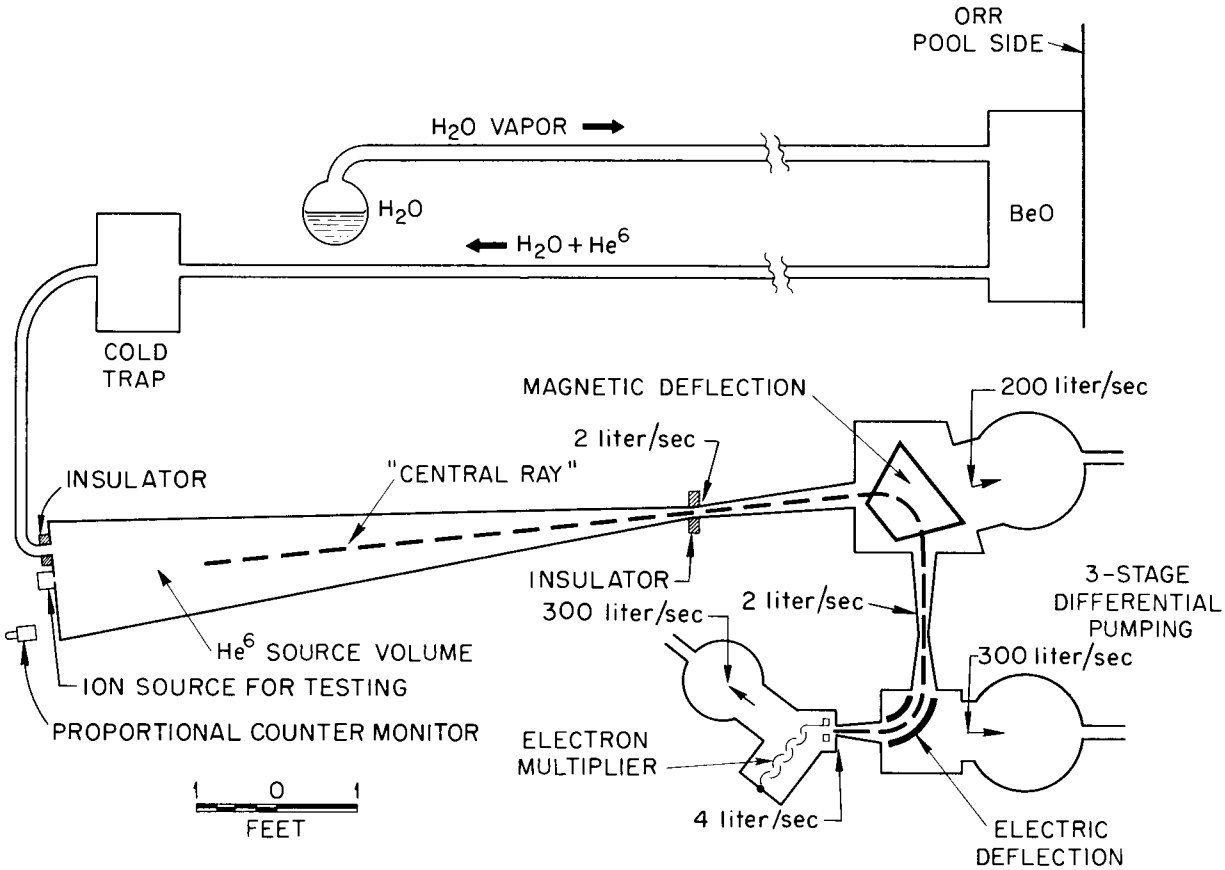

Fig. 1. Spectrometer for He^6 Recoil Experiment.

Figure 2 shows the singly charged recoil spectrum which has been obtained to date. Theoretical curves are shown for pure axial-vector and pure tensor interactions. The two theoretical curves are normalized to the same area, that is, to the same number of recoils. The experimental data are normalized to the area under the upper two-thirds of the axial-vector curve, that is, over the region covered by the data. The axial-vector curve gives an excellent fit to the data; this is in agreement with another recent He^6 recoil experiment.[7] A study of systematic errors has been undertaken in order to assign uncertainties to the asymmetry parameter; however, it should be noted that the measurement is rather insensitive to a small admixture of tensor interaction. For example, for a 20% admixture, the asymmetry parameter changes only about 10% and the momentum distribution is distorted about 5%.

Figure 3 shows preliminary data on the charge 2 spectrum. Within the large statistical uncertainties the two spectra have the same shape, in agreement with Winther's[8] prediction that the probability of double ionization is independent of recoil energy. Comparison of intensities at the peaks of the distributions yields an abundance ratio, charge 2/charge (1 + 2) = (9.5 ± 0.5)%. Winther[8] predicts (10.5 ± 0.5)%.

[7] W. B. Herrmannsfeldt *et al.*, *Phys. Rev. Letters* 1, 61 (1958).

[8] A. Winther, *Kgl. Danske Videnskab. Selskab, Mat.-fys. Medd.* 27, 2 (1952).

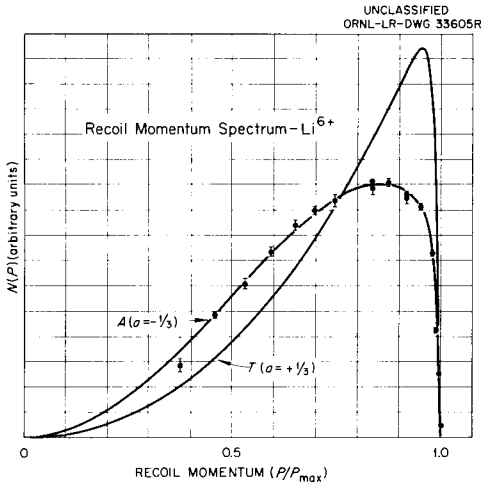

Fig. 2. Recoil Momentum Spectra for Singly Charged Li^6 Ions from the Decay of He^6. The solid curves are theoretical predictions for pure axial-vector and pure tensor interactions. Each curve is normalized to the same area. The data points show the observed recoil spectrum normalized to the upper two-thirds of the theoretical axial-vector curve.

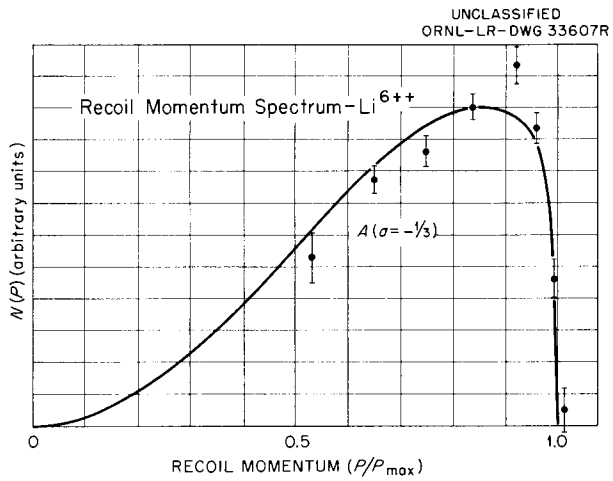

Fig. 3. Recoil Momentum Spectra for Doubly Charged Li^6 Ions. The solid curve is the theoretical prediction for pure axial-vector, assuming that the probability of double ionization is independent of the recoil momentum. The data points give the experimental spectrum normalized at the peak of the theoretical distribution.

POLARIZATION OF GAMMA RAYS IN Pb^{207}[1]

P. H. Stelson W. G. Smith[2] F. K. McGowan

Polarization-direction measurements have been made on the gamma-ray transitions in Pb^{207} resulting from the decay of Bi^{207}. These measurements were made to obtain additional information on both the spin of the level at 2.34 Mev and the multipole character of the decay gamma ray. The observed polarization eliminates the possible spin assignment 9/2. It is concluded that the spin assignment is 7/2 and that the 1.77-Mev gamma ray is predominantly M1.

[1]Abstract of paper to be submitted to the *Physical Review*.

[2]Summer research participant from Purdue University, Lafayette, Ind.

COULOMB EXCITATION OF STATES IN Pt^{195}[1]

F. K. McGowan P. H. Stelson

Gamma rays of 99, 110, 130, 140, 210, and 240 kev have been observed from Coulomb excitation of Pt^{195} (platinum target containing 60.1% Pt^{195}) with 3.0- to 5.5-Mev protons and alpha particles. The energy dependence of the gamma-ray yields indicates direct excitation of states at 99, 130, 210, and 240 kev. The 140-kev gamma ray is a cascade transition between states at 240 and 99 kev. These results do not agree with the conclusions of Bernstein and Lewis, who measured the Coulomb excitation functions of the internal-conversion electrons and found evidence for direct excitation of levels at 31 and 130 kev but no evidence for direct excitation of a level at 99 kev. The angular distributions of the 240- and 210-kev gamma rays and the 140-kev gamma ray in coincidence with K x rays from internal conversion of the 99-kev transition have been measured with respect to the incident ion beam on a thick target. These measured distributions are consistent with an assignment of $5/2(E2)1/2$, of $3/2(E2 + M1)1/2$ with $(E2/M1)^{1/2} = 0.37 \pm 0.02$, and of $5/2(E2 + M1)3/2$ with $(E2/M1)^{1/2} = -(0.13 \pm 0.03)$ for the 240-, 210-, and 140-kev transitions, respectively. The $B(E2)$ and $B(M1)$ for decay of these states have been determined.

[1]Abstract of paper to appear in *Proceedings of the International Congress on Nuclear Physics, Paris, France, July 1958.*

DECAYS OF Rh^{106} AND Ag^{106}

R. L. Robinson F. K. McGowan W. G. Smith[1]

Rhodium-106 (30 sec) decays by beta-ray emission to Pd^{106}, and Ag^{106} (8.3 days) decays by orbital electron capture also to Pd^{106}. The ground-state spins of Rh^{106} and Ag^{106} are 1 and 6, respectively.[2] A previous investigation of the decays of these two isotopes by Alburger and Toppel[3] has indicated that they populate predominantly the same levels in Pd^{106}. This is rather surprising in view of the large difference in the ground-state spins of the two isotopes. Because of this anomaly, the decays of Rh^{106} and Ag^{106} have been re-examined in the present work. The gamma-ray spectra which accompany their decays have been investigated with scintillation spectrometers. The gamma rays were detected with 3-in.-dia × 3-in.-thick NaI(Tl) crystals.

The singles gamma-ray spectrum of Rh^{106} was observed for a source-to-detector distance of 14 cm. One-half inch of Lucite was placed between the crystal and the source to absorb the beta rays. This spectrum is given in Fig. 1. The continuum which can be seen in the spectrum is due to bremsstrahlung produced by electrons from the high-energy, beta-ray groups. With the exception of the peak at 1.13 Mev, this spectrum is in agreement with that presented

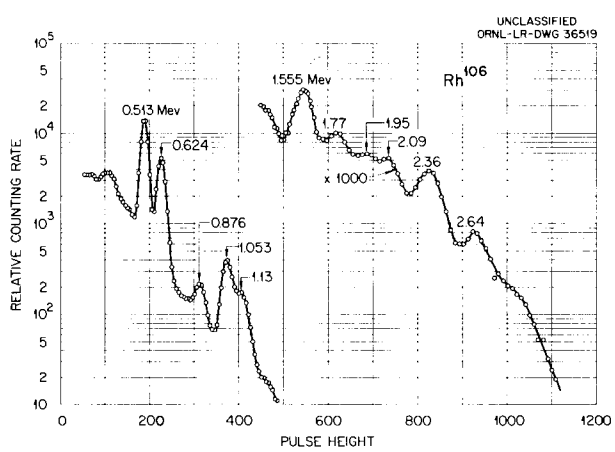

Fig. 1. Gamma-Ray Spectrum of Rh^{106}.

[1]Summer research participant from Purdue University, Lafayette, Ind.

[2]W. B. Ewbank *et al.*, *Phys. Rev.* 110, 595 (1958).

[3]D. E. Alburger and B. J. Toppel, *Phys. Rev.* 100, 1357 (1955).

by Alburger and Toppel.[3] We determined the gamma-ray intensities by measuring the area under each photopeak and correcting for the total intrinsic efficiency and peak-to-total ratio of the crystal, for absorption, and for the gamma-ray summing in the crystal. These intensities, which are normalized to a value of 100 for the 0.513-Mev gamma ray, are given in Table 1. As a large fraction of the peak at 1.13 Mev in Fig. 1 is a sum peak of the intense 0.513- and 0.624-Mev gamma rays, the spectrum was also observed for a source-to-detector distance of 40 cm. In this run the sum peak was relatively smaller. (The ratio of sum counts to crossover counts varies approximately with the solid angle subtended by the crystal.) The same value within experimental errors was obtained for the 1.13-Mev gamma-ray intensity from both spectra. The value is similar to that given by Kahn and Lyon,[4] but it is much larger than the value of 0.8 given as an upper limit by Alburger and Toppel.[3]

The gamma-ray spectra of Rh^{106} in coincidence with the 0.513- and 0.624-Mev gamma rays were also studied. The distance between the source and each detector for these measurements was 5 cm. The resolving time 2τ of the coincidence circuit was 0.2 μsec. The coincidence spectra revealed photopeaks not observed in the singles spectrum at 0.71, 1.49, and possibly 1.19 Mev. The intensities of the gamma rays found in these spectra are included in Table 1. A correction was applied for angular correlation between the coincidence gamma rays when the correlation function was known. A correction was also made for coincidences with pulses accepted by the gating window which were not produced by gamma rays in the photopeak of interest. These pulses were produced by gamma rays Compton-scattered in the crystal and by bremsstrahlung.

A decay scheme which incorporates the data from the three spectra is shown in Fig. 2. The level at 1.13 Mev has been previously observed in Coulomb excitation.[5] It has not been possible to determine from our data whether the 0.71- and 1.95-Mev transitions terminate at the 1.137- or 1.13-Mev level.

[4] B. Kahn and W. S. Lyon, *Phys. Rev.* **92**, 902 (1953).

[5] P. H. Stelson and F. K. McGowan, *Bull. Am. Phys. Soc.* **2**, 267 (1957).

Table 1. Relative Intensities of Gamma Rays from Rh^{106}

Energy (Mev)	Intensities		
	Singles Spectrum	Spectrum in Coincidence with 0.513-Mev Gamma Ray	Spectrum in Coincidence with 0.624-Mev Gamma Ray
0.513	100		52
0.624	52 ± 2	52	
0.71			0.2 ± 0.1
0.876	2.0 ± 0.4	1.1 ± 0.2	1.2 ± 0.1
1.053	7.1 ± 0.3	7.4 ± 0.4	
1.13	2.4 ± 0.2	$\leqq$0.3	$\leqq$0.2
1.49		0.16 ± 0.04	
1.555	0.65 ± 0.07		
1.77	0.17 ± 0.05	0.22 ± 0.03	
1.95	0.09 ± 0.05	0.08 ± 0.04	0.020 ± 0.003
2.09	0.12 ± 0.04	0.17 ± 0.04	
2.36	0.16 ± 0.04	0.22 ± 0.03	
2.64	0.03 ± 0.01		

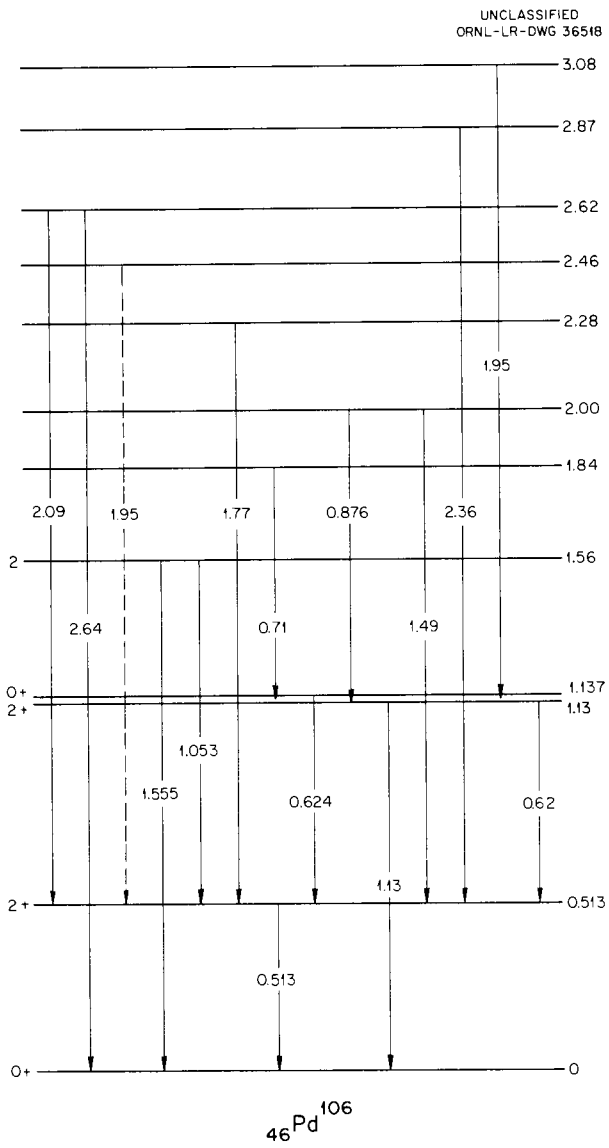

Fig. 2. Proposed Transitions and Energy Levels in Pd^{106} Which Occur in the Decay of Rh^{106}.

However, the decrease in the observed intensity of the 0.876-Mev gamma ray in the coincidence spectra indicates that this transition terminates at the 1.13-Mev level. The discrepancy in the intensity of the 1.95-Mev gamma ray obtained from the spectrum in coincidence with the 0.624-Mev gamma ray and the other two spectra suggests that there are two gamma rays of this energy. The possible second 1.95-Mev transition has been proposed as originating at a 2.46-Mev level.

The intensity of the 0.62-Mev transition between the 0.513- and 1.13-Mev levels was estimated from the gamma-gamma angular correlation data of Klema and McGowan.[6] If the transition is assumed to be pure $E2$, the value of the calculated intensity is 4.9 ± 1.3. For a 10% admixture of $M1$, the value is changed approximately 20%.

Silver-106 was produced by an (α,n) reaction on Rh^{103} with the Purdue University cyclotron. The singles spectrum of Ag^{106} was observed for a source-to-detector distance of 14 cm. The spectrum is shown in Fig. 3. The unresolved peak between 400 and 470 kev appears to be composed primarily of two gamma rays with approximate energies of 0.41 and 0.45 Mev. A second measurement of the spectrum was made with the same source three weeks later. All gamma rays were found to decay with the half life characteristic of Ag^{106}. The intensities of the gamma rays obtained from the analysis of the spectrum in Fig. 3 are given in Table 2. The gamma-ray spectra in coincidence with the 0.513-, 0.725-, 0.808-, 1.051-, 1.21-, and 1.544-Mev gamma rays were observed for a source-to-detector distance of 5 cm.

---

[6] E. D. Klema and F. K. McGowan, *Phys. Rev.* **92**, 1469 (1953).

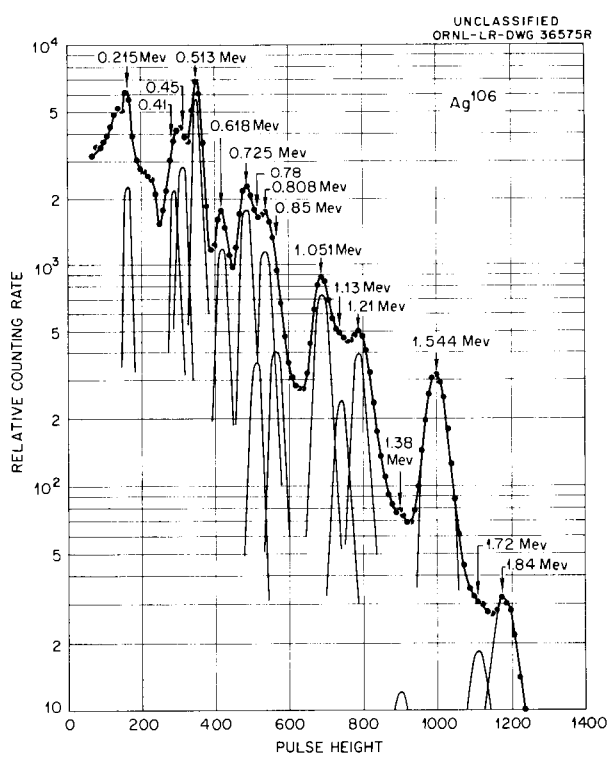

Fig. 3. Gamma-Ray Spectrum of Ag^{106}.

Table 2. Relative Intensities of Gamma Rays from Ag^{106}

Energy (Mev)	Intensity
0.215	11 ± 3
0.400–0.470	63 ± 7
0.513	100
0.618	25 ± 1
0.725	48 ± 4
0.77	?
0.808	36 ± 5
0.85	13 ± 3
1.051	34 ± 2
1.13	11 ± 1
1.21	21 ± 1
1.38	0.8 ± 0.4
1.544	26 ± 1
1.72	2 ± 1
1.83	3.6 ± 0.4

These spectra confirm the presence of the weak 0.77-Mev gamma ray and reveal a new gamma ray with an energy of 0.70 Mev. The 1.21-Mev gamma ray is in coincidence with both the 0.618- and 1.051-Mev gamma rays. This indicates that there are two gamma rays with approximately equal energies of 1.21 Mev. This agrees with the investigation of Alburger and Toppel,[3] who found conversion electrons in the decay of Ag^{106} which corresponded to 1.205- and 1.225-Mev gamma rays. The spectrum in coincidence with the 0.808-Mev gamma ray indicates that there are also two gamma rays with approximately equal energies of 0.81 Mev; furthermore, they are in coincidence.

A tentative decay scheme of Pd^{106} based on the study of the singles and coincidence gamma-ray spectra of Ag^{106} is given in Fig. 4. The decay scheme does not include all of the observed gamma rays. The order of the 0.725-1.544-Mev cascade in Fig. 4 is based primarily on the intensities of the gamma rays observed in the spectrum in coincidence with the 1.544-Mev gamma ray. The order of the proposed 0.70-0.85-Mev cascade cannot be determined from our results. Comparison of this tentative decay scheme with the scheme given in Fig. 2 shows that only the levels at 0.513, 1.13, and 1.56 Mev are populated by the decays of both Rh^{106} and Ag^{106}.

From the decay of Ag^{106} the branching ratio of cascade to crossover gamma rays from the second 2^+ level is 2.3 ± 0.3. This ratio combined with Coulomb excitation data[5] gives a value of 1.2 ± 0.3

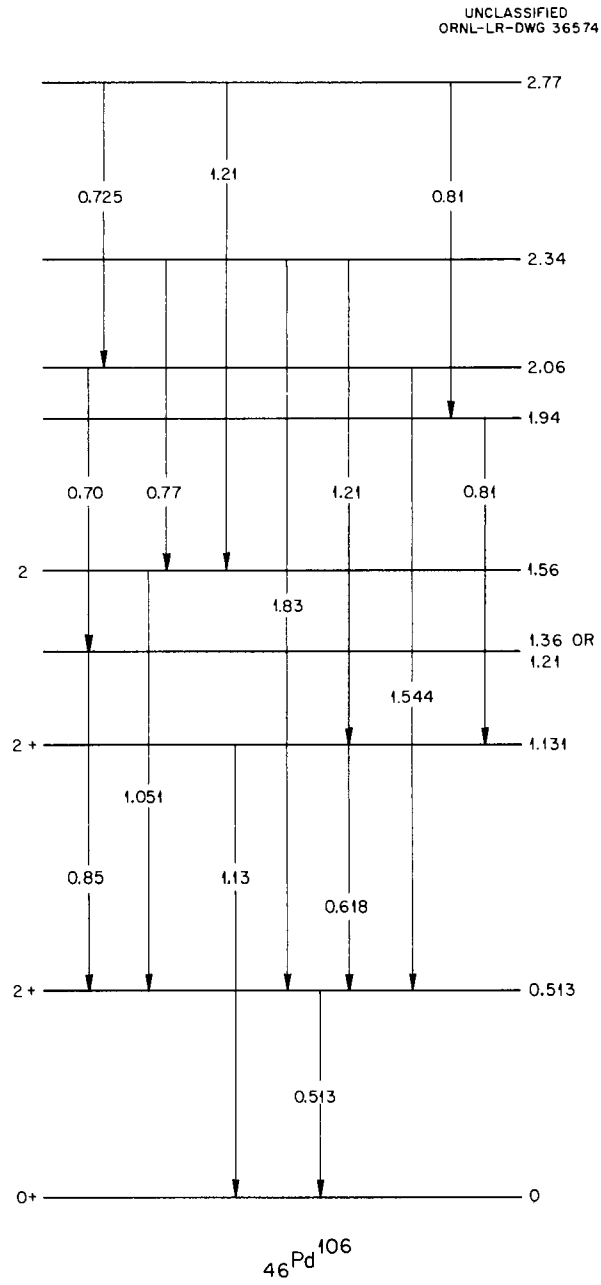

Fig. 4. Suggested Transitions and Energy Levels in Pd^{106} Which Occur in the Decay of Ag^{106}.

for the ratio $B(E2, 2' \rightarrow 2)/B(E2, 2 \rightarrow 0)$. Corrections for double $E2$ excitation and angular correlation effects have not been applied to the Coulomb excitation data. This ratio is smaller than the value of 2.0 which is predicted for it if quadrupole vibrations of spherical nuclei are assumed. However, the value of this ratio for two other even-even, medium-weight nuclei has also been found to be appreciably smaller than the predicted value.[7]

[7] F. K. McGowan and P. H. Stelson, *Phys. Semiann. Prog. Rep. Sept. 20, 1958*, ORNL-2610, p 11.

DECAY OF $I^{130} \rightarrow Xe^{130}$[1]

W. G. Smith[2] P. H. Stelson F. K. McGowan

The decay of I^{130} has been previously studied by two groups of workers,[3] and the following level scheme for Xe^{130} has been proposed: 528 kev (2^+), 1190 kev (4^+), 1930 kev (6^+), and 2340 kev (5^-). Only the states at 1930 and 2340 kev were found to be directly populated by beta decay. However, the recent measurement of spin 5 for I^{130} suggests that the 1190-kev state, if 4^+, should be populated by beta decay. In the present work, such a group was looked for but was not found. A lower limit of 9.8 was set for log ft. Gamma-gamma correlations were also made. The experimental correlation for the 1190-528-0 level sequence can be fitted by $4(Q)2(Q)0$ or by $2(96\%\ D + 4\%\ Q)2(Q)0$ sequences. The 2^+ assignment to the 1190-kev level requires a predominantly $M1$ transition for the 2^+ to 2^+ transition, in contrast with the predominantly $E2$ character of other known transitions of this type. Therefore, either 4^+ or 2^+ assignment to the 1190-kev state leads to an anomalous situation. Six other angular correlations were measured in an attempt to determine the characteristics of the levels at 1930 and 2340 kev. It was not possible to obtain unique assignments.

[1] Abstract of paper submitted to the *Physical Review*.

[2] Summer research participant from Purdue University, Lafayette, Ind.

[3] A. Roberts *et al.*, *Phys. Rev.* **64**, 268 (1943); R. S. Caird and A. C. G. Mitchell, *Phys. Rev.* **94**, 412 (1954).

PRECISION MEASUREMENT OF THE $Be^9(\gamma,n)$ CROSS SECTION[1]

J. H. Gibbons R. L. Macklin J. B. Marion[2] H. W. Schmitt

Measurements have been made of the photoneutron cross section for Be^9 by using gamma rays from radioactive sources of Y^{88} (1.85 Mev) and Sb^{124} (1.69 Mev). The values obtained at these two energies are $(6.54 \pm 0.31) \times 10^{-28}$ and $(12.62 \pm 0.69) \times 10^{-28}$ cm^2, respectively. The limiting factors in the accuracy of these measurements are the uncertainties in the gamma-ray source strength calibration and in the NBS No. 2 Ra-γ-Be neutron source standard, and the lack of precise knowledge concerning the Sb^{124} decay scheme. A new measurement of the gamma-ray branching ratios in the Sb^{124} decay has also been made.

[1] Abstract of paper submitted to the *Physical Review*.

[2] Summer visitor, 1958. Permanent address: University of Maryland, College Park.

TOTAL NEUTRON YIELDS FROM LIGHT ELEMENTS UNDER PROTON AND ALPHA BOMBARDMENT[1]

J. H. Gibbons R. L. Macklin

Total neutron production cross sections have been measured for targets of H^2, H^3, Li^7, Be^9, B^{11}, C^{13}, C^{14}, and F^{19} under proton bombardment and of Li^7, Be^9, B^{10}, and Si^{29} under alpha-particle bombardment. The energy ranges covered differ but were contained between threshold and 6 Mev for protons and between threshold and 9 Mev for alphas. In several cases cross sections for the inverse reactions (n,p) and (n,α) have been computed and compared, where available, with direct measurements.

[1]Abstract of paper submitted to the *Physical Review*.

NEUTRON RADIATIVE CAPTURE CROSS SECTIONS FROM 10 TO 150 kev

J. H. Neiler R. L. Macklin J. H. Gibbons P. D. Miller

A 1-m-dia liquid scintillator tank (Fig. 1) has been constructed and used with the ORNL 3-Mv pulsed Van de Graaff accelerator. Over-all time resolution is 15 to 20 mμsec. Energy resolution on a single gamma-ray peak is 25 to 30%. By use of "kinematically collimated" neutrons from the $Li^7(p,n)$ reaction (29-kev peak intensity, 17 kev full width at half maximum), the radiative capture cross sections for a number of elements have been compared. Absolute cross sections have been assigned by normalization to the absorption cross section of silver as measured by shell transmission at 27 kev (Sb-Be neutrons).[1] Pulse-height spectra in the scintillator have been studied for neutron capture in 19 of the elements studied. Conversion of the full binding energy to a light pulse, even with over 40 cm of gamma absorption path in the scintillator, seems to be relatively rare. The spectra are sufficiently characteristic, however, for neutron binding energies to be identified. Values of 6.5 ± 0.4 Mev for Tb^{159} and 6.2 ± 0.4 Mev for Ho^{165} were found in this way.

The flat-response 4π graphite-sphere neutron detector[2] has been used to establish the absolute neutron flux used in the capture-cross-section experiments described above. This was accomplished by measuring the 54-min beta activity induced in indium samples. A Zr-H^3 target was also used to provide a collimated beam of neutrons from the $H^3(p,n)$ reaction, of average energy 63 kev (full width at half maximum, 40 kev). With the assumption that the response of the neutron detector is uniform, the 29-kev absolute cross sections were extended to this energy. Results are shown in Table 1.

The large liquid scintillator[3] has also been used to study neutron capture cross sections as a function of neutron flight time. The measurement of the absolute cross section was determined[4] earlier at 29 and 63 kev. Relative values were normalized to gamma rays from $B^{10}(n,\alpha\gamma)Li^7$, assuming a $1/v$ behavior for this cross section.[5] The slope of the cross-section results ($\sigma \sim E^{-3/4}$ on the average) in the energy range 30 to 70 kev is in good agreement with the "threshold" measurements at 29 and 63 kev. Cross-section results have been obtained over the energy range from 10 to 150 kev for Ho, Tb, Ta, Pt, Pd, Ag, Au, Nb, In, and Sb. Corrections for the change in tank efficiency for the particular gamma-ray spectra have been made. Cross-section departure from a simple power dependence on energy is particularly noticeable for Pt, Ag, and Au. Results for In, Pt, and Tb are shown in Figs. 2, 3, and 4, respectively. Preliminary measurements among light elements are promising. In the cross-section computations it was assumed that the tank gamma-ray efficiency was equal to that for indium capture gamma rays. An example of studies among light elements is that of aluminum, shown in Fig. 5.

[1]H. W. Schmitt and J. H. Gibbons, unpublished data.

[2]R. L. Macklin, *Nuclear Instr.* 1, 335–39 (1957).

[3]J. H. Neiler *et al.*, *Bull. Am. Phys. Soc.* 4, 43 (1959).

[4]R. L. Macklin *et al.*, *Bull. Am. Phys. Soc.* 4, 43 (1959).

[5]J. H. Gibbons and R. L. Macklin, submitted to the *Physical Review*.

Table 1. Radiative Capture Cross Sections for Threshold Neutrons

Z	Element	Absolute Cross Section (mb)		Z	Element	Absolute Cross Section (mb)	
		29 kev*	63 kev**			29 kev*	63 kev**
6	C	<0.5	<0.3	48	Cd	340 ± 50	190 ± 30
12	Mg	0.5 ± 2	1.8 ± 2	49	In	825 ± 150	480 ± 90
13	Al	3 ± 2		50	Sn	95 ± 20	50 ± 5
24	Cr	11 ± 2	5 ± 2	51	Sb	470 ± 75	270 ± 40
26	Fe	14 ± 3	7 ± 2	65	Tb	2100 ± 300	1250 ± 200
28	Ni	30 ± 10	8 ± 2	67	Ho	2000 ± 300	1300 ± 200
29	Cu	45 ± 10	25 ± 4	73	Ta	780 ± 100	480 ± 70
30	Zn	50 ± 10	27 ± 5	74	W	300 ± 100	205 ± 30
39	Y	13 ± 2	7 ± 2	78	Pt	440 ± 50	270 ± 40
40	Zr	14 ± 3	11 ± 2	79	Au	525 ± 150	350 ± 60
41	Nb	275 ± 50	145 ± 20	82	Pb	2.5 ± 3	<2.5
42	Mo	175 ± 30	85 ± 15	83	Bi	1 ± 3	2.5 ± 2
46	Pd	460 ± 75	275 ± 45	92	U^{238}	450 ± 150	275 ± 90
47	Ag	(950 ± 70)	600 ± 50				

*Full width at half maximum, 16 kev.
**Full width at half maximum, 40 kev.

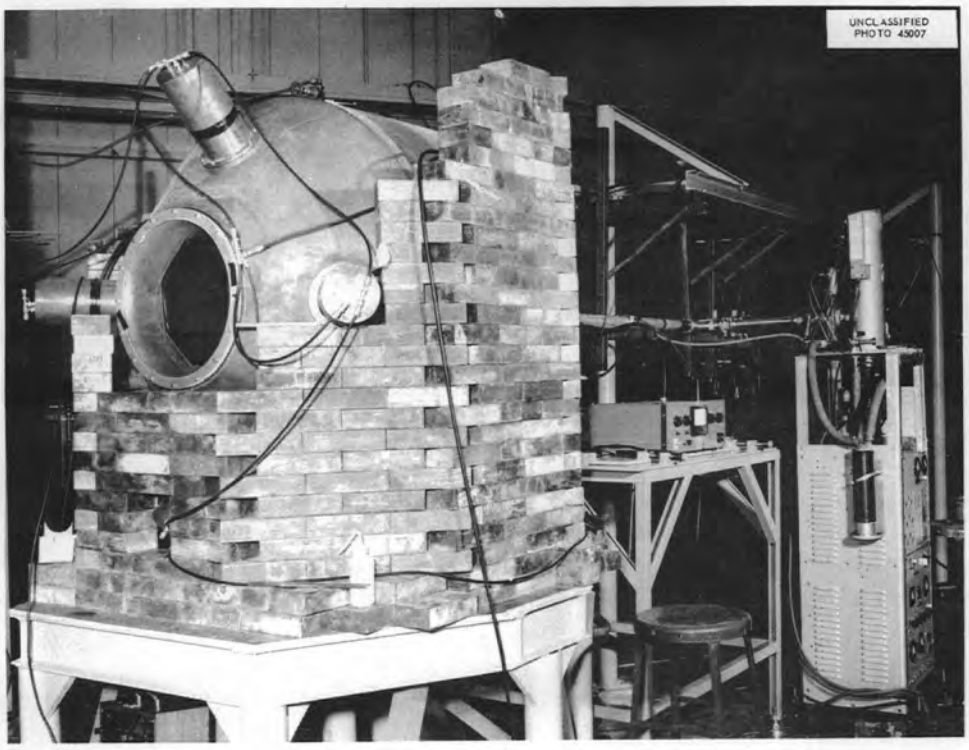

Fig. 1. Photograph of Liquid Scintillator Tank.

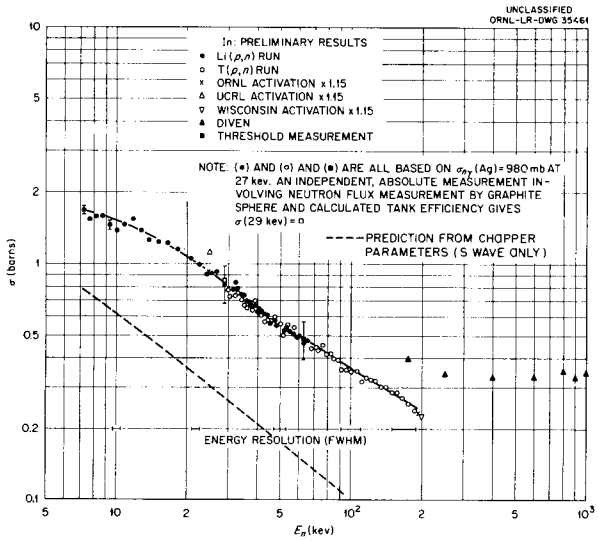

Fig. 2. Capture Cross Section of In as a Function of Neutron Energy.

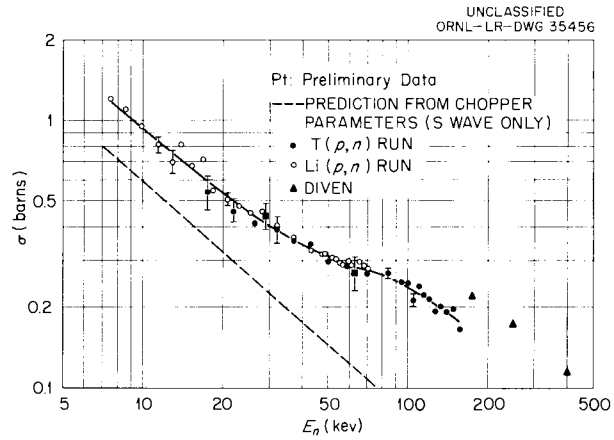

Fig. 3. Capture Cross Section of Pt as a Function of Neutron Energy.

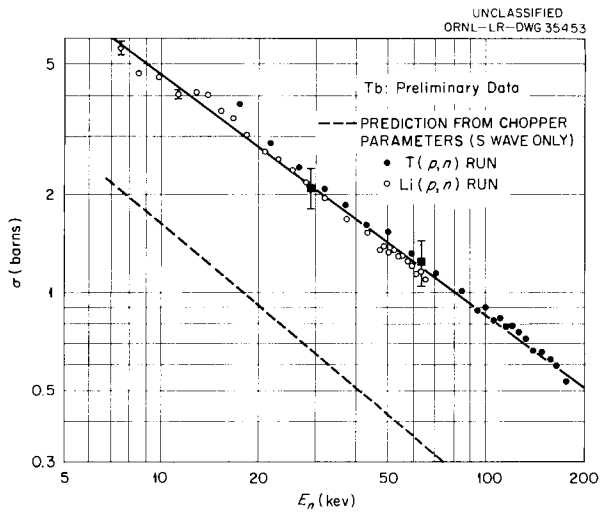

Fig. 4. Capture Cross Section of Tb as a Function of Neutron Energy.

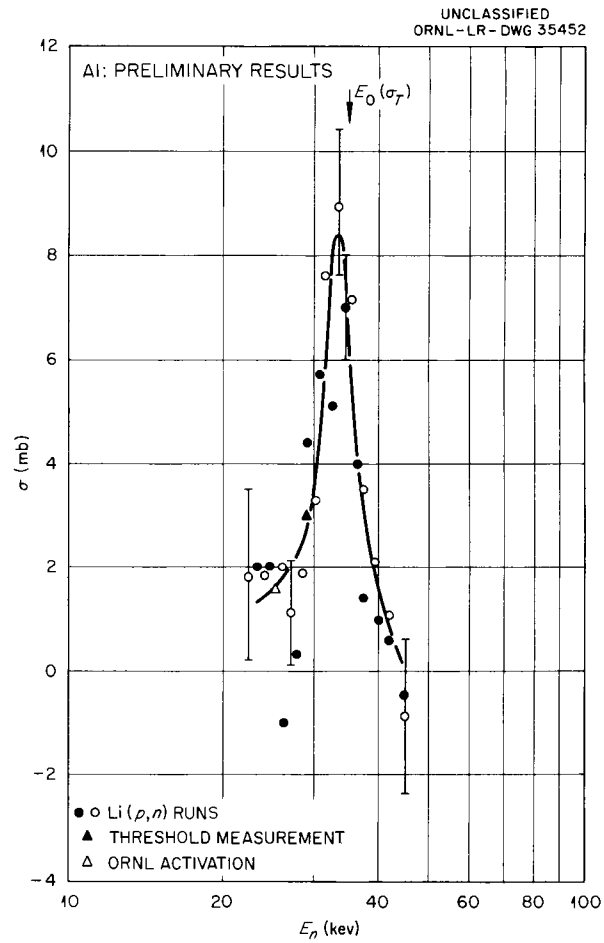

Fig. 5. Capture Cross Section of Al as a Function of Neutron Energy.

NEUTRON SCATTERING FROM BERYLLIUM

J. L. Fowler H. O. Cohn

Before a detailed phase-shift analysis of the differential scattering of neutrons from beryllium was undertaken,[1] it seemed advisable to recheck the total cross section in the energy region 2 to 4 Mev, particularly since the reported peaks in the cross section[2] at about 2.7 Mev seemed anomalously large. Accordingly, the total cross section of beryllium was remeasured in this region. Tritium(p,n) neutrons with an energy spread of about 25 kev were produced by bombarding a tritium gas cell with protons from the 5.5-Mv Van de Graaff machine. The experiment was of the standard transmission type. Forward-direction neutrons were detected with a 2.5-cm-dia propane recoil counter located so that the center of its 10-cm-long sensitive volume was 38 cm from the center of the tritium gas cell. In separate experiments, measurements were made with two beryllium samples each 2.86 cm in diameter which were positioned midway between the neutron source and the detector. One sample was 1.39 cm long, the other 2.38 cm long. The background of neutrons which reached the detector from directions other than that of the source was evaluated by removing the direct neutrons with a Lucite plug.

In Fig. 1 the total cross section has been corrected for these background neutrons and for in-scattered neutrons. For this latter correction, the differential cross sections previously reported[1,3] and shown partially in Figs. 2 and 3 were used. Since isotropic scattering had been assumed for the in-scattering corrections for the data of Bockelman *et al.*,[4] in Fig. 1 their data have been recorrected by use of the recent differential measurements. There is, as can be seen in Fig. 1, good agreement between the measurements reported here and the previous measurements corrected as explained above. The cross section at the peak is about 4% higher than in the published curves.[2]

A preliminary phase-shift analysis based on qualitative arguments,[1] which lead to 2^+ as the spin and parity assignment to one of the levels which contributes to the peak near 2.7 Mev, gives inconsistent results. Neutron and alpha level widths large

[1] H. O. Cohn and J. L. Fowler, *Phys. Semiann. Prog. Rep. Sept. 20, 1958*, ORNL-2610, p 14.

[2] D. J. Hughes and R. B. Schwartz, *Neutron Cross Sections*, BNL-325, 2d ed. (July 1, 1958).

[3] M. Walt and J. R. Beyster, *Phys. Rev.* **98**, 677 (1955).

[4] C. K. Bockelman *et al.*, *Phys. Rev.* **84**, 69 (1951).

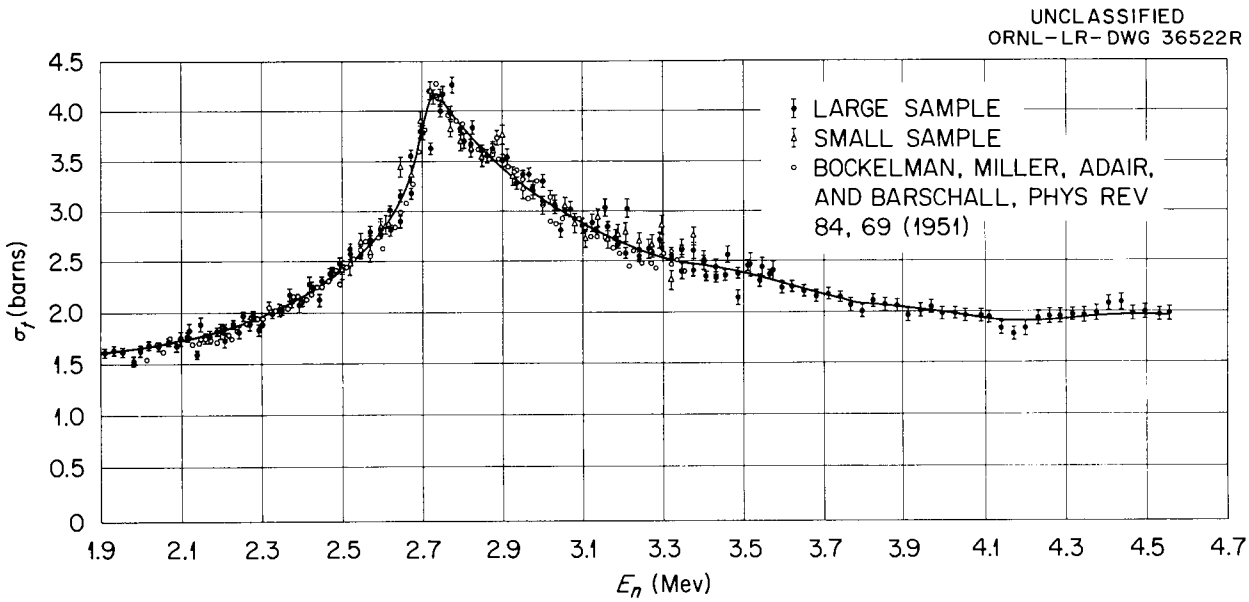

Fig. 1. Total Neutron Cross Section of Be in Region 1.9 to 4.5 Mev.

enough to give the (n,α) cross section in Fig. 3 do not give the correct interference with potential scattering to produce the nearly symmetrical differential cross sections at 2.15 and 2.44 Mev (Figs. 2 and 3). For this purpose, smaller level widths are required. This situation could be remedied if there were a $J = 0^+$ level arising from p-wave neutrons around 1 Mev. This would take care of the low-energy (n,α) cross section and perhaps explain the rather large P_1 contribution to the differential scattering near 1 Mev. The phase-shift analysis is being reinvestigated under the assumptions of a $J = 0^+$ level at about 1 Mev, a 2^+ level around 3 Mev, and an odd-parity high J level (possibly a 4^- level) slightly below 3 Mev.

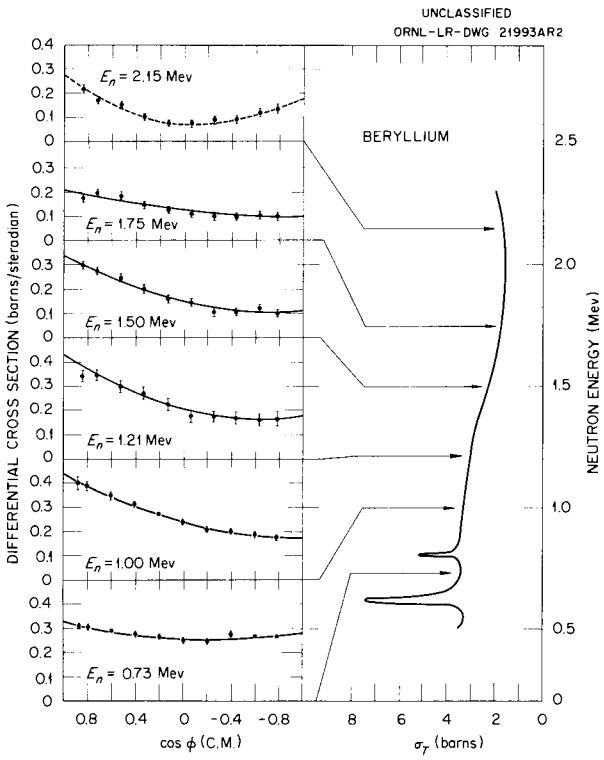

Fig. 2. Center-of-Mass Differential Cross Section of Be from 0.73 to 2.15 Mev.

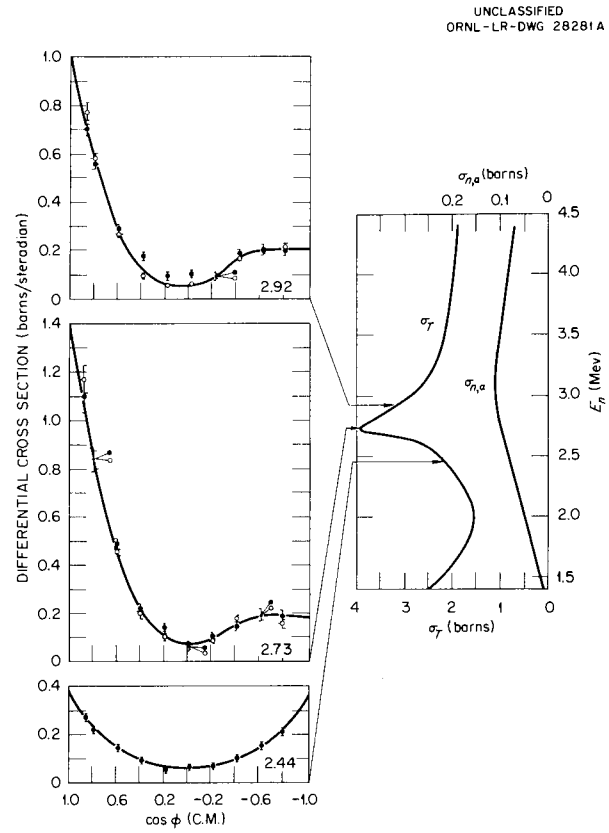

Fig. 3. Center-of-Mass Differential Cross Section of Be in the Vicinity of the Levels near 3.0 Mev.

NEUTRON-INDUCED FISSION FRAGMENT ANGULAR DISTRIBUTION FOR U^{234} AND U^{235}

R. W. Lamphere

The work reported herein covers a period of approximately three years. The data have not been completely analyzed and cross-checked for errors, so the results should be considered tentative.

The purpose of this program has been to establish what, if any, correlations might exist between the extrema in the neutron-induced total fission cross section of an even-even target nucleus and the way in which the angular distribution of the emitted fragments from fission varied in the energy regions of these extrema.

Two foils of U^{234} were mounted back-to-back in a double ionization chamber. A collimator was placed over each foil. A collimator consisted of a sheet of 60-mil-thick aluminum in which a very large number of 20-mil-dia holes were drilled at 45° to the surface. The distance between foils and tritium gas target (neutron source) was kept at 3.93 in. for all measurements. Thicknesses of tritium gas target varied from 60 to 140 kev, the thinner targets being used wherever significant changes in angular distribution with neutron energy were found.

Counting rates under these conditions were very low. The collimators reduced the counting by a factor of 275, compared with uncollimated (2π) counting. Consequently the construction of a gas target capable of yielding a high neutron flux was essential. The one constructed permitted an increase of a factor of 10 in flux over that available from conventional single-foil gas targets. Briefly, it consists of a tritium cell which is separated from the vacuum in the proton beam tube by two 0.1-mil nickel foils, between which helium gas flows at very high velocity.

With this target the curve of the U^{234} fission cross section was rechecked in a short time. This was done with increased precision and greater detail in order to establish the shape more precisely, particularly in the vicinity of the extrema. Two new features of the curve were discovered. First, the shape of the curve was found to change at about 250 kev (where $\sigma_f \cong 0.06$ barn), dropping off much more slowly for lower energies. At 120 kev, $\sigma_f \cong 0.03$ barn, and is about 0.02 barn at 60 kev. Secondly, a tiny dip was found at 330 kev. From 350 kev, where $\sigma_f = 0.15$ barn, the curve rises smoothly to the first maximum of 1.26 barns at 850 kev. There is then a drop to a minimum of 1.11 barns at 1020 kev. At 1900 kev, $\sigma_f = 1.52$ barns, after which there is a small broad dip to 1.47 barns at 2400 kev. The cross section then rises gradually to 1.56 barns at 4000 kev. These values were measured with $\sigma_f(U^{235})$ as a monitor; hence the confidence values will be about those existing for $\sigma_f(U^{235})$, that is, in the neighborhood of 5%. The measured values are reported in detail in Howerton's[1] compilation of fast-neutron cross sections. However, the probable errors quoted therein were unfortunately only the statistical counting standard deviations for the comparison of $\sigma_f(U^{234})/\sigma_f(U^{235})$. These standard deviations must be compounded with the uncertainties in $\sigma_f(U^{235})$.

Table 1 gives representative values of angular distributions as read from a smooth curve drawn through the measured points. The U^{234} foils contained a few per cent of U^{235} as impurity. For the

[1] R. J. Howerton, *Tabulated Neutron Cross Sections*, UCRL-5226 (May 1958).

Table 1. Smoothed Values of $\sigma_f(0°)/\sigma_f(90°)$ for U^{234} and U^{235}

About 20 points with average standard deviation of 2.0% served to estoblish the curve from 400 to 3700 kev for U^{234}

E_n	$\sigma_f(0°/90°)$	
	U^{234}	U^{235}
400	0.73	1.03
500*	0.60	1.05
600	0.87	1.07
800	1.61	1.09
840*	1.67	1.10
900	1.57	1.10
1000	1.20	1.11
1050*	1.09	1.11
1200	1.13	1.12
1500	1.19	1.13
2000	1.20	1.13
2500	1.18	1.13
3000	1.18	1.13
3700	1.20	1.14

*Energies where extrema occur.

most part the corrections for this factor are small. They have not been made as yet, but will be appreciable only for energies below about 500 kev. Uncertainties due to counting statistics were usually about 2%. The total neutron energy spread ran from 60 to 100 kev, being due principally to thickness of the gas target. In addition to the 0°/90° ratio, more complete observations were taken at 840, 1050, and 3700 kev. These consisted of readings taken every 30° around the entire 360°. Symmetry was found relative to 90°, so data referred to 0, 30, 60, and 90° serve to define the distribution. They appear to have an approximately $\cos^2 \theta$ dependence, although detailed analyses have yet to be completed.

Similar measurements, in less detail, were made on U^{235}. Only 13 points were taken, with an average standard deviation of about 2%. Values are listed in Table 1, again as read from a smooth curve drawn through the points. At about 930 kev the total fission cross section has been found by Diven[2] to rise very abruptly from 1.16 to 1.25 barns. This rise takes place within an energy interval of roughly 30 kev. Consequently, in this region a more searching investigation of the angular distribution was carried out, with gas target thicknesses averaging around 60 kev. A measurement at 940 kev yielded 1.08 ± 1.6%, which is only 1½ standard deviations from the smooth curve. At 883 and 983 kev the measured ratios of $\sigma_f(0°/90°)$ were 1.13 and 1.13, respectively, with 2.4% statistical error.

Since a new fission mode clearly comes in around 930 kev, one would expect the angular distribution to be altered. However, since the fissioning nucleus at this energy is about 2 Mev above its threshold, there will already be many channels open to fission. Consequently, the effect on the angular distribution from one additional channel may be expected to be small. Although the data are indicative of the possible presence of such a slight effect, measurements would have to be taken in much greater refinement to permit a valid conclusion to be drawn. This would require about two weeks of generator time.

The theory of Bohr[3] predicts a rising $\sigma_f(0°/90°)$ from sidewise peaking, where this ratio is less than unity, to values above unity as E_n increases above the fission threshold. Following this initial rise, a slow drop toward unity (less asymmetry), up until the point where second chance fissions can come in, is consistent with the theory. This type of behavior has been observed for U^{238} (ref 4).

In the case of U^{234}, however, the observed situation is somewhat different following the first initial rise. The precise correspondence of the extrema in the total fission cross section and 0°/90° ratio and the fact that a minimum occurs in the ratio are yet to be accounted for. If the minimum in the total fission cross section is due to competition from neutron emission from the excited compound nucleus, U^{235}, why should the angular distribution of fission fragments be altered? One must assume that of the population of excited U^{235} nuclei formed, neutrons were preferentially emitted (relative to fission) from compound nuclei existing in those (K, I) rotational states that give rise primarily to large fission-fragment asymmetry, that is, that are oriented with the major axis generally along the z direction (the direction of incident neutron beam).

An alternative explanation is that possibly the major fission mode operative in the vicinity of the first maximum exhibits resonance behavior.

A more thorough analysis of these results is in progress.

[2] B. C. Diven, private communication.

[3] A. Bohr, *Proc. Intern. Conf. Peaceful Uses Atomic Energy, Geneva, 1958* **2**, 151 (1958).

[4] R. L. Henkel and J. H. Brolley, Jr., *Phys. Rev.* **103**, 1292 (1956).

NEUTRON ABSORPTION CROSS SECTIONS AT 27 kev

H. W. Schmitt J. H. Gibbons C. N. Inskeep

The neutron absorption cross sections of a number of elements have been measured at 27 kev by use of a spherical-shell transmission method. Neutrons were obtained from a source consisting of a solid 1-in.-dia sphere of antimony encased in a 0.030-in.-thick beryllium shell. Average neutron energy from this source was 27 kev, with a maximum spread of 3 kev.

The experimental arrangement is shown schematically in Fig. 1. The source was brought to a fixed position at the center of the spherical shell on the axis of the neutron detectors. Successive shell-on and shell-off measurements were made in order to determine the neutron transmission of the sample shell.

Neutron detection was by means of modified long counters, shielded by lead to reduce gamma-ray backgrounds. From the present source, there were about 8×10^4 gamma rays per neutron emitted; hence a gamma sensitivity of say 10^{-7} relative to neutron

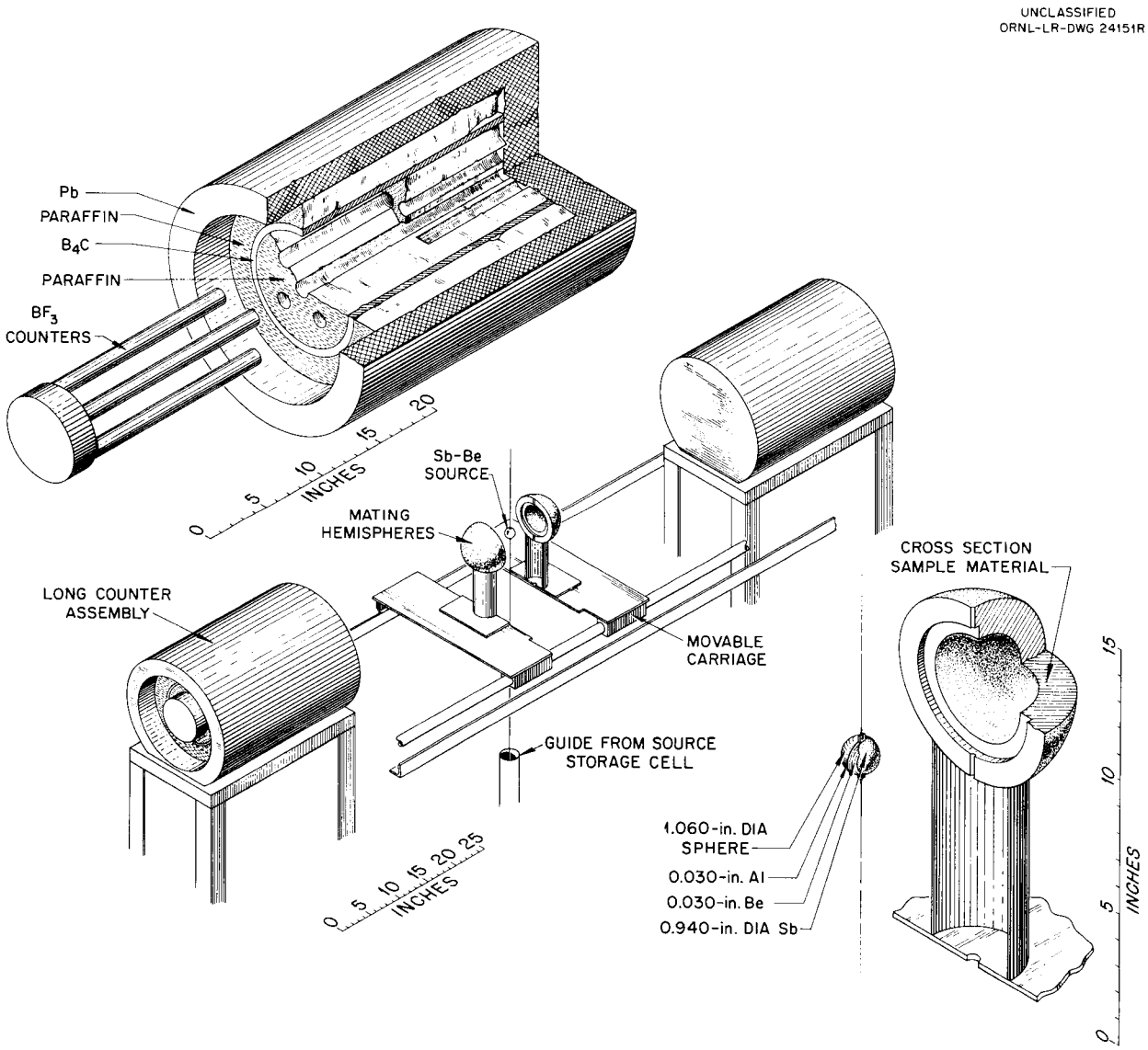

Fig. 1. Apparatus for the Measurement of Neutron Absorption Cross Sections.

sensitivity could introduce an error of about 1% in transmission. Careful experimental checks were made to determine that errors in transmission from gamma-ray backgrounds were less than 0.5%.

A serious attempt was made in these measurements to maintain good geometry; that is, the source was isotropic, source-to-detector distances were large compared with the shell diameters, and the source size was small compared with the inside diameter of the sample shells. While finite size and finite distance effects were minimized, nevertheless they were evaluated and appropriate corrections included in analysis of the data.

Analysis of these measurements, including multiple scattering of neutrons in the sample shells, was carried out by using the method of Bethe, Beyster, and Carter.[1] The transmission of a sphere in the present experiment is given as follows:

$$T = T_0'' + (1 - T_0')\frac{\sigma_{sc}}{\sigma_t}\left[\bar{P}_1 + (1 - P_1)\bar{P}_2\frac{\sigma_{sc}}{\sigma_t} + \frac{(1 - P_1)(1 - P_2)\bar{P}_m\sigma_{sc}^2}{\sigma_t(\sigma_a + \sigma_{sc}P_m)}\right], \quad (1)$$

where

$$T_0'' = T_0' + \frac{r^2}{3b^2}e^{-n\sigma_t(r_2 - r_1)}, \quad (2)$$

$$T_0' = e^{-n\sigma_t(r_2 - r_1)}\left[1 - \frac{n\sigma_t r^2}{3}\left(\frac{1}{r_1} - \frac{1}{r_2}\right)\right]. \quad (3)$$

In these equations, r = source radius; r_1 and r_2 are the inside and outside radii of the sample shell; b = source-to-detector distance; σ_t, σ_{sc}, and σ_a are the total, scattering, and absorption cross sections, respectively, of the sample material. The P_i are the escape probabilities of a neutron after i collisions in the shell. The effects of finite source size and finite source-to-detector distance were derived specifically for the conditions of the present experiment and appear in Eqs. (2) and (3).

Results of the present measurements are given in Table 1. Shell thicknesses in total mean free paths are given, and since the total cross section enters strongly in the analysis, these values are also tabulated. Uncertainties in the measured transmissions include statistical and other small uncertainties associated with the measurements. Uncertainties in the absorption cross sections include uncertainties in the measured transmissions as well as in total cross sections. It is to be noted that each measurement is an absolute measurement, independent of the others.

[1] H. A. Bethe, J. R. Beyster, and R. E. Carter, *J. Nuclear Energy* 3, 207–23, 273–300 (1956).

Table 1. Absolute Neutron Absorption Cross Sections at 27 kev

Spherical-shell transmission measurements

Shell	Thickness (total mean free paths)	σ_t (barns)	T	σ_a (mb)
Cu	1.92	9 ± 1	0.970 ± 0.007	44 ± 10
Zn	1.38	7.0 ± 0.5	0.964 ± 0.008	73 ± 25
Ag	1.34	7.3 ± 0.5	0.703 ± 0.004	970 ± 70
Sb	1.05	6.3 ± 0.2	0.877 ± 0.005	470 ± 30
Sb	0.620	6.3 ± 0.2	0.927 ± 0.003	488 ± 25
Au	1.80	12.0 ± 0.5	0.806 ± 0.005	516 ± 30
Pb	1.49	11.0 ± 0.5	0.999 ± 0.003	3 ± 10

NEUTRON ACTIVATION AT 195 kev[1]

W. S. Lyon R. L. Macklin

Neutron activation cross sections have been measured at 195 kev (50-kev energy spread) for about 30 isotopes, by absolute gamma counting. Absolute calibration was effected by determining the RdTh-D_2O neutron source strength with a flat-response 4π graphite-sphere neutron counter and irradiating indium in the form of a thin, uniform spherical shell. The results are in general agreement with those of other investigators. The 25-kev activation cross sections of Pr^{141}, Zr^{94}, Ga^{71}, and Pd^{108} have been revised.

[1] Abstract of paper submitted to the *Physical Review*.

TOTAL CROSS SECTIONS IN THE KILOVOLT RANGE

P. D. Miller J. H. Gibbons W. M. Good J. H. Neiler

Transmissions of samples in the atomic weight range from 35 to 76 were measured by using an $Li^7(p,n)$ neutron source at 0°. Neutron energies in the range from 3 to 30 kev were used, and energies were determined from their flight times with a resolution of ~ 12 mμsec. Flight paths up to 3 m were used. The detector was a boron-10 carbide–boron-10 disk in front of an NaI(Tl) crystal. One resonance at 26.8 kev in Cl^{35} was observed. This narrow resonance, as well as the others to be described, was area-analyzed by the method of Seth.[1] The width of the resonance, assuming $g = \frac{1}{2}$ and $\Gamma_n = \Gamma$, was 0.09 kev. When this resonance, the resonance at 405 ev observed by Brugger and coworkers at Idaho Falls,[2] and the negative energy resonance found necessary by the Idaho Falls group are used, a strength function

$$\frac{\overline{\Gamma_n^0}}{D} = (0.2 \pm 0.1) \times 10^{-4}$$

is obtained.

Figure 1 shows the cross section obtained for Sc^{45}. Resonances were observed as given below:

E_0 (kev)	Γ_n (kev)
3.25	0.057
4.26	0.25
6.55	0.17
8.0	0.16
9.2	0.26
11.7	0.14
21.2	0.69
33	0.58

The strength function for Sc^{45} on the basis of these data is

$$\frac{\overline{\Gamma_n^0}}{D} = (3.0 \pm 1.1) \times 10^{-4} \ .$$

Preliminary work was done on V^{51}. The broad structure at 7 kev was observed. The structure centered around 12 kev appears to be unresolved. In addition there appear to be a resonance at 17.5 kev, which may also be multiple, and a resonance at 19.5 kev. None of the above resonances have been analyzed to obtain widths.

The situation in Fe^{57} is still not completely clear. The resonance at 3.9 kev may be either $J = 0$ or $J = 1$. The resonance at 6.1 kev is most definitely $J = 1$, and it appears that there is no interference between resonances. On the assumption that the 3.9-kev resonance is $J = 0$ and the 6.1-kev resonance is $J = 1$, the strength function turns out to be $(3.0 \pm 2.1) \times 10^{-4}$.

In Co^{59} the structure at 5.0 kev was not resolved, but its gross area was analyzed. The higher-energy data, up to 30 kev, were in excellent agreement with unpublished Duke work. The strength function on the basis of the first 12 resonances was 4.3×10^{-4}.

The best level statistics were obtained from Cu^{63}, in which 12 resonances were seen, and three others

[1] K. K. Seth, *Nuclear Phys.* (to be published).

[2] R. M. Brugger *et al.*, *Phys. Rev.* 104, 1054 (1956).

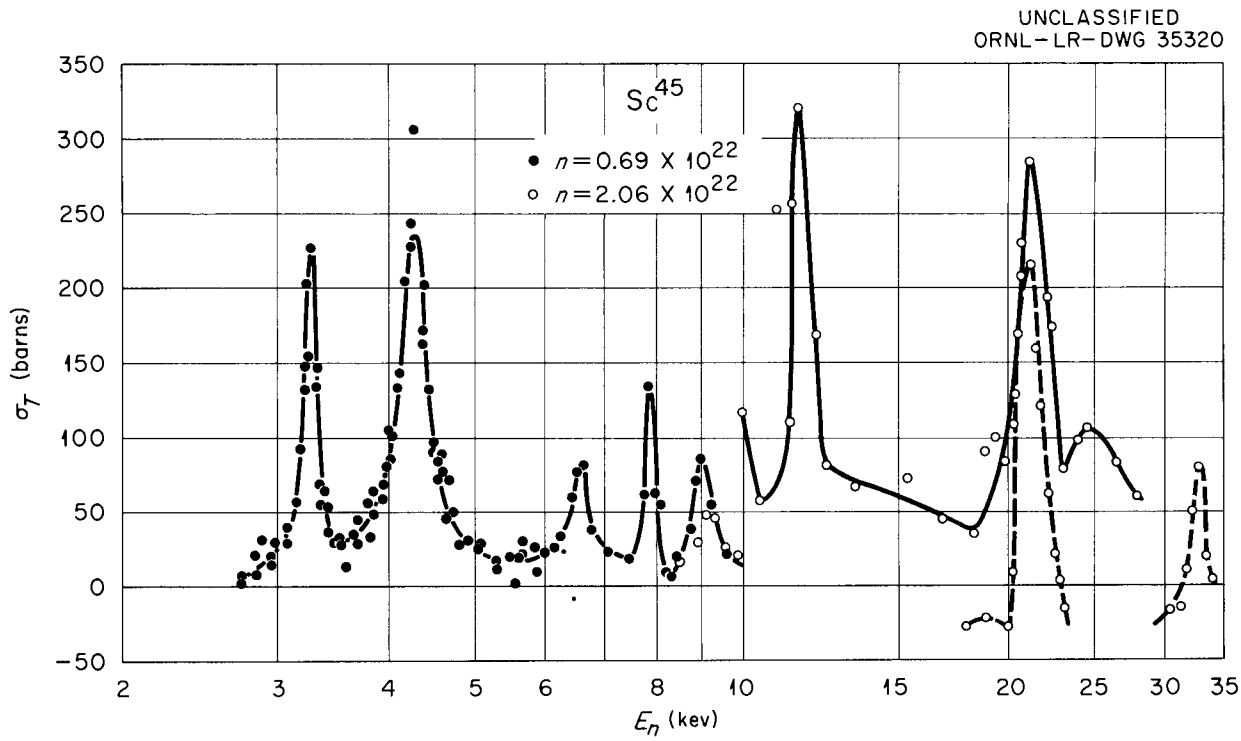

Fig. 1. Sc^{45} Cross Section. The cross sections above 10 kev are plotted times 10. The different cross sections from different runs at high energies result from background uncertainties.

were taken from work at Argonne.[3] Figure 2 shows the cross section obtained, and Fig. 3 shows the distribution of resonances and the distribution of reduced widths. The dotted lines in the distribution of levels show the result of counting resonances that are possibly multiple as two resonances. The strength function obtained from these data is

$$\frac{\overline{\Gamma_n^0}}{D} = (3.3 \pm 0.9) \times 10^{-4} \ .$$

Neither of the zinc isotopes studied, Zn^{66} and Zn^{68}, showed any structure below 10 kev. The transmission of the Zn^{66} sample with $n = 1.44 \times 10^{22}$ atoms/cm^2 is shown in Fig. 4. When these resonances were area-analyzed, a strength function of $(4.2 \pm 1.9) \times 10^{-4}$ resulted, which appears to be rather high. Figure 5 shows the Zn^{68} transmission spectrum. The two resonances at 10.4 and 15 kev are not as convincing as the one at 21.0 kev. When the three are area-analyzed, however, the strength function, including the Argonne results[4] for the 530-ev resonance, is

$$\frac{\overline{\Gamma_n^0}}{D} = (1.5 \pm 0.8) \times 10^{-4} \ .$$

All of the even isotopes of germanium were investigated. In Ge^{70}, six resonances were seen below 15 kev, and the strength function is 1.6×10^{-4}. In Ge^{72}, six resonances were seen below 13 kev, and the resulting strength function is 1.3×10^{-4}. In Ge^{74}, two resonances were seen below 11 kev and their widths are such that the strength function is $(2.2 \pm 1.6) \times 10^{-4}$. In Ge^{76}, five resonances were seen below 30 kev, and the resultant widths yield a strength function of 1.0×10^{-4}.

[3] R. E. Cote, L. M. Bollinger, and J. M. LeBlanc, *Phys. Rev.* 111, 288 (1958).

[4] D. A. Dahlberg and L. M. Bollinger, *Phys. Rev.* 104, 1006 (1956).

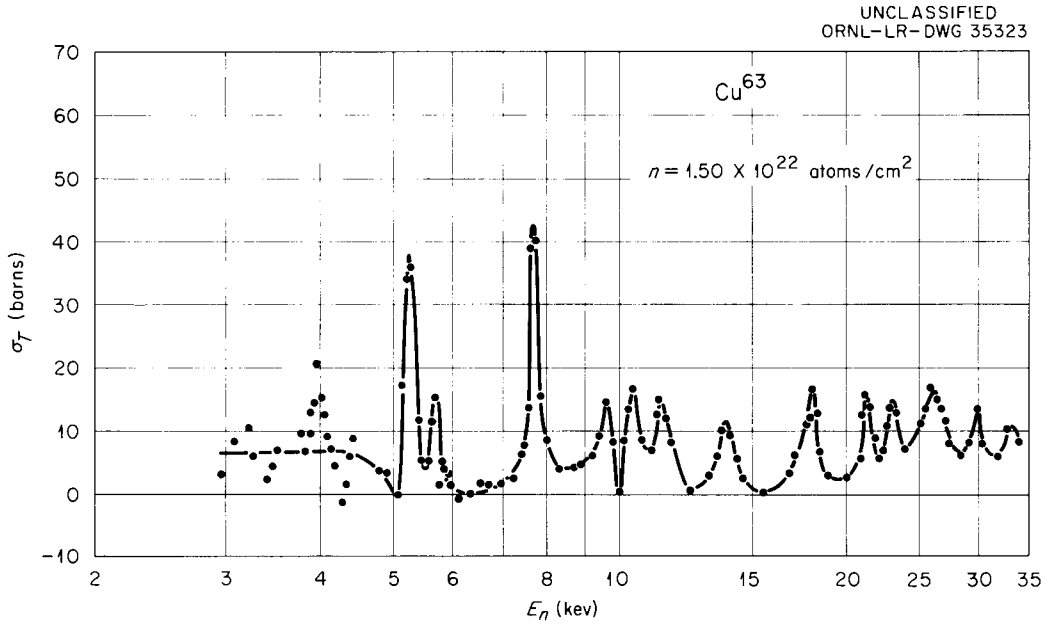

Fig. 2. Cu^{63} Cross Section. More recent experiments with improved resolution have disclosed two additional resonances between 4 and 5 kev.

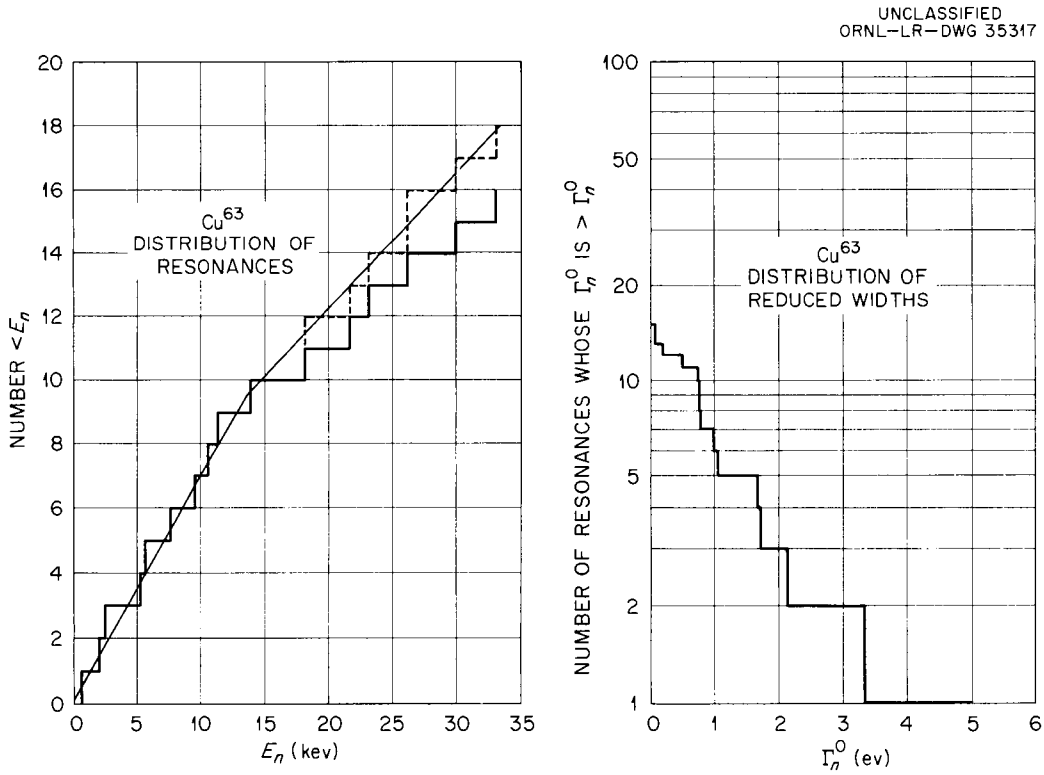

Fig. 3. Distribution of Levels and Reduced Widths for Cu^{63}.

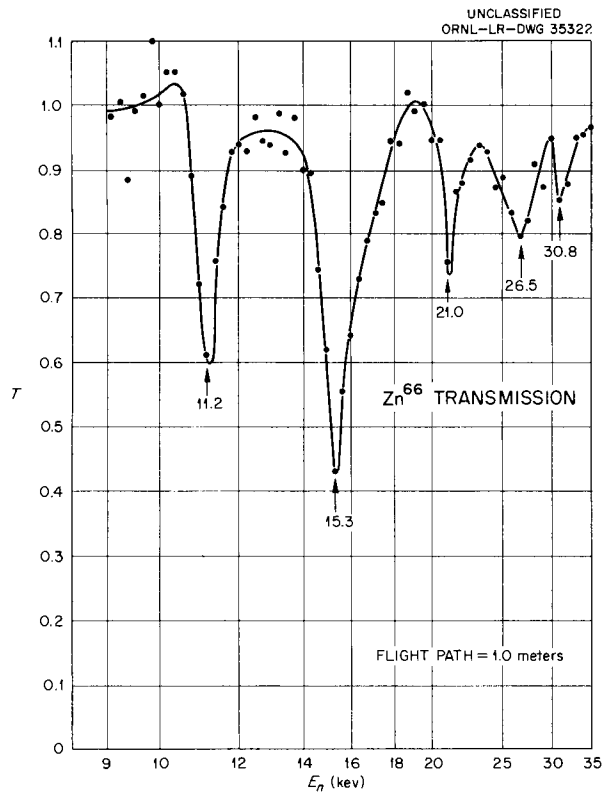

Fig. 4. Zn^{66} Transmission for a Sample with 1.44×10^{22} atoms/cm^2.

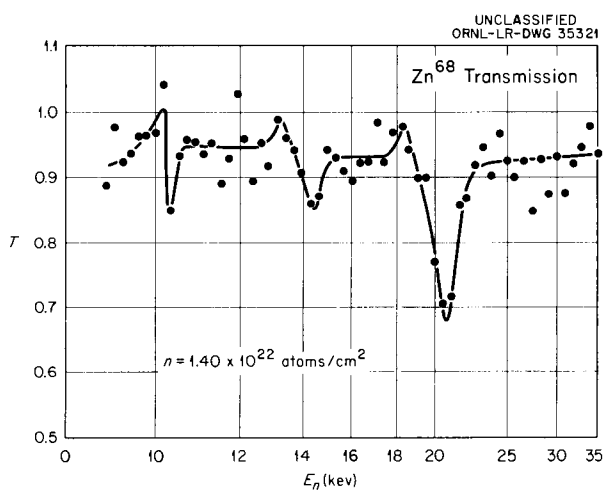

Fig. 5. Zn^{68} Transmission as a Function of Neutron Energy.

Figure 6 shows the above strength functions, together with Duke, Brookhaven, and previously reported Oak Ridge data plotted vs atomic weight of the compound nucleus. The theoretical curves are the Chase-Wilets-Edmunds curves[5] for spherical and deformed nuclei. The latter were calculated at the request of K. K. Seth in the range shown in Fig. 6.

The points corresponding to the Ge^{72} and Ge^{74} samples lie very high from the spherical nucleus curve and are strongly suggestive of deformation effects. The points corresponding to $A < 50$ seem to lie high and might suggest an incorrect radius or well depth in the optical model calculations in this region.

[5]D. M. Chase, L. Wilets, and A. R. Edmunds, *Phys. Rev.* 110, 1080 (1958).

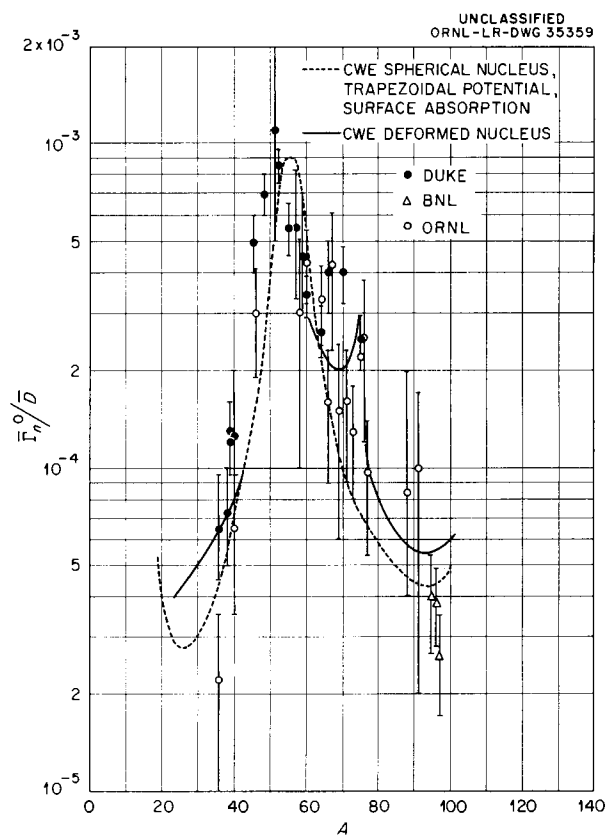

Fig. 6. Observed and Theoretical Strength Functions.

TOTAL NEUTRON CROSS SECTION OF Xe^{135} AS A FUNCTION OF ENERGY[1]

E. C. Smith[2] P. E. F. Thurlow[4] W. J. Martin[5]
G. S. Pawlicki[3] G. W. Parker[5] G. E. Creek[5]
P. M. Lantz[5]

The total neutron cross section of Xe^{135} as a function of energy has been remeasured at ORNL under more favorable conditions than obtained in the measurements of 1948. A sample thickness of 2.5×10^{18} atoms of Xe^{135} gas per cm^2 was procured from the off-gases of a homogeneous reactor. A mechanical time-of-flight chopper was used to produce monoenergetic neutron beams from 0.01 to several hundred ev. The number of Xe^{135} atoms in the sample was determined by means of mass spectrometer measurements on the long-lived daughter Cs^{135}. The data of the low-energy resonance were fitted equally well to the Breit-Wigner formula, taking into account Doppler corrections, with the following two sets of parameters:

Statistical weight factor, g	$\frac{3}{8}$	$\frac{5}{8}$
Resonance energy, ϵ_0 (ev)	0.08472 ± 0.00027	0.08415 ± 0.00028
Neutron width at energy ϵ_0, Γ_n^0 (ev)	0.03477 ± 0.00021	0.02057 ± 0.00012
Capture width, Γ_a (ev)	0.083303 ± 0.00062	0.09493 ± 0.00071

No evidence for resonances at energies greater than 0.085 ev was observed. The results described are interpreted in terms of recent considerations on the statistics of the properties of nuclear energy levels.

The measurements discussed here were taken in 1954. A preliminary analysis of the data was reported at the International Conference on the Peaceful Uses of Atomic Energy, Geneva, 1955.

[1] Abstract of paper submitted to the *Physical Review*; S. Bernstein acted as "editor" and contributor in the preparation of the manuscript. This procedure seemed desirable because those who took the neutron measurements were no longer at ORNL at the time of writing. The authors listed are grateful to him for his counsel and assistance.

[2] Now at Lockheed Aircraft Corp., Marietta, Ga.

[3] Now at Argonne National Laboratory, Lemont, Ill.

[4] Now at American Machine and Foundry Co., Greenwich, Conn.

[5] Chemistry Division.

FAST-CHOPPER TIME-OF-FLIGHT NEUTRON SPECTROMETER

R. C. Block G. G. Slaughter J. A. Harvey

The M1 high-intensity fast chopper installed at the LITR[1] has been used to measure both thermal energy and resonance energy total cross sections. The M2 high-resolution rotor, recently installed at the ORR, has also been used to make thermal energy cross-section measurements on the fissionable uranium isotopes.

This new M2 equipment consists of an 18-in.-diameter rotor fabricated from age-hardened K Monel. The rotor slit system consists of 18 slits parallel to each other. Each slit is 0.045 in. wide at the center of the rotor and is tapered to 0.015 in. at the periphery. At present this equipment can be operated with flight paths of 11 or 45 m. A 2048-channel time analyzer has also been recently received from the Instrumentation and Controls Division and has been used in the U^{233} and U^{235} measurements.

THERMAL CROSS-SECTION MEASUREMENTS OF I^{129}, U^{233}, U^{234}, U^{235}, AND Pu^{240}

Total neutron cross-section measurements were made in the thermal energy region on samples of I^{129}, U^{233}, U^{234}, U^{235}, and Pu^{240}. The I^{129}, U^{234}, and Pu^{240} measurements were carried out at the LITR with the M1 rotor and associated equipment. The M2 equipment installed at the ORR was

[1] G. G. Slaughter, R. C. Block, and J. A. Harvey, *Phys. Semiann. Prog. Rep. March 10, 1958*, ORNL-2501, p 26.

used to make the U^{233} and U^{235} measurements. The I^{129} sample was prepared by G. W. Parker of the Chemistry Division in the form of PbI_2, and the U^{234} and Pu^{240} samples were prepared in the oxide form by J. Halperin and J. Oliver of the Chemistry Division. Since these nuclides were available only in small quantities, the chopper neutron beam was collimated so that less than 6% of the available beam was utilized. The U^{233} and U^{235} samples were prepared as rolled and electropolished metallic foils of very uniform thickness by J. H. Erwin of the Metallurgy Division. Almost all of the chopper beam was utilized in these uranium measurements to average over any small fluctuations in the foil thicknesses.

The results of these measurements are summarized in Table 1. The I^{129}, U^{234}, and Pu^{240} data were fitted by the least-squares method over the energy range from ~0.02 to 0.03 ev to the following expression:

$$\log \sigma_T = a_0 + a_1 \log E \ ,$$

where σ_T is the total cross section, E is the neutron energy, and a_0 and a_1 are the fitted coefficients. From this equation the 2200-m/sec cross section was computed; these results are listed in column 4. For the U^{233} and U^{235} measurements the above equation was modified to

$$\log (\sigma_T - \sigma_S) = a_0 + a_1 \log E$$

to take into account the essentially constant scattering cross section σ_S. When more than one sample thickness was measured, the mean value of all of the measured 2200-m/sec cross sections was listed (column 5).

The absorption cross section is obtained by subtracting the scattering cross section from the total cross section. By use of the scattering cross sections listed in column 6, the absorption cross sections have been computed (column 7). It is to be noted that the Pu^{240} scattering cross section is only ~2 barns. This low scattering cross section is the result of the destructive interference between

Table 1. Thermal-Energy Cross Sections

Nuclide	Isotopic Enrichment (%)	Sample Thickness (atoms/cm^2)	σ_T(2200 m/sec) (barns)	$\langle\sigma_T(2200\ m/sec)\rangle$ (barns)	σ_S (2200 m/sec)	σ_{abs}(2200 m/sec) $= \sigma_T - \sigma_S$ (barns)
		$\times 10^{21}$				
I^{129}	68.0	9.66	36 ± 4		4 ± 1[a]	32 ± 5
U^{233}	99.76	1.195	587 ± 6	588 ± 5	12.5 ± 0.5[b]	576 ± 5
		1.557	590 ± 6			
		3.07	586 ± 6			
U^{234}	96.88	3.11	123 ± 3		10 ± 3[a]	113 ± 5
U^{235}	93.19	1.405	695 ± 7	691 ± 6	15.0 ± 0.5[c]	676 ± 6
		2.90	687 ± 7			
Pu^{240}	92.19	2.377	290 ± 8		~2[d]	288 ± 8

[a] D. J. Hughes and R. B. Schwartz, *Neutron Cross Sections*, BNL-325, 2d ed. (July 1, 1958).

[b] S. Oleksa, *Phys. Rev.* 109, 1645 (1958).

[c] H. L. Foote, Jr., *Phys. Rev.* 109, 1641 (1958).

[d] Based on an estimated potential cross section of ~10 barns and the destructive interference from the 1.055-ev level. The 1.055-ev resonance parameters were obtained from BNL-325, 2d ed.

the potential scattering and the resonance scattering from the 1.055-ev level.

The I^{129} absorption cross section is somewhat higher than the 27 ± 3 barns reported by Chalk River,[2] but both of these values agree within experimental error. The U^{234} total cross section agrees excellently with the Harwell chopper measurements,[3] although the absorption cross section reported here is larger than the 97 ± 5 barn value quoted in BNL-325.[4] The Pu^{240} absorption cross section is in good agreement with the 295 ± 20 barns quoted in BNL-325. Both the U^{233} and U^{235} absorption cross sections are lower than the 585 ± 10 and the 689 ± 7 barn absorption cross sections, respectively, reported in BNL-325 as the "U.S. values." However, these values do agree within experimental error, although it is possible that there are slight systematic effects in our data. Further measurements are being performed to improve the statistical accuracy of the data and to carefully check for any possible systematic effects in the measurements.

RESONANCE PARAMETERS OF Am^{241}

The total cross section of Am^{241} (470-year half life; $I = 5/2$) was measured in the energy range from 0.2 to 45 ev, by using two AmF_3 solid samples and two $Am(NO_3)_3$ liquid samples. These samples were prepared by A. Chetham-Strode of the Chemistry Division and F. N. Case and J. H. Paehler of the Isotopes Division. The thicknesses ranged from 7.87×10^{19} to 1.92×10^{21} atoms/cm^2. The measured total cross section is shown in Fig. 1. The energy resolution was about 1½% over the energy range shown. The data up to 17 ev have been analyzed to give the resonance parameters listed in Table 2. An additional 19 resonances were observed from 17 to 32 ev. From these data were obtained a strength function per spin state ($\overline{\Gamma_n^0}/D$) of $(1.8 \pm 0.5) \times 10^{-4}$ and an average level spacing per spin state (D) of 1.3 ± 0.2 ev up to an energy of 12 ev. For the resonances at 0.306, 0.575, and 1.275 ev the resolution was sufficiently good to permit the determination of the natural widths. The values of Γ_γ inferred from the natural widths of these resonances are 0.036 ± 0.004, 0.034 ± 0.003, and 0.039 ± 0.006 ev, respectively.

[2] J. C. Ray and L. P. Ray, *Progress Report Oct. 1, 1957 to Dec. 31, 1957*, PR-CM-12, p 12.

[3] G. J. McCallum, *J. Nuclear Eng.* 6, 181 (1958).

[4] D. J. Hughes and R. B. Schwartz, *Neutron Cross Sections*, BNL-325, 2d ed. (July 1, 1958).

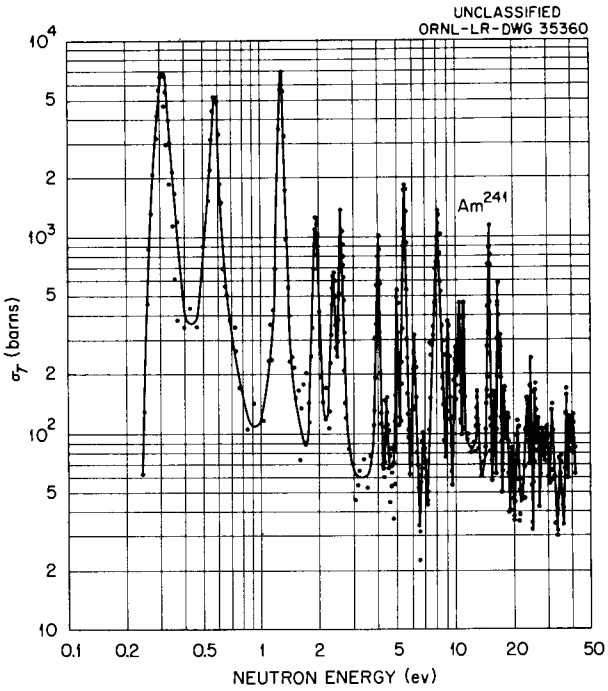

Fig. 1. Total Neutron Cross Section of Am^{241}.

Table 2. Resonance Parameters of Am^{241}

E_0 (ev)	$2g\Gamma_n$ (10^{-3} ev)
0.306	0.060 ± 0.003
0.575	0.075 ± 0.007
1.275	0.39 ± 0.02
1.93	0.125 ± 0.006
2.375	0.080 ± 0.010
2.60	0.20 ± 0.02
3.99	0.26 ± 0.02
4.40	0.027 ± 0.06
5.00	0.21 ± 0.02
5.44	1.3 ± 0.2
6.14	0.23 ± 0.03
6.78	0.059 ± 0.015
8.10	5.0 ± 2.0
9.14	0.80 ± 0.12
9.90	0.71 ± 0.11
10.4	0.7 ± 0.2
11.05	0.65 ± 0.06
12.9	0.24 ± 0.05
14.8	3.5 ± 0.4
15.8	0.40 ± 0.12
16.5	1.8 ± 0.3
17.0	0.7 ± 0.2

These values are not incompatible with the assumption that Γ_γ remains constant from resonance to resonance.

The data previously published[5] concerning the total cross section of Am^{241} indicate resonances at 0.3, 0.53, 0.58, 1.26, and 1.9 ev, with groups at 2.4, 4.0, 5.5, 10.0, and 17.0 ev. The present work does not verify the splitting of the level at 0.575 ev but resolves 18 resonances in the five groups reported in the previous work.

LEVEL SPACING OF ODD-ODD HEAVY NUCLEI

A vast amount of data on the resonances observed in low-energy neutron cross-section measurements has been obtained in the past few years. However, without the use of enriched isotopes it had not been possible to identify with certainty more than one resonance in any heavy odd-odd target nucleus. Since odd-odd target nuclei in general have large thermal-neutron absorption cross sections, which indicate a resonance close to thermal energy, one would expect a small spacing between resonances in these nuclides.

Recently, enriched odd-odd isotopes of lutetium (600 mg enriched to 70.2% in Lu^{176}), tantalum (540 mg enriched to 0.25% Ta^{180}), and lanthanum (359 mg enriched to 0.59% La^{138}) have become available from the Isotopes Division. Transmission measurements on the Lu^{176} sample up to 75 ev, on the Ta^{180} sample up to 11 ev, and on the La^{138} sample up to 5 ev were made by using only one slit of the spectrometer. Total-cross-section measurements were first made on very thick samples of natural tantalum and lanthanum to higher energies than those listed above, since thicker samples of the low-abundant isotope can be obtained by using the natural element, and all 15 slits of the spectrometer could be used. If small resonances were found in these natural-element samples, the enriched samples were then measured in order to assign the resonances to the appropriate isotope. The transmission of an enriched sample of Lu^{175} (99.94%) was also measured up to 140 ev as a further check on the assignment of the lutetium resonances.

In addition to the resonance at 0.43 ev previously assigned to Ta^{180}, two new resonances at 2.07 and 5.96 ev were observed. The neutron widths of these two levels were found to be 0.00063 ± 0.00010 and 0.0031 ± 0.0005 ev, respectively. The resonance at 0.433 ev has a neutron width of 0.00070 ± 0.00007 ev and a radiation width of 0.030 ± 0.003 ev. The parameters for this resonance are in good agreement with those determined by Evans *et al.*,[6] who used a natural tantalum sample.

Transmission measurements of thick samples of lanthanum revealed three previously unobserved resonances at 0.752, 3.06, and 21.3 ev. From measurements with the La^{138} sample the 3.06-ev resonance was assigned to La^{138}, which has a Γ_n of 0.0013 ± 0.0002 ev. The 0.752-ev resonance was not observed in the transmission measurements on the La^{138} sample. It is tentatively assigned to La^{139} since there is no resonance known at this energy in any other nuclide. When assigned to La^{139}, this resonance has a Γ_n of only 8×10^{-8} ev and, hence, is probably not an *S*-wave resonance. The radiation width of this 0.752-ev resonance is only 0.055 ± 0.010 ev, which is considerably smaller than the value of 0.15 ± 0.03 ev (ref 7) for the 73-ev resonance in La^{139}.

The transmission measurements on the lutetium isotopes were analyzed to give the parameters of the resonances. The parameters of the resonances in Lu^{175} and Lu^{176} based on a Γ_γ of 0.060 ev are given in Table 3. An additional 11 resonances were observed in Lu^{175} up to 140 ev, and an additional seven in Lu^{176} up to 75 ev. From the parameters given in the table, the level spacings per spin state, D, are 7.1 ± 1.5 and 4.8 ± 0.8 ev, and the strength functions, $\overline{\Gamma_n^0}/D$, are $(2.4 \pm 0.8) \times 10^{-4}$ and $(1.7 \pm 0.5) \times 10^{-4}$, respectively, for Lu^{175} and Lu^{176}.

The strength functions of these two nuclides are of considerable interest since the two nuclides have very large distortions (quadrupole moments of 5.7×10^{-24} and 8.0×10^{-24} cm^2). The calculated value of the strength function for the distorted nucleus[8] is 1.8×10^{-4} and for the spherical nucleus with a diffuse edge[8] is 4.0×10^{-4}. Hence the experimental values are in good agreement with the value for the distorted nuclear model and are a factor of 2 lower than the value for the spherical diffuse-edge nuclear model.

---

[5] Y. B. Adamchuk *et al.*, *Proc. Intern. Conf. Peaceful Uses Atomic Energy, Geneva, 1955* **4**, 216 (1956).

[6] J. E. Evans, E. G. Joki, and R. R. Smith, *Phys. Rev.* 97, 565 (1955).

[7] A. Stolovy and J. A. Harvey, *Phys. Rev.* **108**, 353 (1957).

[8] D. M. Chase, L. Wilets, and A. R. Edmunds, *Phys. Rev.* 110, 1080 (1958).

Table 3. Resonance Parameters

Lu^{175}		Lu^{176}	
E_0 (ev)	$2g\Gamma_n$ (10^{-3} ev)	E_0 (ev)	$2g\Gamma_n$ (10^{-3}ev)
2.61	0.22 ± 0.02	1.57	0.40 ± 0.06
4.79	0.39 ± 0.05	4.35	0.48 ± 0.04
5.24	1.8 ± 0.2	6.13	1.46 ± 0.14
11.3	3.1 ± 0.3	9.77	1.47 ± 0.13
14.1	22 ± 2	10.8	1.5 ± 0.4
15.4	2.1 ± 0.2	11.5	0.6 ± 0.4
20.6	2.1 ± 0.4	11.9	3.8 ± 1.1
23.6	8.0 ± 1.2	19.1	0.12 ± 0.05
28.15	2.1 ± 0.5	19.9	0.30 ± 0.10
30.28	15 ± 2	21.9	1.6 ± 0.2
31.54	1.6 ± 0.8	24.6	4.5 ± 0.4
36.8	7.5 ± 1.5	27.2	11 ± 3
41.0	35 ± 7	29.8	12 ± 3
49.8	8 ± 2	32.0	7 ± 2
50.9	6 ± 2	33.6	3.7 ± 1.3
57.4	3.4 ± 0.7	37.0	7.9 ± 1.0
		38.9	0.8 ± 0.5
		42.4	16 ± 3
		45.2	3 ± 2
		46.7	5.8 ± 1.2

The average level spacing of the Lu^{176} nuclide is interesting since the target nuclide has the largest measured spin ($I \sim 7$); hence S-wave resonances correspond to excited levels in Lu^{177} of spins, J, of $13/2$ and $15/2$ ($J = I \pm 1/2$). It has generally been accepted by theoretical physicists[9–15] that the level density at high excitation is proportional to $2J + 1$ for low spin values and that there would be deviations for higher spins. This attenuation factor is written in the form

$$D(J) \propto (2J + 1)^{-1} e^{(J+1/2)^2/2\sigma^2} ,$$

and the $2J + 1$ law is obtained on the assumption that $(J + 1/2)^2/2\sigma^2 << 1$. Lang and LeCouteur[11] and Ericson[13] have estimated the cutoff, $J_{critical} \sim (2\sigma^2)^{1/2}$, to be about 6 or 7 for $A \sim 240$; however, there have been no previous experimental data for heavy nuclides so that this estimate could be checked. Since the spin of Lu^{175} is only $7/2$, we can compare the experimental values for the average level spacings of Lu^{175} and Lu^{176} with those predicted from theory without this exponential factor, which increases the spacings of the high spin states. The level spacings of these two nuclides cannot be compared directly since the effective excitation energies[12] of the two compound nuclei are not the same but differ by about 1 Mev due to the odd-even effect. The formulas given by Cameron[15] predict a ratio of average level spacings of Lu^{175} to Lu^{176} of 5.4. Using an experimental ratio of average spacings of 1.5 gives a value for $\sqrt{2\sigma^2}$ of $4\frac{1}{2}$. Since there is some uncertainty in the effective excitation energies, this value of $\sqrt{2\sigma^2}$ is probably good to only ±2.

[9] H. Bethe, *Revs. Modern Phys.* 9, 69 (1937).

[10] C. Bloch, *Phys. Rev.* 93, 1094 (1954).

[11] J. M. B. Lang and K. J. LeCouteur, *Proc. Phys. Soc. (London)* A67, 585 (1954).

[12] T. D. Newton, *Can. J. Phys.* 34, 804 (1956).

[13] T. Ericson, *Nuclear Phys.* 6, 62 (1958).

[14] N. Rosenzweig *et al.*, *Proc. Second U.N. Intern. Conf. Peaceful Uses Atomic Energy, Geneva, 1958*, A/Conf. 15/p/693, United Nations, 1958.

[15] A. G. W. Cameron, *Nuclear Level Spacings*, PD-292 (Oct. 1957).

FUNDAMENTAL-MODE NEUTRON DISTRIBUTION IN PULSED COMPOSITE SYSTEMS

E. C. Campbell

The simple asymptotic solution of the time-dependent neutron diffusion problem in a finite convex homogeneous nonmultiplying medium excited by a pulsed neutron source defines a fundamental-mode neutron density distribution $n(\vec{r})e^{-\lambda t}$ which is characterized by a geometrical buckling

$$B^2 = -\frac{\nabla^2 n}{n} \tag{1}$$

and a decay rate

$$\lambda = v\Sigma_a + DB^2 \ . \tag{2}$$

For a system made up of two or more contiguous regions containing material with different absorption cross section Σ_a and diffusion constant D, the fundamental mode cannot be so characterized. However, the neutron distributions in the various regions behave somewhat like coupled relaxation oscillators in that asymptotically they all decay at the same rate. The coupling between regions is determined by the internal boundary conditions. For each region, then, the sum of leakage and absorption rates is the same and equal to the common decay constant. In each region the flux shape is characterized by a *local* buckling which can be determined experimentally by evaluating Eq. (1) and which satisfies Eq. (2). In a heavily absorbing region the fundamental-mode flux distribution may be characterized by a local buckling $B^2 < 0$, corresponding to a negative leakage (in-flow) and a concave flux shape. In a two-region system bounded by concentric spheres it is of interest to consider the case in which the absorption of the central region is so adjusted to make its local buckling zero. For this case the fundamental-mode flux distribution in the central region is flat, and the decay constant of the system is equal to that of an infinite block of the material in the central region.

In the case that one of the regions of the system is a void which has dimensions large compared with a mean free path, the diffusion approximation is no longer valid and transport theory must be used to describe neutrons in the cavity. Here we may consider that the coupling between the neutrons at opposite sides, say, of the cavity, involves a retardation associated with the free flight of neutrons across the cavity. For simplicity consider a spherical shell of material characterized by Σ_a and D enclosing a void. Inside the cavity the fundamental-mode angular density $\psi(r,\mu,t)$ must satisfy the spherically symmetric time-dependent transport equation

$$-\frac{1}{v}\frac{\partial\psi}{\partial t} = \mu\frac{\partial\psi}{\partial r} + \frac{1-\mu^2}{r}\frac{\partial\psi}{\partial\mu} \ ,$$

which has a solution

$$\psi(r,\mu,t) = e^{-\lambda t}\, e^{r\mu\lambda/v} \ .$$

The neutron density

$$n(r,t) = \int_{-1}^{+1} \psi(r,\mu,t)\, d\mu = 2\,\frac{\sinh r\lambda/v}{r\lambda/v}\, e^{-\lambda t}$$

has a minimum at the center. The decay constant λ is determined by satisfying the (velocity-dependent) internal and external boundary conditions. The dependence of $n(r)$ on the neutron speed v implies that the neutron spectrum is not independent of position inside the cavity, since the depression at the center for low-energy thermal neutrons is relatively greater than for higher-energy neutrons. Attempts to measure the spectrum inside a cavity during a fundamental-mode decay may not be valid unless corrected for these transport effects.

These considerations arose from an attempt to understand the slowly decaying thermal-neutron room background in connection with experiments utilizing a pulsed neutron source.

As is well known, these results are exactly equivalent to those derived from a time-independent solution for a system having a fictitious added negative absorption cross section $-\lambda/v$.

Some of the preliminary considerations on these problems were made during a one-year assignment (1957–1958) at the Centre d'Etude de l'Energie Nucléaire, Mol, Belgium.

ATOMIC-BEAM SPECTROSCOPY

J. E. Sherwood S. J. Ovenshine

During the past year the nuclear spins of I^{130} and I^{132} have been measured by means of the atomic-beam magnetic-resonance technique. A paper covering our work[1] on I^{128} (measured before this report period) and I^{130} has been submitted for publication in the *Physical Review*. The abstract follows:

The nuclear spins of I^{128} and I^{130} have been measured by means of an atomic-beam magnetic-resonance apparatus. A value of 1 was obtained for I^{128}, as predicted by Benczer *et al.* [*Phys. Rev.* **101**, 1027 (1956)]. However, a value of 5 was obtained for I^{130}, in disagreement with the expectations of Caird and Mitchell [*Phys. Rev.* 94, 412 (1954)]. The nature of the discrepancy is indicated.

The apparatus and technique are described, with special attention to the source and detector arrangements.

Recently, the nuclear spin of 2.3-hr I^{132} has been measured. Inasmuch as the apparatus and method were the same as those described,[1] only the method of preparation and results will be dealt with here.

A strip of uranium-aluminum alloy containing 200 mg of U^{235} was bonded to aluminum and hermetically sealed. The sample was then exposed to a flux of 10^{14} neutrons·cm^{-2}·sec^{-1} for ten days in the ORR. Three days after removal, the sample was placed in a quartz tube along with 400 mg of NaI (to provide a carrier of stable I_2). By alternately allowing air to enter the tube (at red heat) and evacuating through a cold trap, good iodine recovery was obtained. Because of the three-day delay, only stable I^{127}, 8-day I^{131}, and 2.3-hr I^{132} were obtained, the latter being present as a daughter of 77-hr Te^{132}.

This mixture of elemental iodines was then introduced into the atomic-beam magnetic-resonance apparatus and examined in the manner described.[1] The scintillation counter detector was adjusted so that it would not count the 8-day I^{131}.

Because of the very large amounts of activity in the machine, it was decided to shorten the experiment by making spot checks for the various possible spin values instead of sweeping a frequency range. This procedure was possible in view of considerable experience with I^{128} in the machine in its present condition; that is, the r-f power level and frequency required for each spin were known with sufficient accuracy. Five-minute depositions and counts were used. Table 1 gives the observed counting rate and corresponding frequency for each point, in the order carried out in the experiment.

The data show a variation in counting rate with time which corresponds to expected buildup and pump-out of activity in the detector chamber, plus two outstanding counting rates, both of which correspond to spin 4, which is therefore taken to be the spin of 2.3-hr I^{132}.

A ground-state spin of 4 is quite consistent with the observed[2] decay of this isotope. According to the rotational model, the second excited level of the Xe^{132} daughter is very possibly a 4^+ level. For this to be beta-populated, as observed, from the I^{132} ground state of spin 4^- (assuming a parity change), one would expect a log *ft* value between 6 and 10. The value corresponding to the data of Finston and Bernstein[2] is 7.5.

Experiments are in progress to determine the spins of 21-hr I^{133} and 7-hr I^{135}. These isotopes are to be prepared in a manner similar to that for I^{132}.

The authors wish to express their indebtedness to G. W. Parker of the Chemistry Division for his generous cooperation in the preparation of I^{132}.

Table 1. Counting Rate vs Frequency

Spin	Frequency (Mc)	Counts
–	Off	2610
6	8.2	3235
5	9.4	3161
4	11.1	4382
3	13.6	3487
2	17.5	3477
1	24.5	3479
2	17.5	3596
3	13.6	3528
4	11.1	3847*
5	9.4	3026
6	8.2	2411

*Ran out of sample during this deposition.

[1] Described in somewhat greater detail in *Phys. Semiann. Prog. Rep. Sept. 20, 1958*, ORNL-2610, p 36.

[2] H. L. Finston and W. Bernstein, *Phys. Rev.* 96, 71 (1954).

DISSOCIATION OF C_6H_5T FOLLOWING BETA DECAY[1]

T. A. Carlson[2] F. Pleasonton A. H. Snell[3]

The relative abundance of the various charged fragments formed following beta decay of monotritiated benzene was measured with a specially designed mass spectrometer. In nearly every case the C–He bond was ruptured, the charge remaining with $C_6H_5^+$. In 28% of the events the $C_6H_5^+$ species were further excited to produce more than 30 different charged fragments. In order to determine the energy required to give rise to this spectrum, a critical evaluation of the Rosenstock[4] theory of decomposition is made and a discussion of some of the modes of decomposition of benzene is given. Calculations are finally made by the use of a semiempirical unimolecular decomposition model which indicates that in 68% of the β^- decays the parent fragment, $C_6H_5^+$, received little or no excitation but that in the remaining events it received from 0 to 39 ev of energy with a distribution of equal probability. The molecular excitation of benzene following beta decay is then shown to result probably from a sudden electronic perturbation following the formation of the doubly charged helium nucleus. The results are compared with those of other tritiated hydrocarbons and found to be in essential agreement.

Some results on the dependence of the collection efficiency of a given ion on its kinetic energy are also discussed.

[1]Abstract of paper to be submitted to the *Journal of Chemical Physics*.

[2]On loan from Chemistry Division.

[3]Director's Division.

[4]H. M. Rosenstock, *Proc. Natl. Acad. Sci. U.S.* 38, 667 (1952).

EXTENSION OF THE ATOMIC ENERGY LEVEL CLASSIFICATION SCHEME FOR SINGLY IONIZED DYSPROSIUM (Dy II)

J. R. McNally, Jr.

Zeeman data of Blank[1] and wavelength data of Gatterer and Junkes[2] on the spectra of dysprosium have been used with IBM-605 calculated wave numbers[3] on the Edlén[4] scale to couple two of the energy-level doublets reported by Paulson[5] and Blank[1]. The results are given in Table 1.

Table 1. Present Status of Low Energy Levels in Dy II for the Configuration $4f^{10}\cdot 6s$

Term	J	Level Value	g_{obs}
^6I	8 1/2	0.00	1.291
^4I	7 1/2	828.31	1.197
^6I	7 1/2	4341.00	1.220
^4I	6 1/2	4755.56	1.121
^6I	6 1/2		
^4I	5 1/2		
^6I	5 1/2	A	0.986
^4I	4 1/2	A – 438.90	0.820
^6I	4 1/2	B	0.739
^4I	3 1/2	B – 846.95	0.451

[1]J. M. Blank, *Zeeman Effect Data and Classification of the First Spark Spectrum of Dysprosium*, MIT Thesis, Cambridge, Mass. (1952).

[2]A. Gatterer and J. Junkes, *Spektren der seltenen Erden*, Specola vaticana, Castel Gandolfo, Città del Vaticano, Italia.

[3]I am indebted to the Y-12 IBM group for these data and especially to J. A. Gillcrist for setting up the necessary routines.

[4]B. Edlén, *J. Opt. Soc. Am.* 43, 339 (1953).

[5]E. Paulson, *Astrophys. J.* 40, 298 (1914).

INFRARED SPECTRA OF SOLID AMMONIA AND SOLID PHOSPHINE

P. A. Staats H. W. Morgan

The existence of two noncubic, crystalline, metastable phases in solid NH_3 has been recently demonstrated by the x-ray diffraction studies of Mauer and McMurdie.[1] These previously unreported phases were obtained when thin films of NH_3 were deposited from the gas phase upon a surface maintained at 77°K. The percentages of the two phases varied with the rate of deposition, the x-ray pattern of the second metastable phase being observed at very slow rates. These observations are of particular significance for the study of low-temperature-solid infrared spectra, since deposition of films is a common technique in preparing samples.

The infrared spectra of NH_3 and ND_3 deposited at 77°K were reported by Reding and Hornig,[2] and interpreted on the assumption of a cubic structure. The selection rules for vibrations in molecular crystals are known,[3] and the reported spectra were not in good agreement with that predicted for cubic symmetry.

In a detailed study of the spectra of solid PH_3, PH_2D, PHD_2, and PD_3, two solid modifications have been observed with a phase transition at about 88°K, in agreement with the heat capacity measurements of Clusius and Frank.[4] These two phases, together with the gas phase spectrum of PH_3, are shown in Fig. 1. Phase (I), above the 88°K transition, was reported by x-ray studies to be cubic;[5] however, its spectrum cannot readily be explained in terms of cubic symmetry, and differs considerably from the reported NH_3 spectra. Because of this disagreement and the recent x-ray evidence of metastable phases, the infrared spectra of ammonia were re-examined.

We have studied the spectra of thin films of solid NH_3 and ND_3 as a function of temperature and of the rate of deposition. Data were taken with a Perkin-Elmer model 21 spectrophotometer, equipped with LiF, NaCl, and CsBr prisms. The low-temperature cell was of conventional design, with liquid N_2, Ar, CH_4, and C_2H_4 used as refrigerants to obtain temperatures of 77, 87, 112, and 169°K. Pentene-1, cooled by liquid nitrogen, was used to obtain intermediate temperatures down to its melting point of 108°K. Studies of the solid phosphine spectra near the transition temperature of 88.5°K indicated that the absorbing solid films, illuminated by the infrared source, were at temperatures not more than 5°K above that of the coolant.

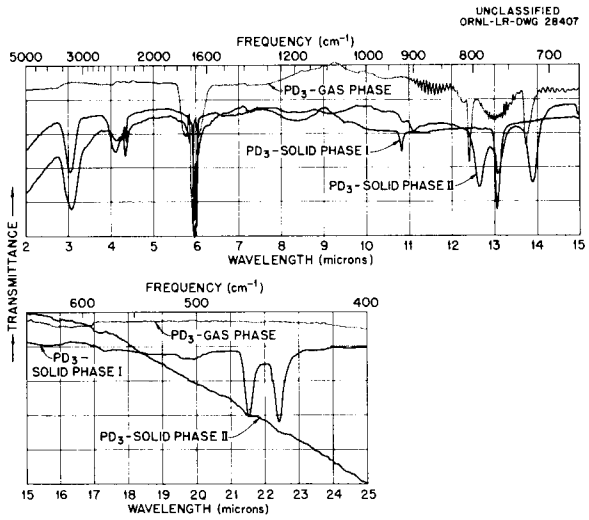

Fig. 1. Infrared Spectra of Phosphine in Gaseous and Solid States.

The spectra of films of ammonia deposited at 77°K were similar to those previously reported.[2] When the films were warmed to 150°K or if they were deposited at about 150°K, a new and previously unreported spectrum was observed. This spectrum persisted, with minor changes, upon cooling of the film to 77°K. It is believed that this spectrum, shown in Fig. 2 for NH_3 at NaCl resolution, arises from the stable modification of the solid, which has been shown by x-ray studies to be cubic.[6,7] Preliminary study has shown that the principal features of the

[1] F. A. Mauer and H. F. McMurdie, private communication.

[2] F. P. Reding and D. F. Hornig, *J. Chem. Phys.* 19, 594 (1951).

[3] H. Winston and R. S. Halford, *J. Chem. Phys.* 17, 607 (1949).

[4] K. Clusius and A. Frank, *Z. physik. Chem.* B34, 405 (1936).

[5] G. Natta and E. Casazza, *Gazz. chim. ital.* 60, 851 (1930).

[6] J. de Smedt, *Bull. classe sci., Acad. roy. Belg.* 11, 655 (1925).

[7] H. Mark and E. Pohland, *Z. Krist.* 61, 532 (1925).

spectrum are in excellent agreement with the selection rules for cubic symmetry.

A metastable phase (I), which transforms to the cubic phase in the range 125 to 135°K, has been observed by the slow deposition of NH_3 upon a window held at 112°K. The spectrum of this phase is shown also in Fig. 2. This spectrum persists upon cooling of the film to 77°K.

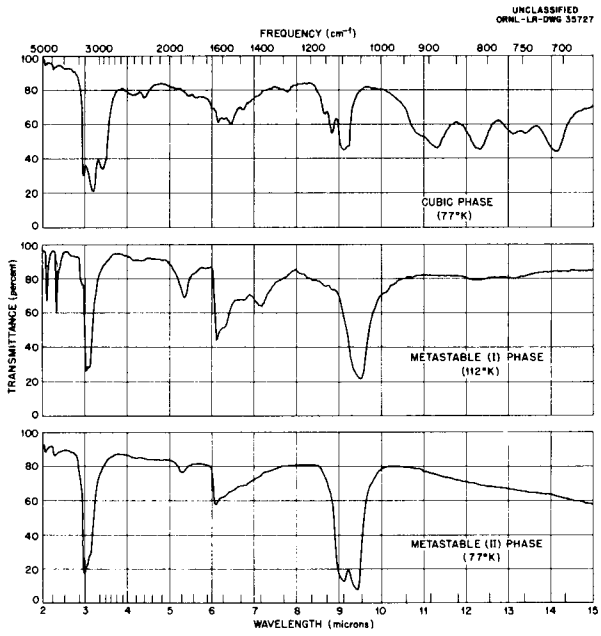

Fig. 2. Infrared Spectra of Solid NH_3.

The second metastable phase (II) has been obtained by the slow deposition of films upon a window at 77°K, from a reservoir maintained near 160°K. Under these conditions the spectrum always shows a small varying percentage of (I). Warming of the film to 112°K causes this metastable phase (II) to transform completely to the metastable phase (I). Figure 2 shows a spectrum obtained from metastable phase (II), in which the content of (I) is believed to be less than 10%. The spectra show that the slow deposition of additional solid ammonia upon a previously deposited film of the cubic phase held at 77°K produces a layer of metastable phase (II), indicating that the nature of the cold surface does not determine the phase deposited.

The spectra of solid ammonia previously reported by Reding and Hornig[2] have been determined to represent a mixture of metastable phases (I) and (II), with phase (II) predominating. A study of the spectra of NH_3, NH_2D, NHD_2, and ND_3 in the cubic and in the metastable phases (I) and (II) is being made in an attempt to correlate the features of these spectra with the intermolecular forces in the different crystal structures.

PRELIMINARY CLASSIFICATION OF THE SINGLY IONIZED PLUTONIUM ATOM (Pu II)[1]

J. R. McNally, Jr. P. M. Griffin

A preliminary energy-level scheme for Pu II has been established based on 125 Zeeman patterns obtained with an echelle-Littrow spectrograph and a magnetic field of approximately 24,000 oersteds. The low electronic configuration involves the $^{6,8}F$ terms from $5f^6 7s$. Seven low even levels and 84 high odd levels are given.

[1]Abstract of published paper: *J. Opt. Soc. Am.* **49**, 162 (1959).

APPLICATION OF A DIGITAL COMPUTER TO THE ZEEMAN METHOD IN ATOMIC SPECTROSCOPY[1]

K. L. Vander Sluis

The existence of high-speed computers with their large-capacity memories makes feasible the concept of generating complete sets of derived data in the problem of spectrum classification. This possibility leads to a closer examination of the relative merits of the three types of generating operations as judged according to the probability of generating real data and according to the generated statistical noise level. This examination shows that the treatment of the observed data in terms of the concept of Zeeman tags is by far the most fruitful approach to be taken. A quantitative evaluation of the derived data is also given.

A specific set of computer routines designed to do both the computational and bookkeeping operations of the Zeeman method on the Oracle is described.

[1]Abstract of paper to be submitted to the *Journal of the Optical Society of America.*

ANTIFERROMAGNETISM IN $CrCl_3$ AND $FeCl_3$

J. W. Cable M. K. Wilkinson E. O. Wollan

The neutron diffraction measurements made on polycrystalline samples of $CrCl_3$ and $FeCl_3$ were reported previously.[1] These compounds, which have similar hexagonal layer type structures, both become antiferromagnetic below 17°K. For $CrCl_3$ a structure consisting of ferromagnetically aligned moments within the hexagonal layers with a relatively weak antiferromagnetic coupling between the layers was suggested, while a more complex structure involving antiferromagnetic coupling within the hexagonal layers was indicated for $FeCl_3$. In neither case were the data sufficient for a unique structure determination. The investigation has now been extended to single-crystal samples of these two compounds.

$CrCl_3$

The single $CrCl_3$ crystals were grown from the gas phase by sublimation of the anhydrous material in a vacuum at 950°C. The crystals obtained were in the form of thin sheets of only a few mils thickness but as large as 1 in. in diameter. As would be expected from the two-dimensional nature of the chemical bonding, the thin sheets lie parallel to the hexagonal layers of the crystal. A specimen was selected with dimensions $\frac{1}{4} \times \frac{1}{2} \times 0.004$ in. and mounted between two 0.020-in. aluminum plates in a cylindrical cell. The cell was suspended in the low-temperature cryostat in such a manner that the hexagonal layers of the crystal were parallel to the incident neutron beam. Neutron diffraction patterns were obtained at temperatures above and below the Néel temperature of 16.8°K, and the results are shown in Fig. 1. In the upper curve, taken at a sample temperature of

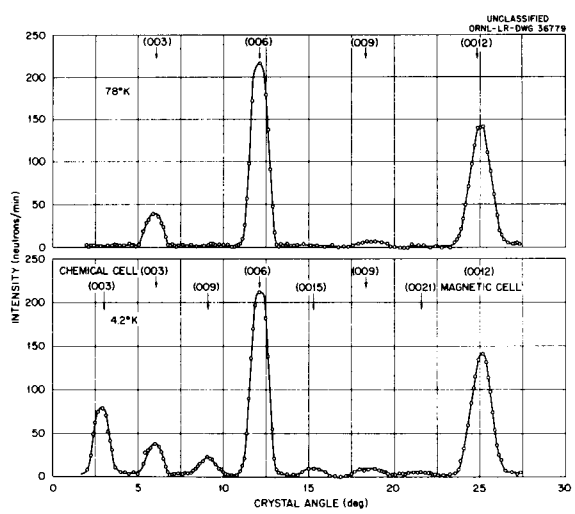

Fig. 1. The (00*l*) Reflections from a Single Crystal of $CrCl_3$.

[1]J. W. Cable, M. K. Wilkinson, and E. O. Wollan, *Phys. Semiann. Prog. Rep. Sept. 20, 1958,* ORNL-2610, p 28.

78°K, the expected (00l) nuclear reflections are observed. At 4.2°K additional (00l) reflections are observed at superlattice positions. These are indexed on the basis of a cell for which the A axis remains the same but the C axis is twice that of the chemical cell and are the reflections expected for the structure suggested by the powder data. Quantitative calculations confirm this structure.

For single crystals the integrated intensity, E_{bkl}, of a Bragg reflection is given by

$$E_{bkl} = \frac{KI_0 \, F^2_{bkl}}{\sin 2\theta} A_{bkl} \ ,$$

in which θ is the Bragg angle and F_{bkl} is the geometrical structure amplitude; KI_0 depends on the instrumental geometry and the particular crystal under observation but for a fixed set of experimental conditions is an instrumental constant which can be determined from the observed nuclear reflections; A_{bkl} is an absorption correction term which for this small crystal is nearly the same for all reflections and is included in the instrumental constant. The geometrical structure amplitude is a function of the positional coordinates of the ions which, in this case, includes an unknown parameter z for the chloride ions. Figure 2 shows a plot of the instrumental constant, KI_0, vs z for the four observed nuclear reflections. The intersection of the curves gives the values of KI_0 and z which satisfy the above relationship for the four reflections. The instrumental constant can then be used in calculating the intensities of the magnetic reflections. For the (00l) magnetic reflections

$$F^2_{00l} = (0.1348 \times 10^{-12})^2 \, f^2 \, q^2_{00l} \mu^2 \ ,$$

in which f is the form factor of the magnetic electrons, μ is the ordered atomic magnetic moment in Bohr magnetons, and $q^2 = \sin^2 \alpha$, where α is the angle between the scattering vector and the axis of magnetization. The intensities of the antiferromagnetic (00l) reflections are given below:

bkl	E_{bkl} Calculated	E_{bkl} Observed
003	710	640
009	195	175
0015	69	68
0021	28	29

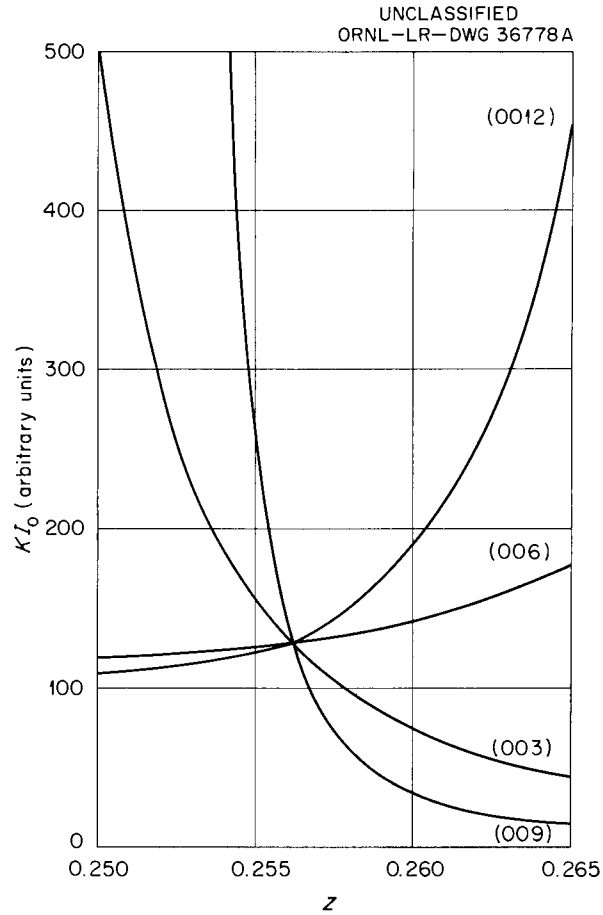

Fig. 2. Determination of the Instrumental Constant and Chlorine Parameter for $CrCl_3$.

The calculated intensities were obtained by using the iron form factor,[2] by using a spin-only value for the moment with $S = 3/2$, and by assuming that the axis of magnetization is perpendicular to the C axis of the crystal. The agreement with the observed intensities is quite satisfactory and confirms the ferromagnetic layer antiferromagnetic structure for $CrCl_3$.

Chromic chloride exhibits the same type of anomalous magnetic behavior as the dichlorides of iron, cobalt, and nickel.[3] The magnetization curve rises rapidly, saturation being attained with an applied field of a few kilo-oersteds. Figure 3 shows the

[2] C. G. Shull and E. O. Wollan, *Solid State Physics*, vol II, p 210, Academic Press, New York, 1956.

[3] For a summary of the magnetic properties of these compounds see: C. Starr, F. Bitter, and A. R. Kaufmann, *Phys. Rev.* 58, 977 (1940).

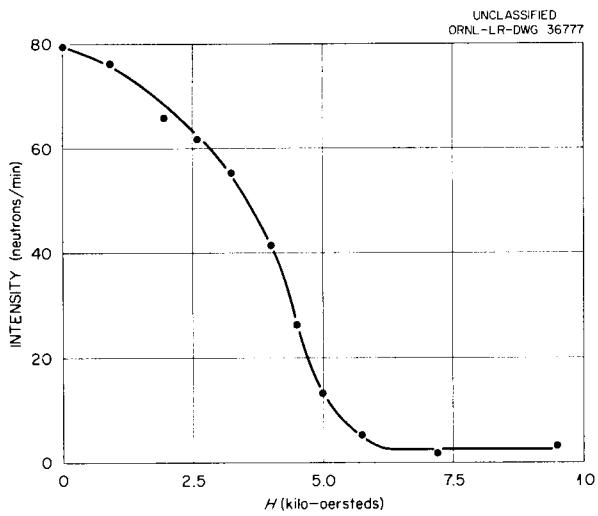

Fig. 3. Variation of the Intensity of the (003) Magnetic Reflection with an Externally Applied Field.

variation of the intensity of the (003) magnetic reflection with an external magnetic field applied parallel to the C axis. This curve fits the expected $\cos^2$ function corresponding to a rotation of the atomic moments and a saturation field of 5.4 kilo-oersteds. (A sharper dependence would be expected if the field were applied perpendicularly to the C axis. In the instrument used the field direction can be displaced from the scattering vector by a maximum of 30°. When the field was applied at 26° to the C axis, saturation was attained at 3.5 kilo-oersteds.) For comparison, no effect was observed in $CoCl_2$ with fields up to 16.5 kilo-oersteds when applied parallel to the C axis, and only a 20% effect was observed with the field applied perpendicular to the C axis.[4] The lower field required for saturation in $CrCl_3$, even though applied along the most difficult direction for obtaining a net magnetization, indicates a smaller anisotropy constant and a weaker antiferromagnetic interaction between the layers.

$FeCl_3$

The $FeCl_3$ single crystal was grown from a melt of the anhydrous material. The sample was cut in the shape of a disk approximately $\frac{1}{4}$ in. in diameter and $\frac{3}{16}$ in. thick with (00l) cleavage planes forming the flat sides of the disk. The specimen was mounted in the low-temperature goniometer, with the C axis of the crystal parallel to the horizontal rotation axis of the goniometer. The nuclear reflections were examined in order to relate the crystal axes to the goniometer settings and to determine the instrumental constant, KI_0. Magnetic reflections were observed at 4.2°K, and all these reflections had either threefold or sixfold symmetry about the C axis, which indicates either a magnetic cell with at least threefold symmetry or a structure domain situation in which the domains grow along the three equivalent hexagonal axes of the chemical cell. Since structure domains have been observed in the structurally similar and isoelectronic manganous halides[5,6] and also because the required hexagonal magnetic unit cell contains 2700 magnetic ions, it was considered more profitable to pursue the structure domain situation.

The most convenient unit cell on which the magnetic reflections can be indexed is monoclinic, with $a = 3A_1$, $b = A_1 + 5A_2$, and $c = 2C$, and contains 180 magnetic ions. The antiferromagnetic structures found in the manganous halides consist of ferromagnetic bands of moments tilted with respect to the hexagonal layers and with alternate bands oppositely aligned. In calculating the geometrical structure amplitudes for the magnetic reflections of such a cell, the relative phases of the magnetic moments at the individual ionic sites are first assigned in one layer of the magnetic cell. This layer is then either repeated or reversed along with a shift in origin in the other layers which make up the unit cell. For the best fit of the experimental data with a model which contains ferromagnetic bands and a single magnetic axis, positive amplitudes were assigned at the following 16 ionic positions in the base plane:

$$[000,\ 0\,\tfrac{1}{3}\,0]\quad \begin{matrix} +(000,\ \tfrac{4}{15}\,\tfrac{3}{15}\,0) \\ \pm(\tfrac{1}{15}\,\tfrac{12}{15}\,0,\ \tfrac{2}{15}\,\tfrac{9}{15}\,0,\ \tfrac{3}{15}\,\tfrac{6}{15}\,0) \end{matrix}$$

Negative amplitudes were assigned at the other 14 positions:

$$[\tfrac{8}{15}\,\tfrac{6}{15}\,0,\ \tfrac{8}{15}\,\tfrac{11}{15}\,0]\quad \begin{matrix} +(000) \\ \pm(\tfrac{1}{15}\,\tfrac{12}{15}\,0,\ \tfrac{2}{15}\,\tfrac{9}{15}\,0,\ \tfrac{3}{15}\,\tfrac{6}{15}\,0) \end{matrix}$$

[4] M. K. Wilkinson *et al.*, *Phys. Rev.* 113, 497 (1959).

[5] E. O. Wollan, W. C. Koehler, and M. K. Wilkinson, *Phys. Rev.* 110, 638 (1958).

[6] M. K. Wilkinson *et al.*, *Phys. Semiann. Prog. Rep. Sept. 10, 1957*, ORNL-2430, p 65.

This layer was then repeated at (000, $0\,\frac{1}{3}\,\frac{1}{3}$, $0\,\frac{2}{3}\,\frac{2}{3}$) and reversed at ($0\,\frac{2}{3}\,\frac{1}{6}$, $0\,\frac{1}{3}\,\frac{5}{6}$, $00\,\frac{1}{2}$) so that the structure amplitude is given by:

$$F_{hkl} = \left(1 - \exp \pi i l + 2 \cos 2\pi \frac{k+l}{3} - 2 \cos 2\pi \frac{4k+l}{6}\right)\left\{\left(1 + \exp 2\pi i \frac{k}{3}\right)\left[\left(1 - \exp 2\pi i \frac{8h+6k}{15}\right)\times\right.\right.$$
$$\left.\left.\times\left(1 + 2\cos 2\pi \frac{h+12k}{15} + 2\cos 2\pi \frac{2h+9k}{15} + 2\cos 2\pi \frac{3h+6k}{15}\right) + \exp 2\pi i \frac{4h+3k}{15}\right]\right\} .$$

The only reflections allowed are those for which $k + l = 3n$ and $4k + l = 6n + 3$, where l is odd and n is any integer. Also,

$$F^2_{hkl} = 0.389 \ , \quad \text{if } l = 6n + 3 \ ,$$
$$F^2_{hkl} = 0.0972 \ , \quad \text{if } l = 6n + 1 \ .$$

In Table 1 are listed the magnetic reflections expected from such a model. The scattering angles in column two are for a wavelength of 1.222 Å, with the lattice constants obtained from the nuclear reflections at 4.2°K. In the third and fourth columns, γ is the angle between the scattering vector and the C axis, while β is the angular position about that axis (relative to a <100> direction in the chemical cell of 79°). The observed values of 2θ, γ, and β agree with these calculated values within experimental error. In the calculated values of the integrated intensities, a spin-only moment and the iron form factor were used, while the axis of magnetization was chosen to give agreement with the observed intensities of the ($10l$) reflections. This axis makes an angle of 35° with the C axis and lies in the (100) plane of the magnetic cell.

A comparison of the calculated and observed intensities shows general agreement, but there are a few rather serious discrepancies. It should be pointed out that the calculations are based on a crystal structure in which one-third of the lattice sites in the metal ion layers are vacant. These vacancies are assumed to occur in the regular manner prescribed by the space group to which the crystal structure has been assigned. Any alteration of this pattern of vacancies in the actual crystal will affect the observed intensities. This was not apparent in the ($00l$), ($h0l$), and (hhl) nuclear reflections from which the instrumental constant was determined, but there were large discrepancies in the intensities of the (hkl) reflections. No satisfactory agreement could be obtained for these reflections by varying only the chlorine parameters. It is possible that the discrepancies in these nuclear intensities and in the magnetic intensities are due to a slight variation of the vacancies in the metal ion lattice sites.

Table 1. Antiferromagnetic Reflections of $FeCl_3$

hkl	2θ*	γ	β	E_{hkl} Calculated**	E_{hkl} Observed
103	7° 26′	33° 58′	68°	11,900	11,800
$\bar{1}03$			248°	11,900	12,500
109	19° 0′	12° 39′	68°	2,340	2,020
$\bar{1}09$			248°	2,340	1,970
1015	31° 24′	7° 50′	68°	870	670
$\bar{1}015$			248°	870	850
$5\bar{3}3$	20° 40′	72° 39′	45°	4,490	3,260
$\bar{5}33$			225°	5,680	4,370
$5\bar{3}9$	27° 11′	46° 52′	45°	870	1,930
$\bar{5}39$			225°	2,950	2,410

Table 1 (continued)

hkl	2θ*	γ	β	E_{hkl} Calculated**	E_{hkl} Observed
$7\bar{3}3$	28° 24′	77° 24′	52°	2,840	2,250
$\bar{7}33$			232°	3,190	3,450
263	21° 34′	73° 23′	116° 30′	5,140	4,070
$\bar{2}\bar{6}3$			296° 30′	3,120	2,810
269	27° 52′	48° 10′	116° 30′	3,160	2,340
$\bar{2}\bar{6}9$			296° 30′	870	1,800
463	27° 44′	77° 6′	103°	3,270	2,730
$\bar{4}\bar{6}3$			283°	2,500	2,560
$2\bar{9}3$	24° 2′	75° 8′	339°	1,840	2,090
$\bar{2}93$			159°	3,850	1,650
$2\bar{9}9$	29° 52′	51° 26′	339°	230	1,550
$\bar{2}99$			159°	2,870	1,150
$4\bar{9}3$	25° 34′	76° 1′	358° 30′	1,880	1,910
$\bar{4}93$			178° 30′	3,520	1,510
$\bar{2}\bar{1}1$	9° 46′	77° 55′	264°	3,700	4,450
215	14° 2′	43° 2′	84°	1,950	1,700
$\bar{2}\bar{1}7$	17° 17′	33° 40′	264°	790	1,170
2111	24° 40′	22° 59′	84°	550	490
151	15° 36′	82° 27′	124°	1,900	1,650
$\bar{1}\bar{5}5$	18° 36′	56° 30′	304°	470	910
157	21° 11′	47° 9′	124°	1,310	870
$\bar{1}\bar{5}11$	27° 35′	35° 28′	304°	100	430

*$\lambda = 1.222$ Å, $A_0 = 5.962$, $C_0 = 17.08$.

**Spin-only moment; iron form factor.

NEUTRON DIFFRACTION INVESTIGATIONS OF THE FERROMAGNETIC ORDERING IN HoN

M. K. Wilkinson H. R. Child E. O. Wollan J. W. Cable

The number of magnetically ordered systems of rare-earth ions which have been investigated is relatively small, and most of these systems have been complicated by crystal distortions or by the presence of other magnetic ions. Since all the rare-earth elements form nitrides which possess the simple NaCl-type structure and consequently permit relatively easy theoretical analyses, it was of interest to investigate the existence of magnetic ordering in these compounds at low temperatures. The first investigation was performed on HoN because of its reasonable cross section and the large atomic magnetic moment which is associated with the Ho^{+++} ion. This report contains the preliminary results of the experiments on this compound.

The sample was prepared[1] from holmium metal with a spectroscopic purity of 99.9%. Since the metal was obtained in a large ingot to reduce oxide impurities, it was first cut into small chunks and then treated with H_2 up to 1000°C in a closed system to form HoH_3. This material was pulverized in a dry box to small pieces, after which the nitride was formed by passing NH_3 over this powder at temperatures up to 1100°C. The product was then heated in a vacuum at 1000°C to remove any remaining hydrogen, after which it was treated again with NH_3. Quantitative chemical analyses have determined that the resulting sample has closely the proper stoichiometry.

Neutron diffraction investigations have been performed on HoN at temperatures from 298 to 1.3°K. At room temperature the nuclear reflections are superimposed on a very high paramagnetic diffuse scattering as shown in Fig. 1*a*, and the observed cross section of this paramagnetic scattering at low angles appears to be consistent with that calculated for the free-ion moment (10.6 Bohr magnetons). Furthermore, the relatively few coherent reflections permit a good determination of the paramagnetic scattering and the corresponding magnetic form factor associated with the spin and orbital contributions to the atomic moments of the 4*f* electrons in the Ho^{+++} ion. The present data were limited to the angular region shown in the figure by the construction of the cryostat, and the form factor in this region agrees satisfactorily with that which was obtained[2] for the Ho^{+++} ions in Ho_2O_3. The analysis will be extended to much larger scattering angles when the cryostat is modified to permit these investigations.

Ferromagnetic reflections were observed in the diffraction pattern at liquid-helium temperatures, and these reflections are shown in Fig. 1*b*, where the data represent the difference in results obtained at 1.3 and 78°K. It is interesting to note that the (111) and (311) magnetic reflections actually occur at positions where nuclear reflections would be expected, but the latter are missing because the nuclear coherent amplitudes of holmium and nitrogen are almost equal. The negative background in this difference pattern represents the change in the magnetic diffuse scattering when the magnetic lattice orders. The very pronounced small-angle scattering and the large increase in diffuse scattering near the (111) and (200) reflections are indicative of some type of magnetic inelastic scattering from the ordered magnetic lattice. There is little change in the pattern when the sample temperature is raised to 4.2°K, and additional experiments will be performed at temperatures near the Curie point (about 20°K) in an attempt to obtain a better understanding of this scattering.

The large angular variations in the diffuse scattering from the ordered magnetic lattice make calculations of the atomic magnetic moments in this ferromagnetic structure somewhat uncertain. Preliminary calculations based on the change in the diffuse scattering between 298 and 1.3°K and on the coherent magnetic intensities indicate a value of about 8.0 ± 1.0 Bohr magnetons, depending on the background analysis. This value is somewhat lower than that expected for the ordered moment of the free ion (10.0 μ_B) and suggests that there is a crystalline

[1]We are very much indebted to D. E. LaValle of the Analytical Chemistry Division for preparing the sample.

[2]W. C. Koehler, E. O. Wollan, and M. K. Wilkinson, *Phys. Rev.* 110, 37 (1958).

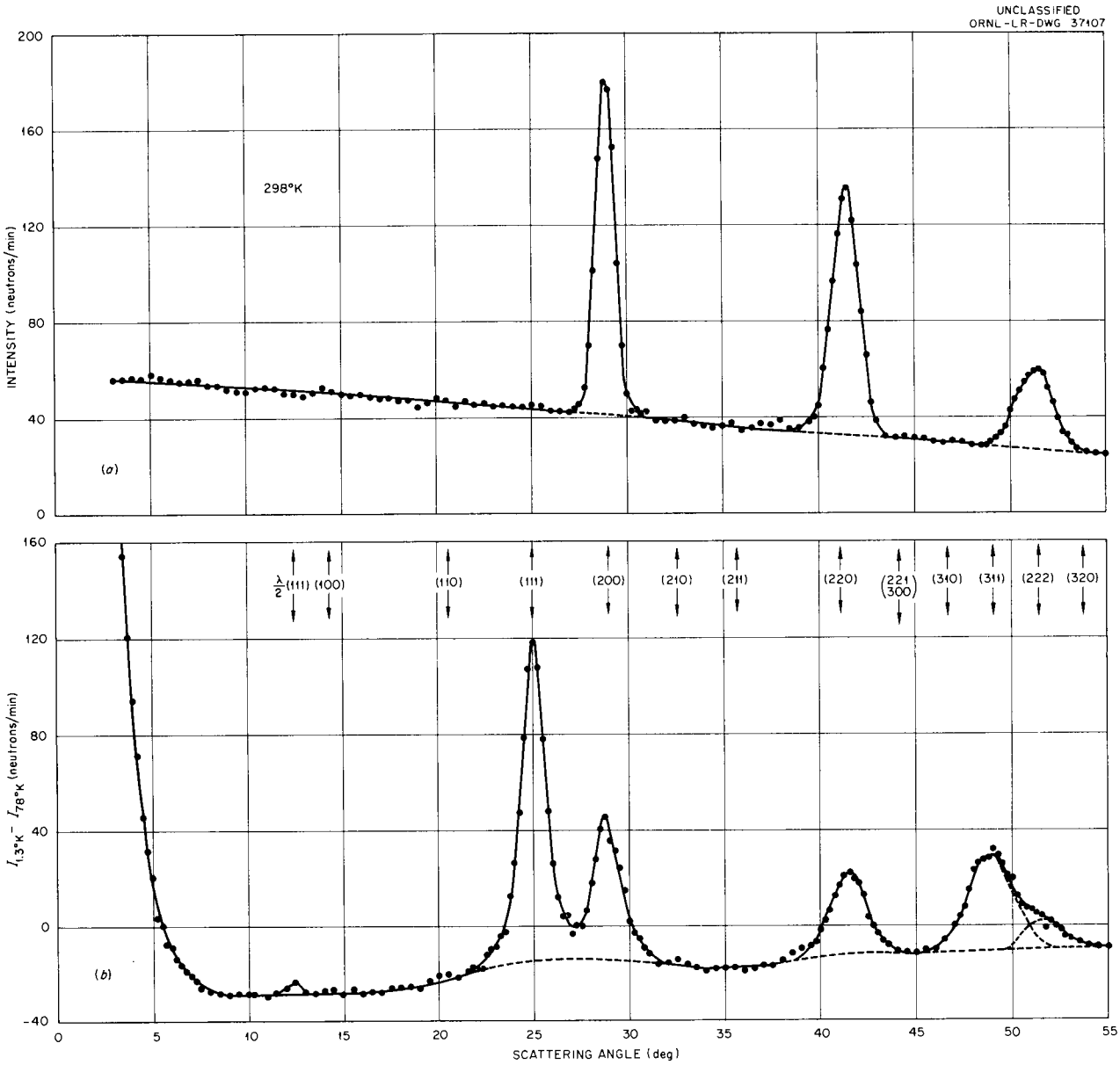

Fig. 1. (*a*) **Neutron Diffraction Pattern from Polycrystalline HoN at 298°K;** (*b*) **Temperature Difference Pattern** ($I_{1.3°K} - I_{78°K}$) **for HoN.**

field interaction which splits the energy levels so that the lowest level does not have the maximum value of J_z. The observed moment value, nevertheless, includes a large orbital contribution, and it was of interest to determine the effect of an external magnetic field on this type of moment.

Figure 2 shows the intensities of the (111) and (200) reflections when a magnetic field was applied parallel to their scattering vectors. The (111) reflection was unaffected by the magnetic fields which were applied, while the magnetic contribution in the (200) reflection was almost eliminated with fields of 12 kilo-oersteds. This difficulty in rotating the moments is merely indicative of the interaction of the crystalline field with the orbital currents of the 4*f* electrons. Furthermore, since relatively small fields applied perpendicular to the (200) planes can align the moments in that direction, the experiment indicates that the moments are oriented in directions parallel to the cube edges.

The results which have been reported are preliminary, and additional investigations will be made on the HoN sample. Furthermore, similar investigations are planned for all the rare-earth nitrides which have sufficiently large magnetic moments and sufficiently small absorption cross sections to permit analysis by neutron diffraction.

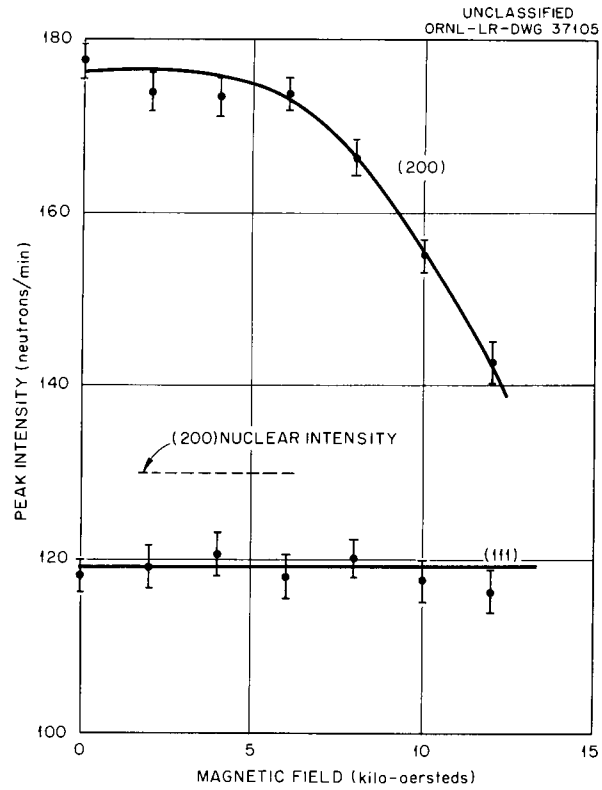

Fig. 2. Intensity Variation of the (111) and (200) Reflections from HoN at 4.2°K in an External Magnetic Field.

NEUTRON DIFFRACTION INVESTIGATIONS OF METALLIC CERIUM AT LOW TEMPERATURES

M. K. Wilkinson H. R. Child E. O. Wollan

The anomalous behavior exhibited in the specific heat[1,2] and magnetic susceptibility[3] measurements on metallic cerium has been difficult to interpret and has led to considerable speculation regarding the magnetic properties of this metal. Both types of measurements show large hysteresis effects which are strongly dependent on the previous history of the sample. Although it has been known for many years that cerium exists in a number of crystallographic states, recent x-ray measurements by McHargue, Yakel, and Jetter[4] were the first detailed investigations of the phase transformations. These experiments showed that three crystallographic forms exist between 77 and 450°K and that the relative concentrations are dependent both on

[1] D. H. Parkinson, F. E. Simon, and F. H. Spedding, *Proc. Roy. Soc. (London)* A207, 137 (1951).

[2] D. H. Parkinson and L. M. Roberts, *Proc. Phys. Soc. (London)* B70, 471 (1951).

[3] J. M. Lock, *Proc. Phys. Soc. (London)* B70, 566 (1957).

[4] C. J. McHargue, H. L. Yakel, Jr., and L. K. Jetter, *Met. Ann. Prog. Rep. Oct. 10, 1957*, ORNL-2422, p 207 (classified).

the sample temperature and on the condition of the sample. For example, in a previously uncooled annealed sample a face-centered cubic phase (fcc) with $a_0 = 5.15$ Å is stable at room temperature, but as the sample is cooled, a double hexagonal close-packed (hcp) structure starts to develop at about 263°K and a collapsed face-centered cubic phase (α-fcc) with $a_0 = 4.85$ Å starts to form at about 103°K. There is a large hysteresis in the phase transformations, so that when the sample temperature is raised, the formation of the original phases starts to occur at much higher temperatures. Furthermore, strains introduced in the sample by cold-working or thermal-cycling can produce entirely different phase concentrations as a function of temperature.

Since the nuclear reflections in a neutron diffraction pattern permit a determination of the relative phase concentrations, this technique provided an excellent method for investigating the magnetic properties of cerium under known crystallographic conditions. In addition to the anomalous hysteresis effects in the cryomagnetic measurements, there were two particular points of interest which these experiments could possibly clarify. Lock's susceptibility measurements had indicated an antiferromagnetic transition at about 12.5°K, and Zachariasen[5] and Pauling[6] had suggested that the formation of the α-fcc phase involved the promotion of a $4f$ electron to a $5d$ level.

Neutron diffraction experiments were performed from room temperature to 4.2°K on three specimens of polycrystalline cerium rod, furnished by McHargue, Yakel, and Jetter of the Metallurgy Division. These samples were conditioned by various methods to give considerably different concentrations of the three crystallographic phases of cerium as a function of temperature. As previously reported,[7] these investigations showed that the anomalous hysteresis effects in the specific heat and magnetic susceptibility measurements could be correlated with the hysteresis in the formation of the α-fcc phase.

The neutron diffraction patterns at 4.2°K for all three samples showed the presence of three additional very weak reflections, and the relative intensities of these reflections in the three samples corresponded to the relative concentrations of the hcp phase. The largest reflection in one sample was scanned with the sample at various temperatures[7] above 4.2°K and was found to disappear near 12.5°K, thereby indicating that the susceptibility and specific heat anomalies observed at this temperature were associated with an antiferromagnetic transition in the hcp phase.

Additional analyses have now been performed on these magnetic reflections which further substantiate antiferromagnetic ordering in the hcp phase. The reflections cannot be associated with the α-fcc phase since their intensities in the three samples disagree violently with the relative concentrations of this phase at 4.2°K. Furthermore, the largest of the three antiferromagnetic reflections cannot be indexed by any sensible enlargement of the normal fcc unit cell. Since this phase is practically absent at 4.2°K in all three samples, it is impossible to show that antiferromagnetic ordering does not also exist in this phase, but the largest observed reflection is undoubtedly the result of an antiferromagnetic transition in the hcp phase. All three observed reflections can be indexed satisfactorily for a hexagonal cell with the same c axis as that of the chemical cell ($ABAC$ layers) and an a axis which is twice that of the chemical cell. Such a magnetic structure can be formed by stacking ferrimagnetic layers of moments of the type shown in Fig. 1*a*. Calculations have been made for several models in which stacking sequences of +−+− and ++−− were considered. Since only three reflections were observed and since these reflections could not be accurately determined because of their very small intensities, it has been impossible to find a unique structure. However, three models for each stacking sequence do predict the proper relative intensities within experimental error if the moment orientation is parallel to the c axis. The best agreement was obtained for the structure shown in Fig. 1*b*. Calculations of the value for the atomic magnetic moment in the ordered lattice consistent with these models varied between about 0.50 μ_B and 0.75 μ_B, with the model of Fig. 1*b* giving 0.62 μ_B. A determination of the magnetic moment from the change in diffuse scattering above and below the transition temperature was unfortunately hindered by the large change

[5]Cited by A. W. Lawson and L. Y. Yang, *Phys. Rev.* 76, 301 (1949).

[6]Cited by A. F. Schuck and J. H. Sturdivant, *J. Chem. Phys.* 18, 145 (1950).

[7]H. R. Child *et al.*, *Phys. Semiann. Prog. Rep. Sept. 20, 1958*, ORNL-2610, p 32.

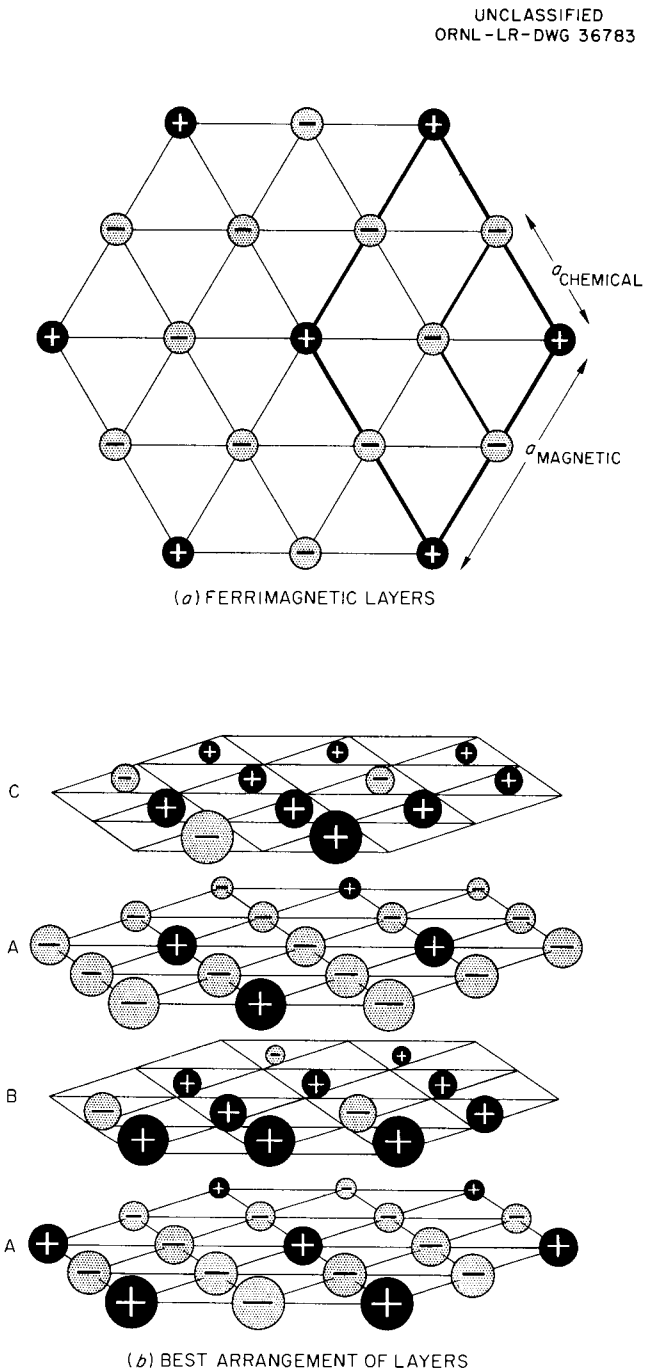

Fig. 1. Possible Magnetic Ordering in Hexagonal Cerium.

in diffuse scattering which accompanied the formation of the α-fcc phase. However, this diffuse scattering change limited the atomic magnetic moment to a maximum value of 0.90 μ_B and suggested a value of $0.6 \pm 0.3\ \mu_B$. Of course, the diffuse scattering analysis does not prove that any of the proposed structures are correct; it merely verifies that they predict a satisfactory value for the atomic moment in the ordered lattice.

Since the paramagnetic scattering from a magnetic material is proportional to $g^2J(J+1)$, an analysis of the diffuse scattering can, in principle, determine the specific electronic configuration of the magnetic electrons within an atom. This type of analysis is particularly good for metallic cerium since there is practically no diffuse scattering from the sample other than the paramagnetic scattering. There are only two isotopes, Ce^{140} and Ce^{142}, which constitute 99.55% of the element, and since both have even-even nuclei, there is no nuclear-spin-incoherent scattering. Furthermore, the two isotopes have closely the same values of nuclear coherent scattering amplitudes, so that isotopic incoherence is essentially negligible. Therefore the only sources of diffuse scattering in addition to the magnetic scattering are disorder scattering due to lattice distortions and multiple scattering. Both of these should be small.

Figure 2 shows the diffuse scattering at small angles for the three cerium samples at various temperatures, and it is immediately apparent from these curves that a large decrease is associated with the formation of the α-fcc phase. Such a change would be expected if there is a different electronic configuration of the atoms in the α-fcc structure. Calculations have been made of the paramagnetic diffuse scattering which would be expected for various possible electronic configurations and have been compared with the experimental values. The intensities of all curves shown in Fig. 2 can be explained if the atoms in the normal fcc and hcp structures have one magnetic electron in the electronic state $4f^1(^2F_{5/2})$ and the atoms in the α-fcc phase do not have an atomic magnetic moment. Of

UNCLASSIFIED
ORNL-LR-DWG 36784

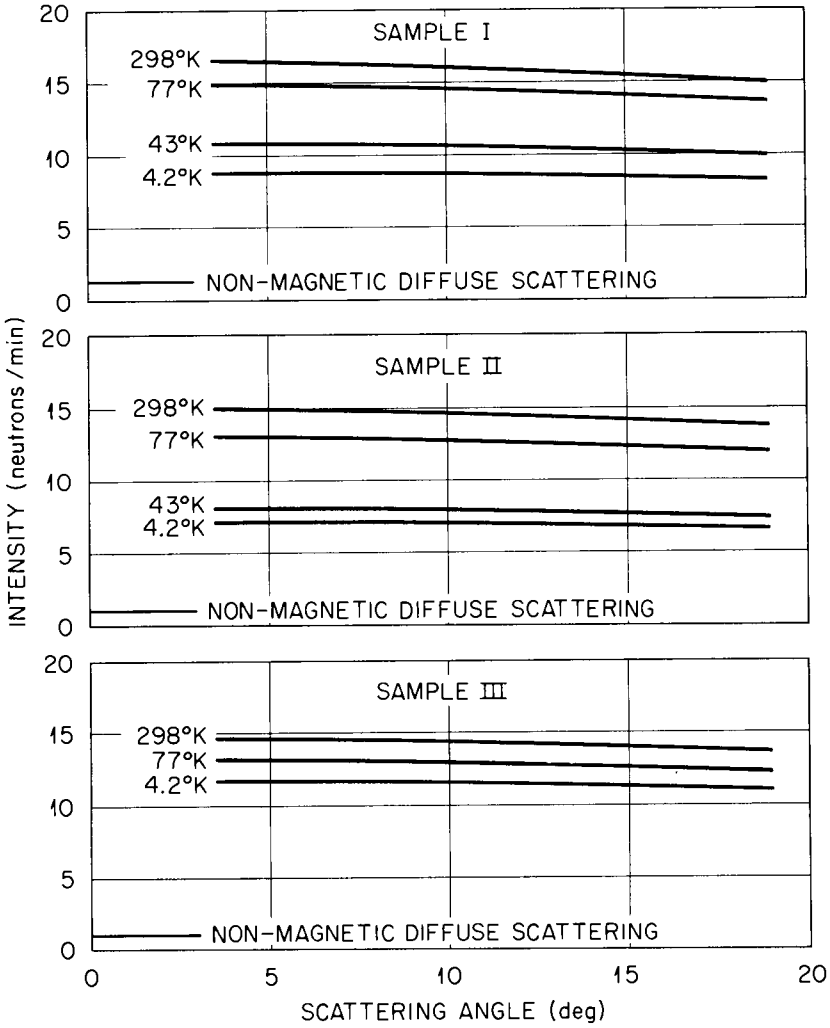

TEMP PHASE PERCENTAGES

(°K)	NORMAL fcc (%)	hcp (%)	COLLAPSED fcc (%)
298	100		
77	10	80	10
43	5	55	40
4.2	5	45	50

(°K)	(%)	(%)	(%)
298	75	25	
77	57	35	8
43	8	40	52
4.2	5	40	55

(°K)	(%)	(%)	(%)
298	10	90	
77	10	87	3
4.2	8	84	8

Fig. 2. Diffuse Neutron Scattering from Cerium.

the many configurations considered, this combination is the only one which gives satisfactory agreement with the data, and, as shown in Table 1, the agreement is quite good when a small term is included to account for the estimated diffuse scattering from other sources. The configuration $^2F_{5/2}$ corresponds to that predicted for the free ion Ce^{+++}, and Lock's susceptibility measurements above 110°K were also consistent with such a state. Furthermore, the change in the atomic magnetic moment in the α-fcc phase explains why susceptibility measurements were sensitive to the amount of this phase present in the samples. Previous predictions that the α-fcc phase involved the promotion of a $4f$ electron to a $5d$ level are apparently also verified by these experiments if the electrons in the $5d$ level are in a bonding orbital with compensating spins. The intensity of the diffuse

Table 1. Comparison of Calculated Diffuse Scattering with Experimental Value (Extrapolated to $2\theta = 0°$)

Sample	Temperature (°K)	Phase Concentrations (%)			Diffuse Scattering (neutrons/min)			
		Normal-fcc	hcp	α-fcc	Calculated* Paramagnetic	Other	Total	Observed
I	298	100			15.3	1.2	16.5	16.5
	77	10	80	10	13.8	1.2	15.0	15.0
	43	5	55	40	9.1	1.2	10.3	10.8
	4.2	5	45	50	7.3	1.2	8.5	9.0
II	298	75	25		14.0	1.0	15.0	15.0
	77	57	35	8	12.9	1.0	13.9	13.3
	43	8	40	52	6.7	1.0	7.7	8.0
	4.2	5	40	55	5.9	1.0	6.9	7.3
III	298	10	90		14.0	1.0	15.0	14.8
	77	10	87	3	13.5	1.0	14.5	13.5
	4.2	8	84	8	12.0	1.0	13.0	12.0

*Calculated values for the paramagnetic scattering from one magnetic electron in the $4f^1(^2F_{5/2})$ electronic state in the normal fcc and hcp phases and no paramagnetic scattering in the α-fcc phase.

scattering would not permit even a spin-only value for the magnetic moment of the atoms in this structure.

Lawson and Yang have calculated that the energy separation of the $4f$ and $5d$ levels is about 0.04 ev, and large strains in the sample could presumably modify these levels sufficiently to affect the $4f \rightleftharpoons 5d$ transition. This could be the reason why little α-fcc phase was formed in sample III (which had been cycled between 300 and 4.2°K 100 times) and could also explain the apparent lack of formation of this phase in slightly impure samples examined by previous workers.

It is interesting that the value of the atomic magnetic moment associated with the ordered magnetic lattice is much smaller than that ($2.14\mu_B$) calculated for the maximum gJ_Z in the $^2F_{5/2}$ state. This indicates that the energy levels are affected by the crystalline field. Although calculations have not been made for the hcp phase, Murao and Matsubara[8] have calculated the level splitting of this electronic state in cubic cerium. Their results predict a value for the atomic moment at low temperatures of $0.71\mu_B$, which is within the limits of possible values obtained in this experiment.

[8] T. Murao and T. Matsubara, *Progr. Theoret. Phys. (Kyoto)* 18, 215 (1957).

NEUTRON DIFFRACTION INVESTIGATIONS OF ANTIFERROMAGNETISM IN CrF_2 AND $CrCl_2$

M. K. Wilkinson J. W. Cable E. O. Wollan

Recent investigations at ORNL of antiferromagnetic structures in compounds containing $3d$ transition-group elements have suggested specific coupling mechanisms[1] when the magnetic cations are located in octahedral sites of the anions. This coupling scheme predicts that trivalent manganese, Mn^{+++}, and divalent chromium, Cr^{++}, are unique in these surroundings, since there should be both ferromagnetic and antiferromagnetic coupling with neighboring magnetic ions via the intervening anions. Although the chromium positions in CrF_2 and $CrCl_2$ are not exactly octahedral sites, it was of interest to determine the existence of magnetic ordering in these compounds and compare the magnetic structures with those of similar compounds involving other divalent ions of the iron group. Both CrF_2 and $CrCl_2$ crystallize in slightly different distortions of the rutile structure and are consequently very similar to the difluorides of Mn, Fe, Ni, and Co, which were studied at ORNL by Erickson.[2]

The crystal structure of CrF_2 has recently been investigated by Jack and Maitland,[3] and they determined that the unit cell is monoclinic with a = 4.732 Å, b = 4.718 Å, c = 3.505 Å, and β = 96.52°. The cell is bimolecular with two chromium atoms at (000) and ($\frac{1}{2}\,\frac{1}{2}\,\frac{1}{2}$) and with four fluorine atoms at $\pm(xyz)$ and $\pm(\frac{1}{2}+x,\ \frac{1}{2}-y,\ \frac{1}{2}+z)$, where $x = y =$ 0.297 and z = 0.044. The crystal structure of $CrCl_2$ was previously undetermined, but investigations at ORNL by Yakel and Steele[4] have revealed that it is orthorhombic with a = 6.638 Å, b = 5.984 Å, and c = 3.476 Å. The unit cell is also bimolecular, with two chromium atoms at (000) and ($\frac{1}{2}\,\frac{1}{2}\,\frac{1}{2}$) and with four chlorine atoms at $\pm(u\ v\ 0)$ and $\pm(\frac{1}{2}+u,\ \frac{1}{2}-v,\ \frac{1}{2})$, where u = 0.36 and v = 0.28. The nuclear reflections in the neutron diffraction pattern agree satisfactorily with both structure determinations.

Neutron diffraction investigations have been performed on polycrystalline samples of CrF_2 and $CrCl_2$ at temperatures from 300 to 4.2°K. Antiferromagnetic reflections were observed in the patterns from both compounds at 4.2°K, and Fig. 1 shows the difference in the results obtained at 4.2 and 78°K. In these plots the nuclear contributions to the scattering have essentially been eliminated so that the diffraction peaks represent coherent magnetic scattering from the ordered magnetic lattice at 4.2°K, while the negative backgrounds give the change in the magnetic diffuse scattering which occurred with the formation of the antiferromagnetic structures. In both patterns shown in Fig. 1 the backgrounds do not have the true form-factor variation exhibited by paramagnetic scattering, thereby indicating that magnetic short-range order existed at 78°K.

A complete analysis of these magnetic structures has not been finished, but preliminary calculations indicate that different types of magnetic ordering occur in the two compounds. The magnetic reflections in CrF_2 have been indexed for a unit cell which has the same dimensions as the chemical cell, and they can be explained by a magnetic structure in which the atomic moments of the chromium ions at the lattice corners are antiparallel to those at the center of the cell. This is the same magnetic structure as those observed for the other iron-group difluorides. However, the antiferromagnetic reflections in $CrCl_2$ require a magnetic unit cell in which the b axis and c axis are twice those of the chemical cell, but the a axis is the same as that of the

[1] E. O. Wollan *et al.*, *Phys. Rev.* 112, 1132 (1958).

[2] R. A. Erickson, *Phys. Rev.* 90, 779 (1953).

[3] K. H. Jack and R. Maitland, *Proc. Chem. Soc. (London)* 1957, 232.

[4] H. Yakel and R. Steele, private communication.

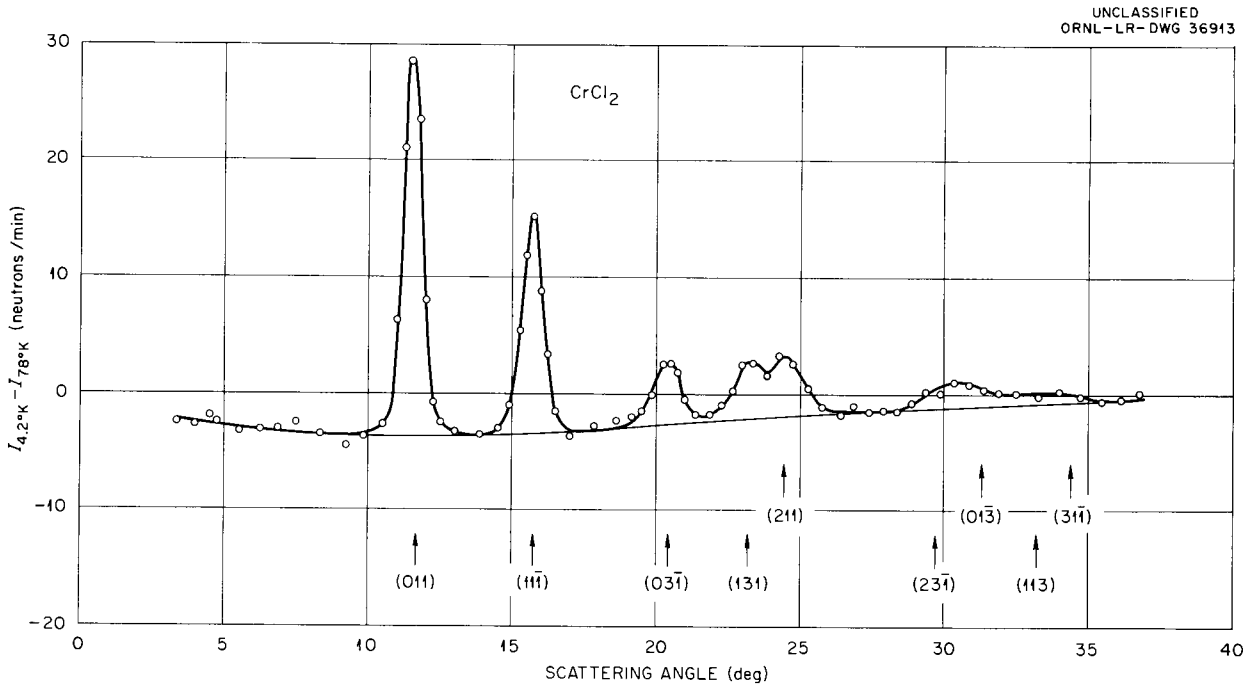

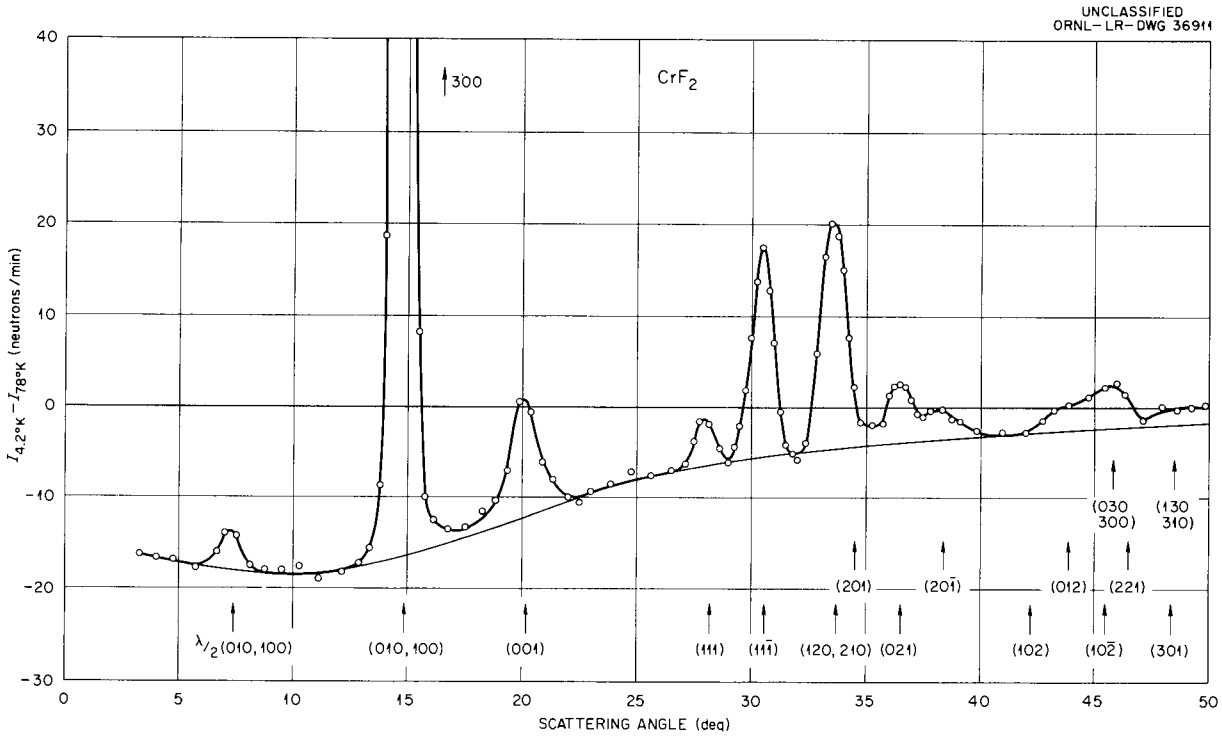

Fig. 1. Temperature Difference Patterns ($I_{4.2°K} - I_{78°K}$) for $CrCl_2$ and CrF_2.

chemical cell. The suggested magnetic structure of this compound has ferromagnetic (011) planes with adjacent planes antiparallel. Since the analysis is incomplete, the exact orientation of the magnetic moments has not been determined and no moment value has been obtained from the coherent scattering. Analyses of the difference in the diffuse scattering at 4.2 and 300°K suggest that in both compounds the atomic moments have values that are close to those expected for the Cr^{++} ions if the orbital contribution is quenched. Furthermore, the magnetic form factor appears to be very similar to that which has been previously determined[5] for divalent manganese, Mn^{++}.

The Néel temperatures have been determined for both compounds by observing the variation of the largest antiferromagnetic reflections as a function of temperature. Figure 2 shows the temperature variation of the (100) reflection from CrF_2, and these results indicate a transition temperature of about 51°K. Similar data observed for the (011) magnetic reflection from $CrCl_2$ give a Néel temperature of about 20°K.

[5]C. G. Shull and E. O. Wollan, *Solid State Physics* (ed. by F. Seitz and D. Turnbull), vol II, p 211, Academic Press, New York, 1957.

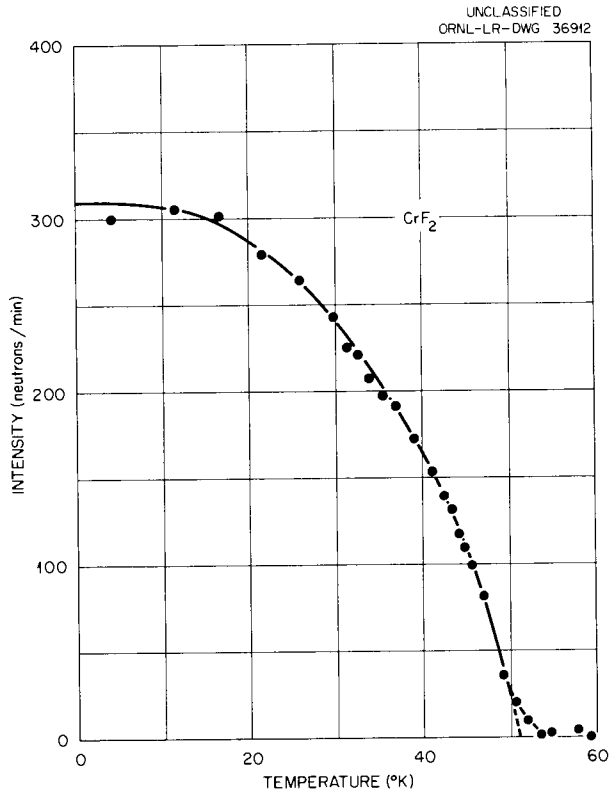

Fig. 2. Temperature Variation of the (100) Antiferromagnetic Reflection from CrF_2.

A DUO-PLASMATRON ION SOURCE FOR USE IN ACCELERATORS

C. D. Moak
H. E. Banta[1]
J. N. Thurston[2]
J. W. Johnson[1]
R. F. King[1]

Evaluations of various sources for accelerator use at proton currents above 10 ma indicate that a variation of Von Ardenne's Duo-Plasmatron will give a performance superior to that of any other source presently available. Operating characteristics for various sizes of the source have been examined for H_1^+, H_2^+, H_3^+, H_1^-, He^+, and He^{++} ions and electrons. Experience with protons in the current range from 1 to 30 ma indicates that the Duo-Plasmatron can deliver up to 100 amp per square centimeter of exit aperture area. A current density such as this cannot be maintained in the accelerator-extractor section because of space-charge forces, even at the highest gradients normally available for well-polished electrodes in vacuum; thus it can be said that proton current densities will be space-charge-limited by the accelerator rather than emission-limited by the source. Operation for He^+ ions and electrons is similar to proton operation. Currents of 11 μa of H_1^- ions and 5 μa of He^{++} ions were extracted directly from a source which had been designed for a proton current of several milliamperes. The most striking features of the Duo-Plasmatron are its remarkably high brilliance, high gas efficiency, good power economy, and compactness.

[1]Instrumentation and Controls Division.

[2]Summer participant from Clemson College, Clemson, S. C.

LOW-TEMPERATURE HELIUM-VAPOR PULSE IONIZATION CHAMBER

J. W. T. Dabbs S. H. Hanauer L. D. Roberts[1]

Since helium is the only substance which is gaseous at 4.2°K and lower, operation of a gas-filled ionization chamber in this temperature range is governed by the properties of helium. Recent measurements[2,3] have shown that W (average energy to form an ion pair in the gas) for helium is very sensitive to small traces of foreign gases. The value of W for helium continuously purified[3] is $\sim$1.5 times the value for "spectroscopically pure" cylinder gas. We have investigated the properties of helium gas in the temperature range 2 to 2.6°K, where no other gas has a vapor pressure as high as 10^{-12} mm Hg. The measurements were made by use of a small gridded ionization chamber which fitted available low-temperature apparatus. Little effort was made to get good energy resolution; the experiment was performed to obtain design parameters for larger low-temperature ionization chambers, which might be used in nuclear alignment studies.

The experimental arrangement is shown schematically in Fig. 1. The electrodes of a parallel-plate gridded ionization chamber[4] were enclosed in a cylindrical copper can with walls 0.3 cm thick. The side walls of the can were extended downward 15 cm below the bottom of the enclosed section to form a "skirt." The chamber assembly was mounted in a Dewar vessel containing liquid helium, the liquid level being always below the bottom of the enclosed (chamber) section and above the bottom of the skirt. Holes cut in the bottom and top of the chamber allowed helium vapor boiled off from the bath to flow freely through the chamber. The copper can and skirt provided an isothermal enclosure at the temperature of the bath. Alpha particles from a thin source[5] of Am^{241} were collimated so that their paths lay approximately perpendicular to the electric field in the chamber.

The apparatus was first used at 300°K, with the chamber filled with a mixture of 90% Ar and 10% CH_4. In this preliminary test, W for the gas mixture was found to be 24.7 ± 1.0 ev per ion pair, in satisfactory agreement with 26.2 ± 0.3 ev per ion pair as measured by Moe, Bortner, and Hurst.[6]

Typical helium data obtained with a single-channel pulse-height analyzer are shown in Fig. 2. The spread in observed pulse height when signal-generator pulses were being counted is due to noise in the electronics. The alpha-particle ionization straggling was small compared with this: the

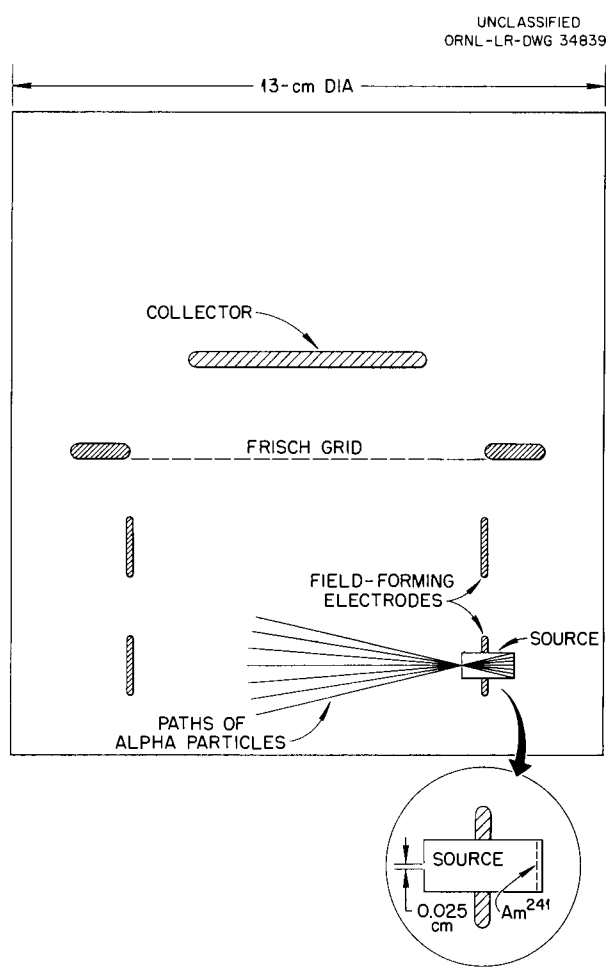

Fig. 1. Helium-Vapor Pulse Ionization Chamber.

[1]On leave at Oxford University, England, under a Guggenheim Fellowship and a Fulbright Fellowship.

[2]W. P. Jesse and J. Sadauskis, *Phys. Rev.* **90**, 1120 (1953).

[3]T. E. Bortner and G. S. Hurst, *Phys. Rev.* **93**, 1236 (1954).

[4]O. Bunemann, T. E. Cranshaw, and J. A. Harvey, *Can. J. Research* **A27**, 191 (1949).

[5]The assistance of G. W. Parker with source preparation is gratefully acknowledged.

[6]H. J. Moe, T. E. Bortner, and G. S. Hurst, *J. Phys. Chem.* **61**, 422 (1957).

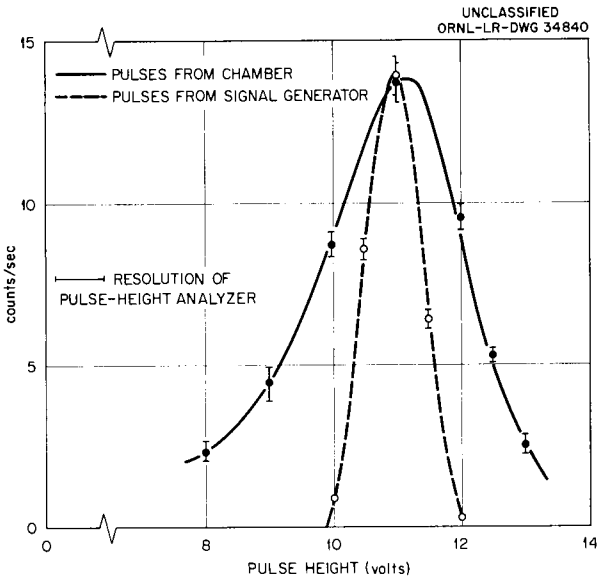

Fig. 2. Typical Data Obtained with Low-Temperature Helium-Vapor Pulse Ionization Chamber.

spread in alpha-particle pulse hieght when the chamber was filled with Ar-CH_4 (not shown in Fig. 2) was comparable with the spread caused by electronic noise alone. The increased spread when alpha pulses from the helium-filled chamber were counted may be attributed partly to pressure fluctuations in the chamber, for which there was some evidence. Increased microphonic noise probably accounts for the remaining spread.

Because of the absence of measurable ionization straggling, the pulse height for which the counting rate was a maximum was taken to be the measured pulse height.

The gain of the amplifiers was measured with a precision pulse generator and the single-channel pulse-height analyzer. The capacitance of the input circuit was 26 $\pm$ 0.3 $\mu\mu$f.

The pulse rise time, RT, shown in Fig. 3, increased slowly with decreasing voltage (N = density of gas, E = voltage gradient between collector and grid). A simple theory[7] gives $RT \propto (E/N)^{-1/2}$; this form of variation is not excluded by the data. Note that in this and other equations the gas density must be used rather than the pressure, as is more usual where temperature variation is negligible.

[7]For example, see L. B. Loeb, *Basic Processes of Gaseous Electronics*, chap III, Univ. of Calif. Press, 1955.

The pulse-height data shown in Fig. 4 are corrected for amplifier clipping and for ionization lost within the collimator volume. The latter correction was calculated by using a Bragg curve[8,9] altered to take into account the difference between air and other gases.[10] The data taken at 20 mm Hg gas pressure also had to be corrected for ionization outside the effective volume of the chamber, since the alpha-particle range at this gas density is larger

[8]M. G. Holloway and M. S. Livingston, *Phys. Rev.* **54**, (1938).

[9]M. S. Livingston and H. A. Bethe, *Revs. Modern Phys.* **9**, 245 (1937).

[10]E. T. Segre (ed.), *Experimental Nuclear Physics*, vol I, p 236, Wiley, New York, 1953.

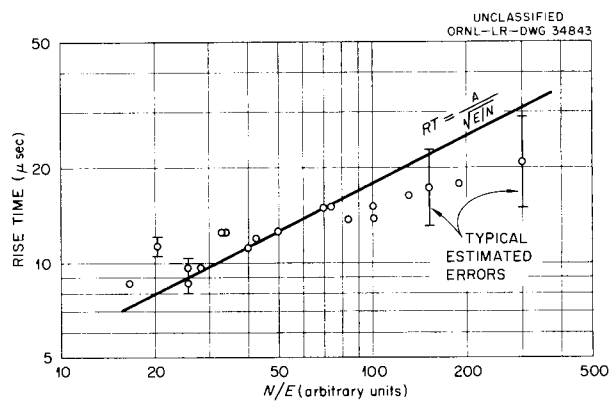

Fig. 3. Rise-Time Data Obtained with Low-Temperature Helium-Vapor Pulse Ionization Chamber.

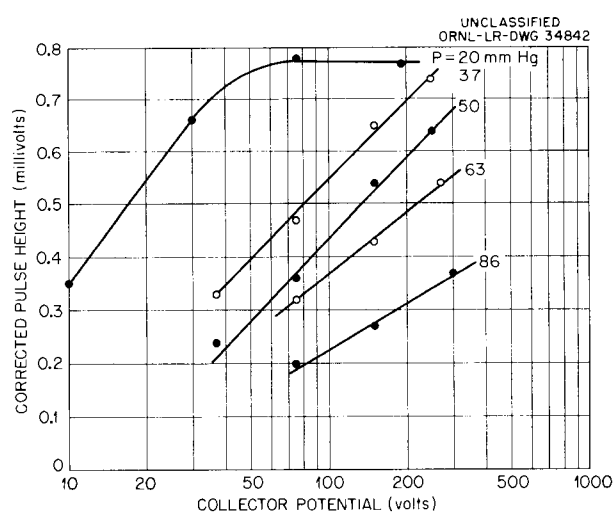

Fig. 4. Pulse-Height Data Obtained with Low-Temperature Helium-Vapor Pulse Ionization Chamber.

than the diameter of the field-forming electrodes. This large correction (~55%) increases the uncertainty in the absolute value of these pulse heights.

The evidence for saturation is suggestive but inconclusive. The collector potential which could be applied was limited by breakdown, and it was not possible with this apparatus to reach the saturation region – if it exists – at higher pressures. If the two points on the horizontal portion of the $P = 20$ mm curve in Fig. 4 are taken as representing the saturated pulse height, then W is calculated to be 46 ± 6 ev per ion pair. This agrees well with $W = 46.0 \pm 0.4$ ev from accurate experiments[3] at 300°K. An interesting way of plotting the data is shown in Fig. 5. If the reciprocal of the corrected pulse height be plotted as a function of N^3/E, the experimental data are consistent with a single curve, whose greater portion, shown on Fig. 5, can be represented by a straight line. We have found no satisfactory explanation of this functional form. The intercept of the least-squares straight-line fit to these data plotted in this way is a measure of the saturated pulse height, if this plot has any validity. The value for W determined in this way is 40 ev per ion pair.

From these measurements we conclude that (1) the recent measurements[2,3] of W for highly purified helium at 300°K are probably representative of the pure gas; (2) a helium-gas pulse ionization chamber clearly can be operated at low temperatures with rise times and pulse heights such that alpha particles may be counted with good energy resolution. The question of maximum acceptable values for N^3/E will require further measurements.

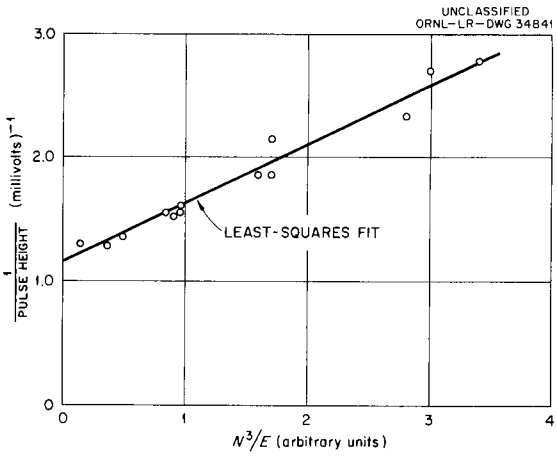

Fig. 5. Extrapolation of Data Taken with Low-Temperature Helium-Vapor Pulse Ionization Chamber.

It is a pleasure to acknowledge helpful discussions with C. J. Borkowski and E. Fairstein.

BROAD-AREA GERMANIUM SURFACE BARRIER COUNTERS

F. J. Walter
J. W. T. Dabbs
L. D. Roberts[1]
H. W. Wright[2]

In a previous semiannual report[3] a brief description of initial work on germanium surface barrier counters was given. The study of these counters has been continued, both on a theoretical and an experimental basis. For purposes of coherence, certain information is repeated in this report, which is comprehensive of all our work done to date. It should be noted that this investigation was directed primarily at obtaining satisfactory counters for fission fragments and alpha particles in connection with nuclear alignment work at low temperatures. No attempt has been made to study surface treatments which produce barriers at room temperature.

INTRODUCTION

When a charged particle, such as an alpha particle, enters germanium, it produces free electrons and holes at an average rate of 1 electron-hole pair for each 3 ev of energy lost.[4] If these free carriers are created in a surface barrier[5] where a significant

[1] On leave at Oxford University, England, under a Guggenheim Fellowship and a Fulbright Fellowship.

[2] Analytical Chemistry Division.

[3] J. W. T. Dabbs, F. J. Walter, and L. D. Roberts, *Phys. Semiann. Prog. Rep. March 10, 1958*, ORNL-2501, p 73.

[4] K. G. McKay, *Phys. Rev.* **84**, 829 (1951).

[5] J. W. Mayer and B. R. Gossick, *Rev. Sci. Instr.* **27**, 407 (1956).

electric field exists, they will drift in the field and induce a charge on the ungrounded electrode (see Fig. 1). The size of the voltage pulse resulting from this induced charge will depend on the total amount of charge created, the capacitances of the device and external circuits, and the efficiency of charge collection. The speed with which the counter responds to an ionizing event is determined by the time required for the charge carriers to traverse the voltage gradient. The large electric field and short collection distances associated with surface barriers, together with high carrier mobilities, give these devices very short pulse rise times. The absence of large trapping or recombination effects leads to good proportionality between particle energy and pulse height provided that the range of the radiation is comparable to the barrier depth. The use of a surface barrier device has the additional advantage of providing a large, uniform, and well-defined area which is sensitive to ionizing radiation.

The purposes of this study were to extend the work of Mayer and Gossick[5] to the detection of fission fragments; to detect both alpha particles and fission fragments with large detectors at low temperatures in connection with nuclear alignment experiments; and to compare the experimentally observed counter characteristics with the predictions of a simple theory.

UNCLASSIFIED
ORNL-LR-DWG 33930

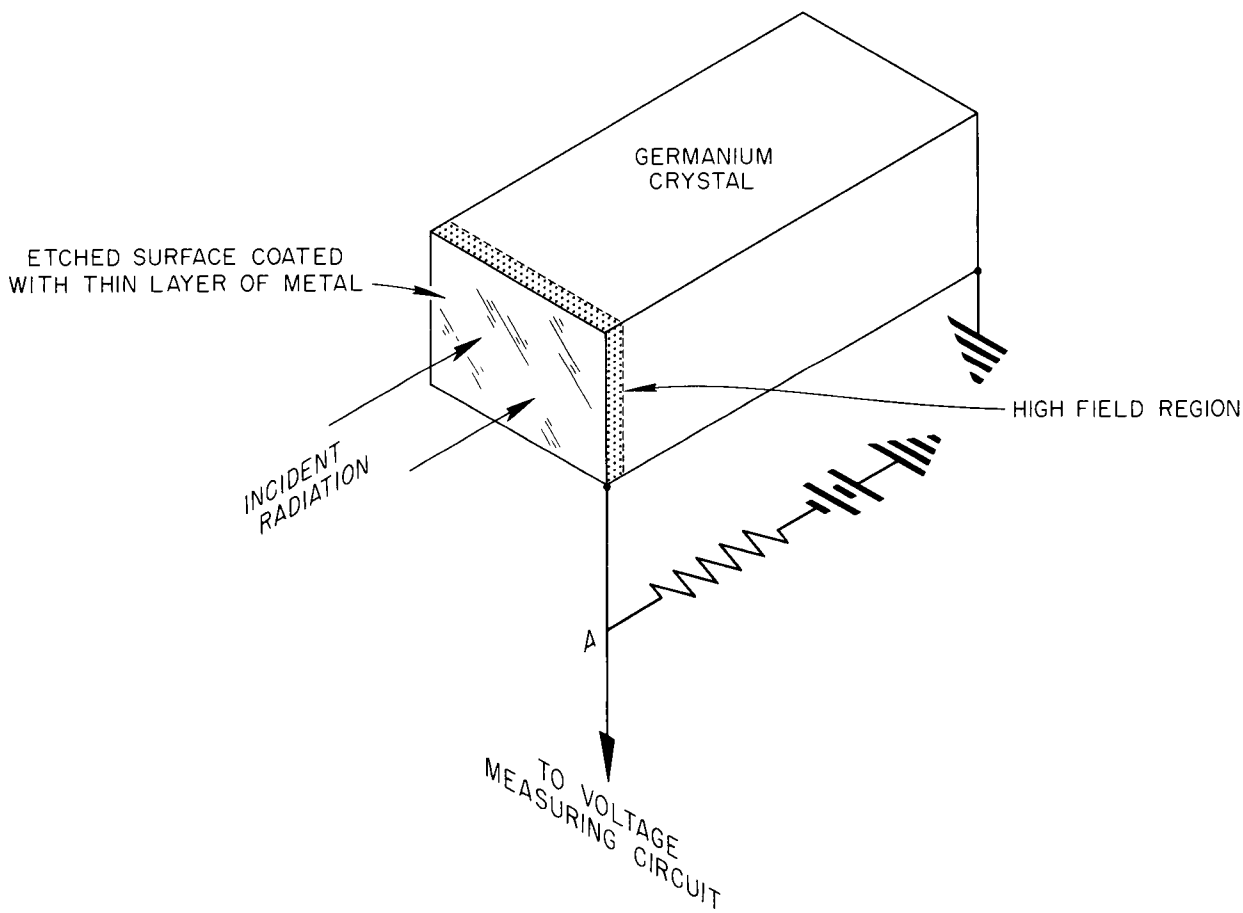

Fig. 1. Typical Surface Barrier Counter or Photovoltaic Cell.

THEORY

In order to give a theoretical description of the characteristics of a surface barrier counter, it is necessary to know the electrostatic potential distribution in the crystal and the resulting effective (small-signal) capacitance of the device.

The existence of surface states on n-type germanium is well established.[6] These states are able to trap electrons from the crystal until the Fermi level in the surface is equalized with the Fermi level in the interior. This leaves the crystal with a positive space charge and also warps the band structure as shown in Fig. 2. The resulting

[6] R. H. Kingston (ed.), *Semiconductor Surface Physics*, Univ. of Pennsylvania Press, Philadelphia, 1957.

UNCLASSIFIED
ORNL-LR-DWG 34169

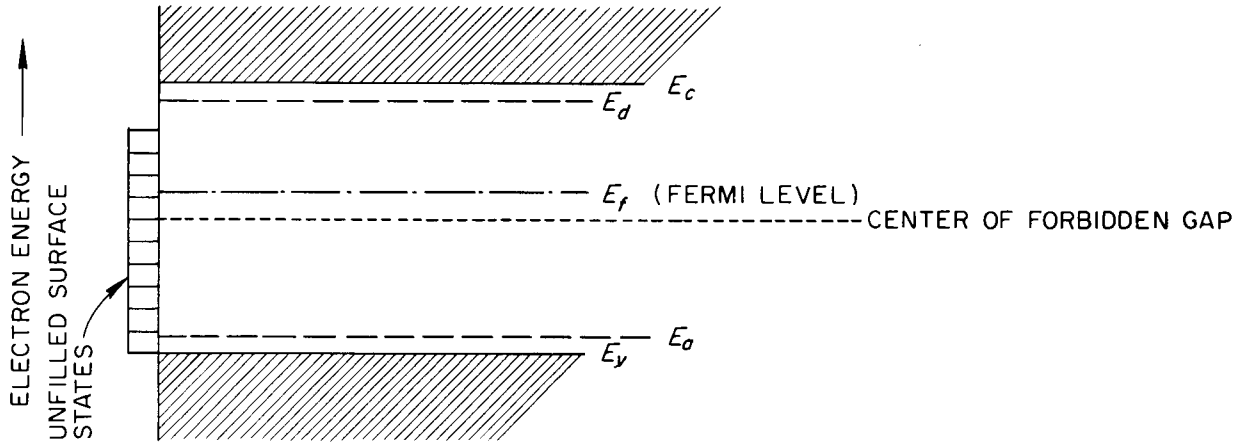

(*a*) SEMICONDUCTOR NOT AT EQUILIBRIUM WITH SURFACE STATES

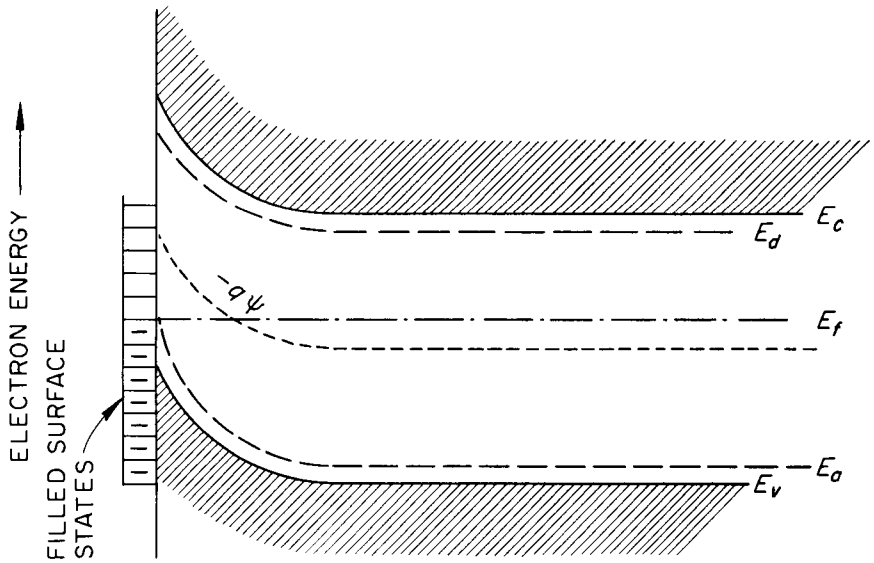

(*b*) SEMICONDUCTOR AT EQUILIBRIUM WITH SURFACE STATES; FORMATION OF SPACE CHARGE LAYER

Fig. 2. Electron Energy Relations at the Surface of n-Type Germanium.

high density of charge on the surface and relatively low density of charge in the interior produce an asymmetric potential distribution, which is called a surface barrier. In the descriptions which follow, the exact density and location of the surface states will remain unspecified. The following assumptions will also be made:

1. Image effects, work function differences, and barrier tunneling are negligible.
2. The distance between ionizable donor centers is small compared with the depth of the positive space-charge region.
3. All ionized impurity sites are immobile.
4. The density of donor and acceptor centers is constant.
5. The surface barrier is formed on the plane surface of a semi-infinite crystal.
6. All the donor centers are located at a well-defined energy level E_d, and all the acceptor centers are located at a well-defined energy level E_a.

At the temperatures and impurity concentrations of interest in this work, the Fermi-Dirac distribution associated with the carriers can be approximated accurately by a Boltzmann distribution. In this case the charge distribution in the crystal is given by

$$\rho = q(N + C_1 e^{-q\psi/kT} - C_2 e^{q\psi/kT}) \quad , \qquad (1)$$

where

ρ = charge density,

q = magnitude of the electronic charge,

ψ = electrostatic potential,

$N \equiv N_d - N_a$,

N_d = density of donor centers,

N_a = density of acceptor centers,

$$C_1 \equiv N_v e^{(E_v - E_f)/kT} + N_a e^{(E_a - E_f)/kT} \quad ,$$

$$C_2 \equiv N_c e^{(E_f - E_c)/kT} + N_d e^{(E_f - E_d)/kT} \quad ,$$

N_v = density of states in valence band (below energy E_v),

N_c = density of states in conduction band (above energy E_c),

E_f = Fermi level energy,

kT = Boltzmann's constant times the absolute temperature.

Substituting Eq. (1) into Poisson's equation in one dimension and integrating, one obtains

$$x = -\frac{1}{2L} \int_{u_0}^{u} [Nu + C_1(e^u - 1) + C_2(e^{-u} - 1)]^{-1/2} \, du \quad , \qquad (2)$$

where

x = normal distance from the surface of the crystal,

$L \equiv q^2/kT\epsilon_0 K$,

$u \equiv -q\psi/kT$,

K = dielectric constant,

ϵ_0 = permittivity of free space.

Here, u_0 is proportional to the barrier height $(-\psi_0)$, which cannot exceed a value of a few times kT less than $(E_f - E_v)/q$. In n-type material, the term $C_1(e^u - 1)$ produces what is known as an "inversion layer" at the surface. The term $C_2(e^{-u} - 1)$ produces a "tailing out" of the potential distribution at large x which is unimportant if $-q\psi_0 \gg kT$.

A numerical integration of Eq. (2) showed that at the temperatures and impurity concentrations of interest here, the terms involving C_1 and C_2 are not particularly important. In this case Eq. (2) integrates into the usual equations for a Schottky barrier, which are

$$x = A \frac{(-\psi_0)^{1/2} - (-\psi)^{1/2}}{N^{1/2}} \quad , \qquad (3)$$

$$\lambda_0 = A \left(\frac{-\psi_0}{N} \right)^{1/2} \quad , \qquad (4)$$

$$-E(x) = \left(\frac{\partial \psi}{\partial x} \right)_x = \frac{2N(\lambda_0 - x)}{A^2} \quad , \qquad (5)$$

where $A \equiv (2K\epsilon_0/q)^{1/2}$, E is the electric field, and the barrier depth (λ_0) is defined as the value of x at which ψ becomes zero. A comparison of the two calculated potential distributions is shown in Fig. 3.

When an external potential bias (ψ_a) is placed across the crystal, the potential distribution changes, since the original conditions for equilibrium and neutrality are no longer valid. For the case where the electrical resistivity of the bulk

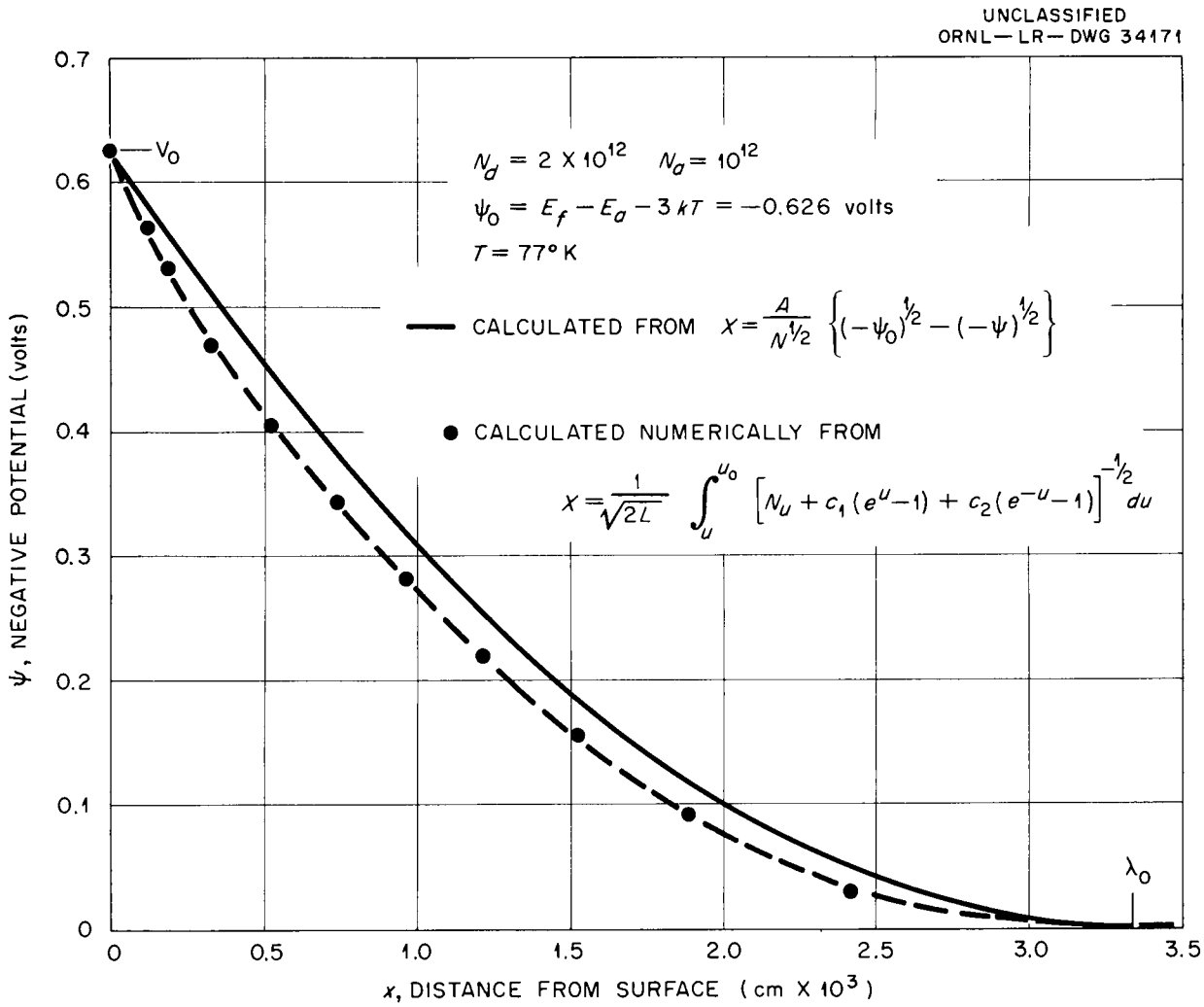

Fig. 3. Electrostatic Potential in Germanium Due to Surface States.

crystal is small, it can be assumed that all of the applied potential difference occurs across the barrier region. In this case, with the current flow neglected, the potential distribution, barrier depth, and electric field in the crystal may be obtained by replacing ψ_0 with $\psi_T \equiv \psi_0 + \psi_a$ and λ_0 with λ.

Equations (3), (4), and (5) characterize a typical Schottky barrier whose dynamic capacitance (C_c) is given by

$$\frac{1}{C_c^2} = \frac{8\pi}{KqN}(-\psi_T) = \frac{1.41 \times 10^8 (-\psi_T)}{KN}, \quad (6)$$

if C_c is to be in $\mu\mu f/cm^2$ and ψ_T in volts. For the cases under consideration we have demonstrated that these relations hold at least down to 77°K by the measurements of capacitance as a function of applied potential shown in Fig. 4. However, the experimental evidence indicates that Eqs. (3) through (6) are not valid at liquid-helium temperatures, where the resistivity of the crystal approaches that of a good insulator.

The magnitude of ψ_0 depends on the energy location and density of surface states and on the location of the Fermi level in the crystal. In the very pure n-type crystals used in these experiments, the location of the Fermi level energy ranged from within kT of the center of the forbidden band gap at 300°K to very near E_d at liquid-helium temperatures. This is shown in Fig. 5. No experimental attempt was made to determine either the densities or energies of the surface states.

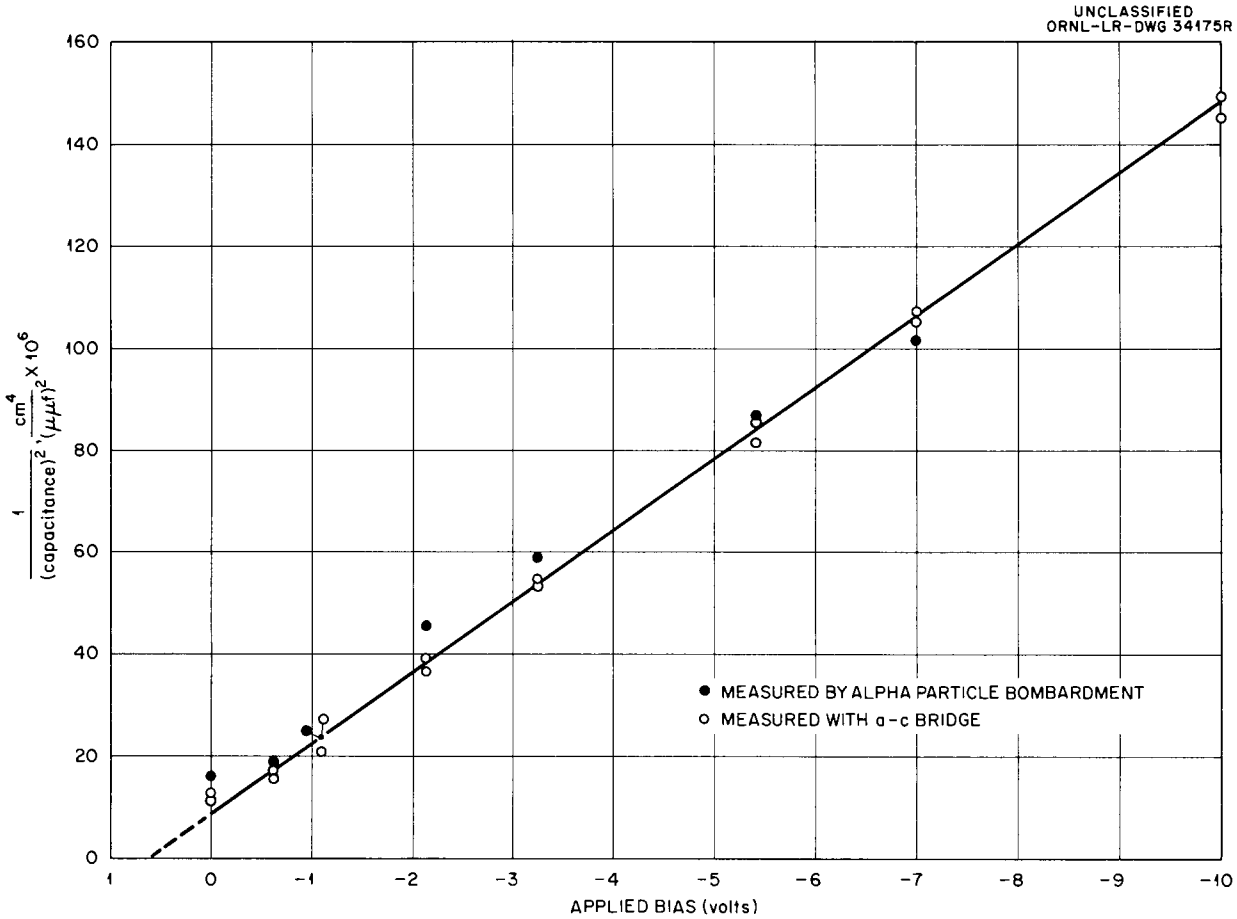

Fig. 4. Capacitance of Counter G-4-4 at 77°K as a Function of Applied Bias.

The size of the voltage pulse induced across the counter by a short-range ionizing particle with energy W is given by

$$V = \frac{1}{C_c + C_p} \frac{qW}{\epsilon} \eta \ , \qquad (7)$$

where C_p = stray capacitance in circuit, ϵ = average energy need to create a free electron hole pair in germanium, and η is the apparent efficiency of charge collection. The quantity η includes all possible mechanisms for charge-carrier loss, such as recombination and short-term trapping (for times in excess of either the RC time constant of the circuit or the pulse-clipping time constant in the amplifier). If, as was usual in this work, the capacitance of the counter is large compared with C_p, Eq. (7) becomes

$$V = \left(\frac{8\pi q}{K}\right)^{1/2} \frac{-\psi_T}{N} \frac{W\eta}{\epsilon} \ . \qquad (8)$$

The rise time of the voltage pulse may be estimated from the mobilities of the charge carriers and the electrostatic potential distribution in the crystal. Consider the case where an alpha particle with a range (R) of 2×10^{-3} cm enters a counter in which $N = 10^{12}$ cm^{-3}. If ψ_T is 5.5 v, λ is 10^{-2} cm and the maximum value of the electric field is approximately 10^3 v/cm. The time required for any small element of charge to move from position x_1 to position x_2 is given by

$$t \cong \frac{A^2}{2N\mu} \left| \ln (\lambda - x) \right|_{x_2}^{x_1} \ . \qquad (9)$$

The time required to move from potential ψ_1 to ψ_2 is

$$t \cong \frac{A^2}{N\mu} \left| \ln \psi \right| \frac{\psi_2}{\psi_1} \ , \qquad (10)$$

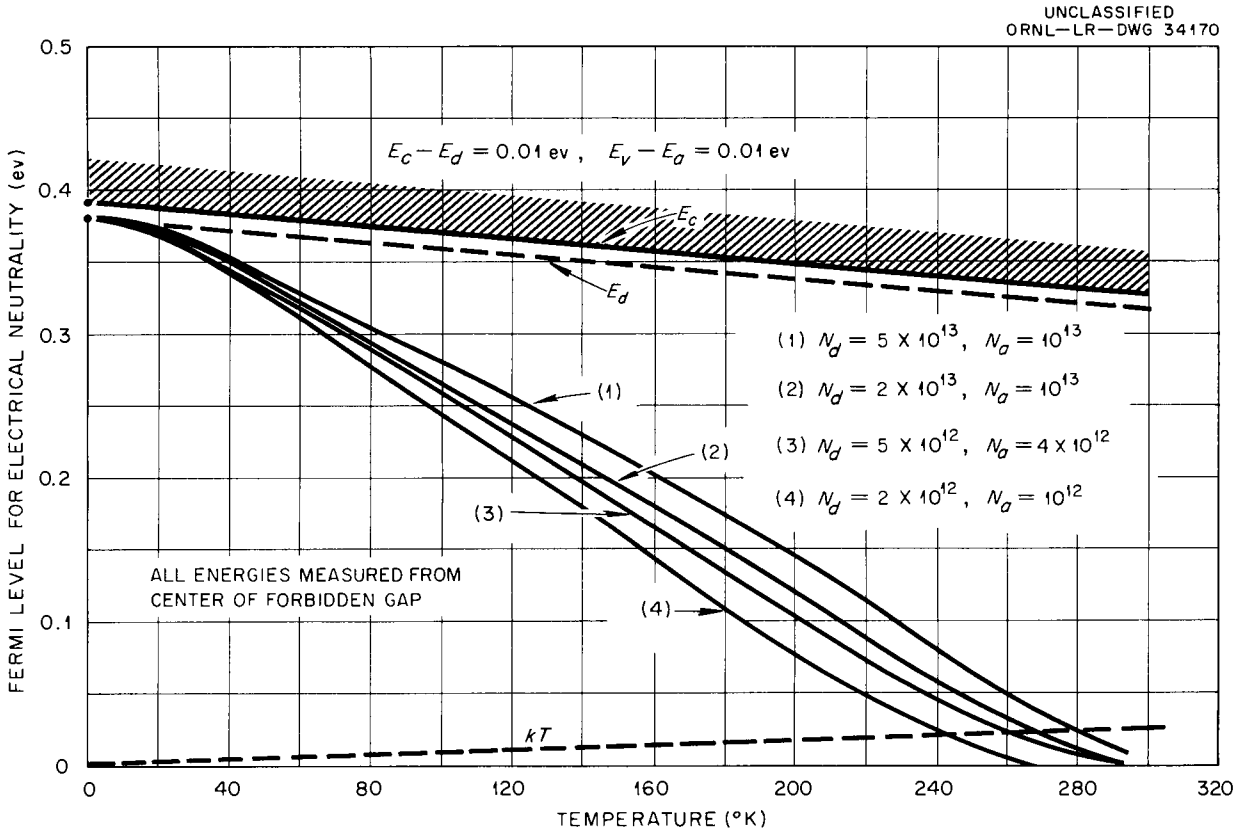

Fig. 5. Fermi Level as a Function of Temperature.

where μ is the average mobility of the charge carrier. At 77°K the average mobility of the holes is on the order of 2×10^4 cm^2/v-sec, and the longest distance any hole must travel is R. From Eq. (9) the time required for all the holes to traverse the barrier region is $\sim 10^{-10}$ sec. The longest distance any electron must travel is λ. It is immediately apparent that Eqs. (9) and (10) diverge under these conditions. However, all that is actually required is for the electron to get within 1 mean free path of λ, or, from a more practical point of view, for it to traverse most of the voltage gradient. If an average electron mobility of 1.5×10^4 cm^2/v-sec is assumed, the time required for the electron to traverse 90% of the electric field is $\sim 6 \times 10^{-9}$ sec.

DESCRIPTION OF COUNTER AND EQUIPMENT

The counters used in this study were made from high-purity (30 ohm-cm, $N = 10^{12}$ to 5×10^{13} cm^{-3}) single-crystal germanium. The active elements of the counters consisted of plates cut from a germanium crystal with a diamond saw. The plates were prepared by lapping and etching in CP4 (by volume, 5 parts concentrated HNO_3, 3 parts 48% HF, 3 parts glacial acetic acid). The electrodes were applied by vacuum evaporation of a thin (200 to 2000 Å) layer of gold onto the two large faces of the plate. The residual air pressures ranged from 0.1 to 1 μ Hg. After the gold electrodes were applied, the counters were installed in a mounting similar to the one illustrated in Fig. 6. Approximately 20 successful counters, with counting areas ranging from a few square millimeters to 5 cm^2, were constructed.

Figure 7 shows a typical electrical circuit for detection of charged particles with a surface barrier counter. The symbols C_c and R_c represent, respectively, the effective (small signal) capacitance and d-c resistance of the counter. The effective capacitance was of the order of several hundred micromicrofarads per square centimeter of counting area, and the d-c resistance was usually several megohms or more.

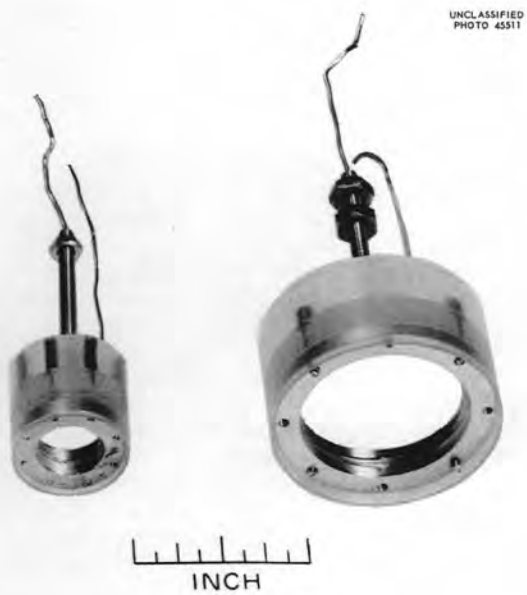

Fig. 6. Germanium Surface Barrier Counters.

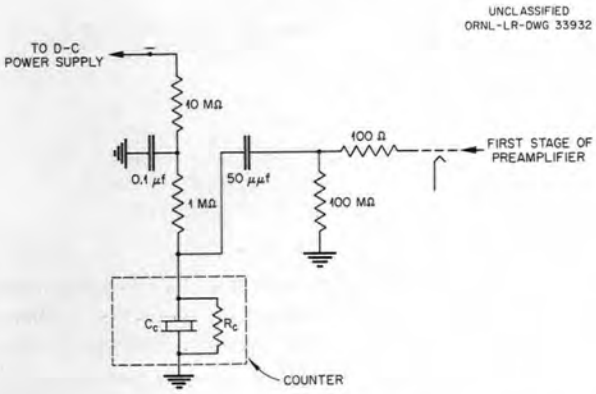

Fig. 7. Surface Barrier Counter and Preamplifier.

Data on the properties of surface barrier counters as alpha-particle and fission-fragment detectors were obtained in a liquid-helium cryostat which was capable of cooling the counter and uranium source to 1.3°K. A sample containing U^{233} served as a source of alpha particles and also emitted fission fragments when bombarded with thermal neutrons.

EXPERIMENTAL RESULTS

Figure 8 shows the pulse-height distribution obtained from a thin U^{233} source with a 1-cm-dia counter. The 4% full width at half maximum in the main peak is close to that expected from noise in the preamplifier. The two small satellite peaks and several additional peaks at higher pulse heights (not shown in Fig. 8) were caused by impurities in the source.

Figure 9 shows the pulse-height distribution obtained for fission fragments from thermal-neutron-induced fission of U^{233}. These data were obtained at 4.2°K with the use of a 1-cm-dia counter. Comparison of the location of the peaks in Fig. 9 to the known energy distribution of fission fragments indicates that, at this temperature, the response of the counter to particle energy was nearly linear.

The effective capacitance of the barrier layer at any applied voltage, as well as the value of ϵ/η,

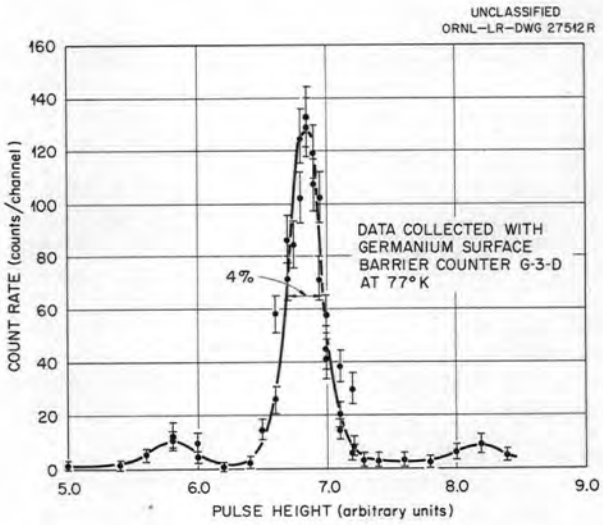

Fig. 8. Pulse-Height Distribution for U^{233} Alpha Particles.

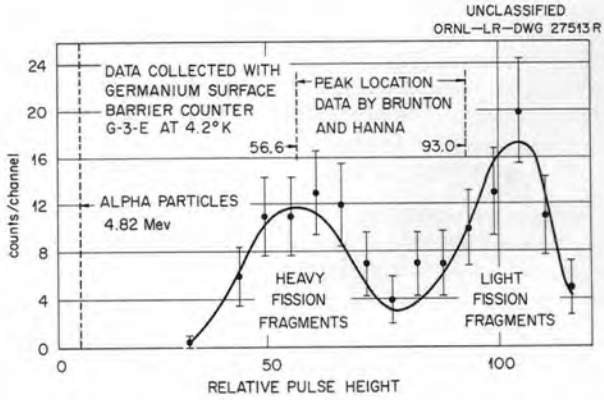

Fig. 9. Pulse-Height Distribution of U^{233} Alpha Particles and Thermal Fission Fragments.

was determined by measuring the pulse height resulting from bombardment with monoenergetic alpha particles at 77°K. These measurements were accomplished by placing a variable capacitor in parallel with the counter and measuring the pulse height as a function of applied voltage and external capacitance. The barrier capacitance as a function of applied bias at 77°K was also measured with a small-signal a-c bridge. Figure 4 shows the capacitance of a 1-cm-dia counter as a function of applied bias. Within the accuracy of the measurements, the values of C_c, as determined by the bridge method, were independent of frequency from 100 cps to 10 kc and were independent of a-c signal from 10 to 100 mv peak to peak. According to Eq. (6) the values of N and ψ_0 can be determined directly from the slope and intercept of Fig. 4. Although the accuracy of the data was insufficient to permit a precise determination of ψ_0, the experimental value of 0.6 v is in reasonable agreement with the maximum possible value at this temperature. The value of N as determined from Fig. 4 is 1.4×10^{12}; this agrees quite well with the value of 1.5×10^{12} determined by Hall coefficient measurements on the parent crystal.

Figure 10*a* shows the pulse height (V) as a function of applied bias (V_a) resulting from bombardment of a 1-cm-dia counter with U^{233} alpha particles at 77°K. The variation of pulse height with applied bias is caused both by a change in the capacitance of the counter and by an increase in η with increasing bias. The failure of the pulse height to go to zero as the externally applied bias goes to zero is a direct consequence of the fact that the barrier exists even in the absence of externally applied bias.

Figure 10*b* shows the measured values of ϵ/η at 77°K as a function of externally applied bias. If it is assumed that η goes to unity as the bias is increased, the limiting value of ϵ/η is in good agreement with McKay's[4] value of $\epsilon = 3.0 \pm 0.4$ ev per pair.

The rise time of pulses resulting from bombardment with monoenergetic alpha particles at 77°K was measured for a 1- and a 0.1-cm-thick counter. In both cases the experimentally determined rise time was $\sim 2 \times 10^{-8}$ sec, which is in reasonable agreement with the predictions of simple surface barrier theory.

At 4.2°K the pulse rise time for the 1-cm-thick counter was 2×10^{-7} sec. Since the carrier mobilities would be expected to be larger at 4.2°K than at

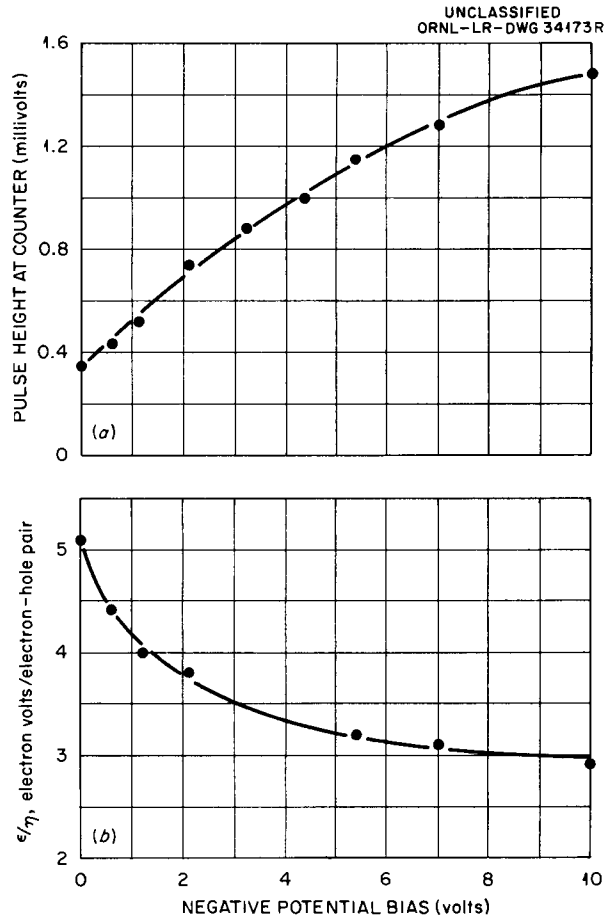

Fig. 10. (*a*) Pulse Height as a Function of Bias Voltage for U^{233} Alpha Particles on Germanium Surface Barrier Counter G-4-4 at 77°K; (*b*) Ratio of Energy per Electron-Hole Pair to Apparent Collection Efficiency as a Function of Applied Bias.

77°K, this relatively long pulse rise time indicates that at very low temperatures (where the resistivity of germanium approaches that of a good insulator), there were significant electric fields extending through a substantial portion of the crystal when external bias was applied. However, measurements of the details of pulse shape, the effective capacitance, and the apparent charge collection efficiency which would be needed to provide a detailed picture of this behavior have not been performed.

One counter has been operated successfully at temperatures down to 0.15°K. It was noted that alpha-particle pulses were completely suppressed in fields of a few kilogauss applied parallel to the surface.

CONCLUSIONS AND POSSIBILITIES FOR FUTURE STUDY

Under proper operating conditions, germanium surface barrier counters make excellent detectors for short-range charged particles. Their apparent freedom from direct recombination makes them particularly useful for resolving pulses from particles which create different specific ionization densities. The very fast rise time associated with pulse formation indicates that they might also prove useful for fast coincidence counting, particularly in experiments which involve counting of fission fragments.

The range of sizes and the compactness of a complete unit make them potentially very useful in experiments where space is an important consideration. Their compactness might also make them useful for constructing matrices containing a large number of small individual counting elements.

Since this investigation was primarily concerned with counting of short-range particles at low temperatures, no attempt has been made to develop a device which would operate successfully at room temperature. None of the counters produced by the techniques described under "Description of Counter and Equipment" have been successfully operated at temperatures above 216°K (dry-ice temperature). However, Mayer and Gossick[5] have produced small counters of this type which work quite well at room temperature. Their success, combined with the fact that other investigators have produced large surface barrier photovoltaic cells,[7] indicates that additional work might lead to the development of a large-area surface barrier counter with reasonably large resistance and small capacitance at room temperature. Development of a reliable surface treatment which produces a large density of surface states near the bottom of the forbidden gap would be a large step toward this goal.

[7] E. Simon, unpublished thesis, Purdue University (Jan. 1955).

A 60° DEFLECTION, DOUBLE FOCUSING, UNIFORM FIELD, REACTION PRODUCT MAGNET

H. B. Willard J. K. Bair

A double focusing, uniform field magnet has been designed and constructed[1] for the analysis of charged particles from nuclear reactions. The theory developed by Cross[2] gives the relationships for conditions of double focus. In his notation our design parameters were:

Bending radius, ρ	15 in.
Object distance, l'	1 (in units of ρ)
Image distance, l_d''	2.061 (in units of ρ)
Angle of incidence, ϵ_1	56° 34′
Angle of deflection, ϕ	60°
Angle of emergence, ϵ_2	−32° 16′
Sector angle, Ω	35° 42′
Total gap width, $2g$	0.75 in.
Entrance half angle (bending plane), α_{max}	±5.5°
Entrance half angle (direction of H), ω_{max}	±1.1°
Solid angle, S_{max}	0.006 steradian

This choice of values assures that the second-order focusing terms (in α^2) will be zero, minimizing aberrations. The theoretical momentum resolution will then be

$$\Delta s \frac{p}{\Delta p} = 809 \text{ mm} \quad ;$$

that is, the momentum resolution for a 1-mm-wide object should be 0.12%, while the energy resolution would then be 0.24%. The magnification in the bending plane should be −0.77, while in the direction of the gap it should be +4.47.

The actual pole face boundaries were then corrected for the fringing field by a method due to Bainbridge,[3] displacing the entrance edge inward by 0.92 in. and the exit edge inward by 1.16 in. The corrected object and image were displaced 0.26 and 0.88 in. from the median ray, respectively. Figure 1 illustrates all the above geometrical considerations.

[1] Constructed to our specifications by Pacific Electric Motor Co., Oakland, Calif.

[2] W. G. Cross, *Rev. Sci. Instr.* 22, 717 (1951).

[3] K. T. Bainbridge (E. T. Segre, ed.), *Experimental Nuclear Physics*, vol I, part V, p 582, Wiley and Sons, New York, 1953.

UNCLASSIFIED
ORNL-LR-DWG 36655

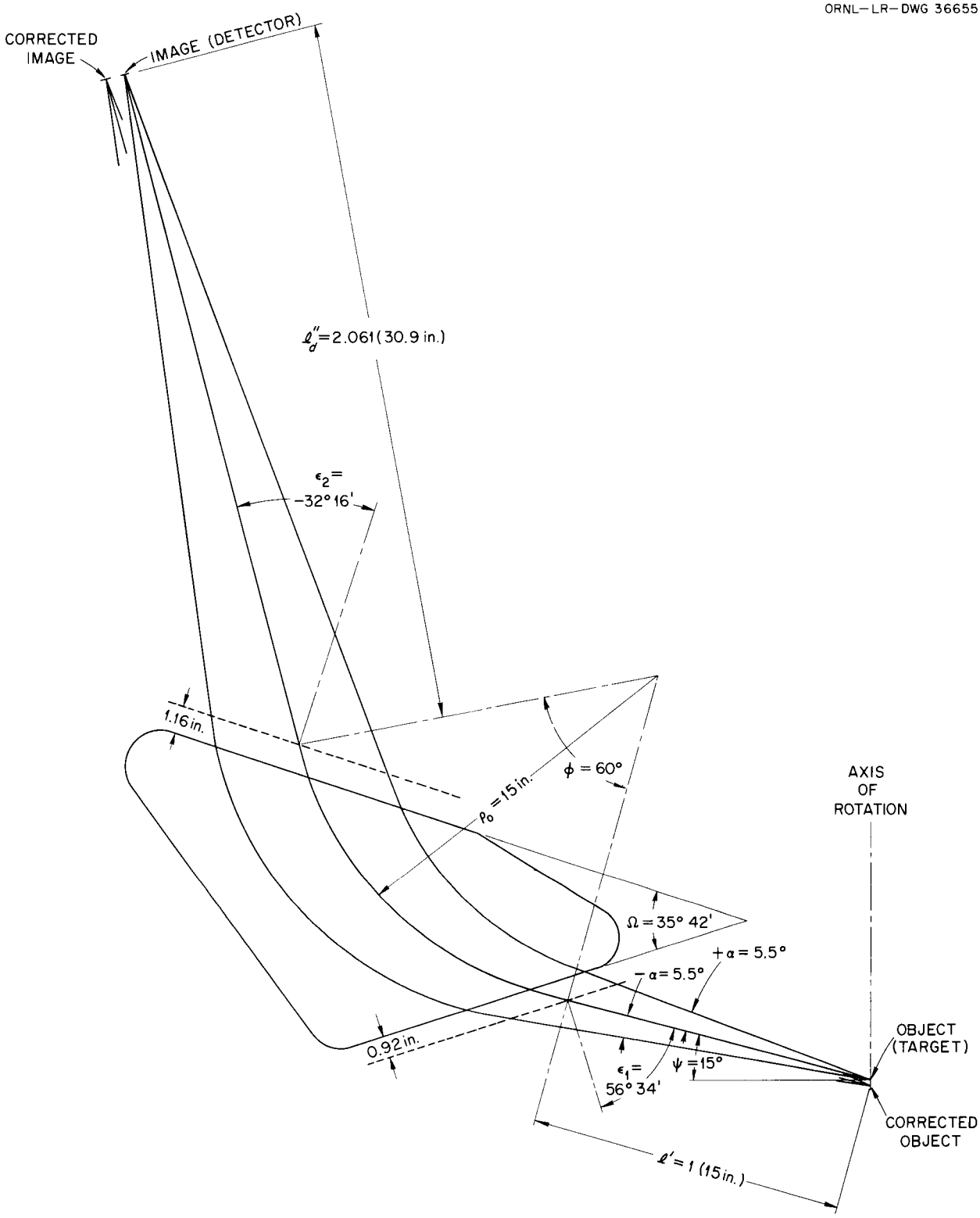

Fig. 1. Geometrical Drawing of Focusing Arrangement.

In order to achieve the maximum solid angle with the minimum gap, the sides of the vacuum chamber are the pole faces, with a stainless steel strip welded around the edges to form a seal. Both pole faces and the H-type yoke of the magnet are made of Armco iron. This allows a maximum field of 16,000 oersteds to be reached, which will bend 17.6-Mev protons. The measured curve of H vs I is shown in Fig. 2. Current stabilization to better than 1 part in 10^4 is achieved by a three-phase electronically regulated power supply.[1]

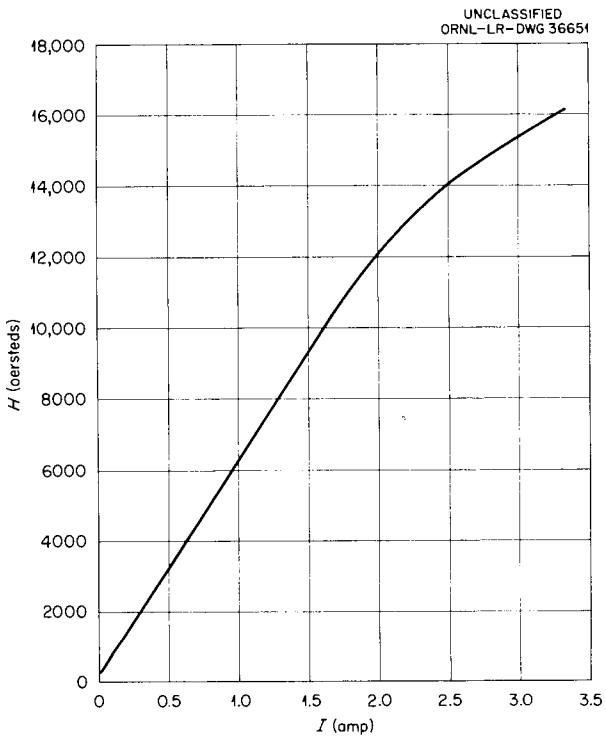

Fig. 2. Magnetic Field as a Function of Magnet Current.

The magnet is located so as to deflect particles upward vertically after being emitted from a target at an angle of 15° above the horizontal plane. A sliding vacuum seal in the target chamber then permits continuous rotation of the magnet for laboratory angles of 15 to 145°.

Momentum resolutions were measured, with both thick and thin targets of gold, by elastic scattering of protons. Figure 3 shows this resolution in per cent as a function of the entrance angle $\pm\alpha$. When a 1- by 1-mm object size is observed with a 0.6- by 15-mm exit slit, the theoretical resolution is achieved at small angles. Utilizing the full solid angle it is a factor of 2 worse, presumably due to aberrations. Figure 4 is a curve of the resolution at full solid angle as a function of exit slit width, again for a 1- by 1-mm object size. A typical resolution curve, this time in energy, is shown in Fig. 5 for protons elastically scattered by gold.

A determination of the maximum solid angle of the magnet was obtained from the thick target data, making use of the known Coulomb scattering cross section. The result of 0.005 ± 0.001 steradian is in good agreement with the theoretical value.

Preliminary data on the elastic scattering of protons by Si^{28} has also been obtained.

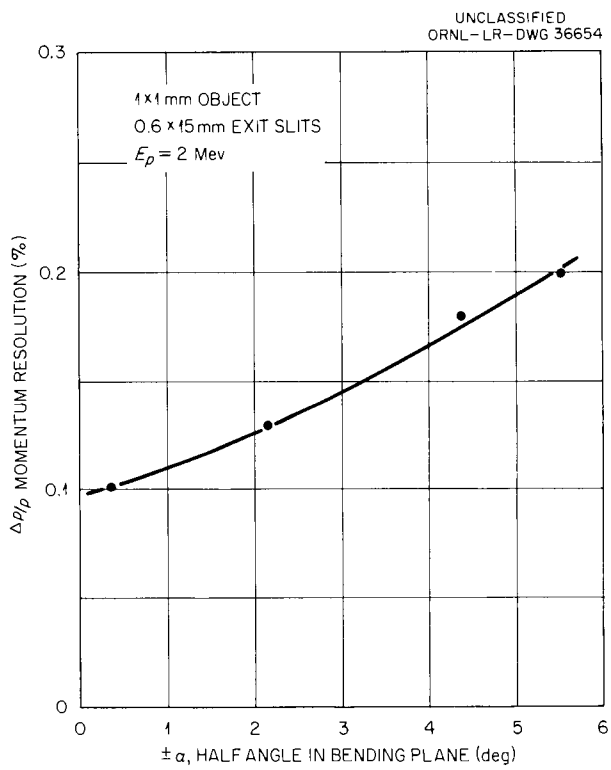

Fig. 3. Momentum Resolution as a Function of Entrance Half Angle α.

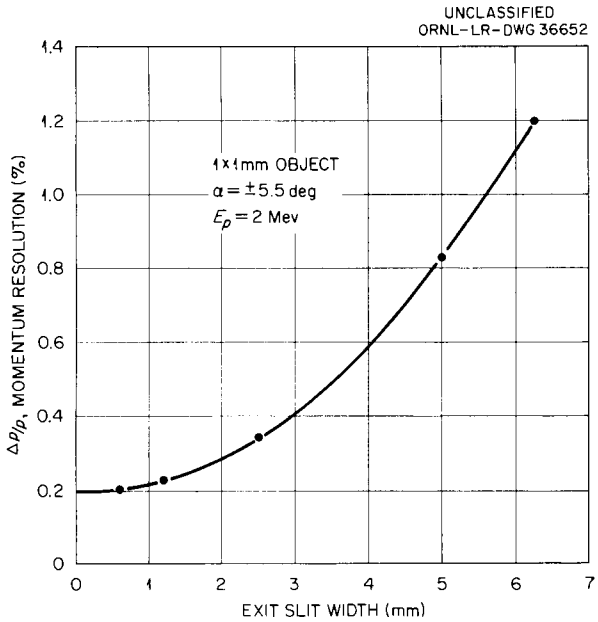

Fig. 4. Momentum Resolution as a Function of Exit Slit Width.

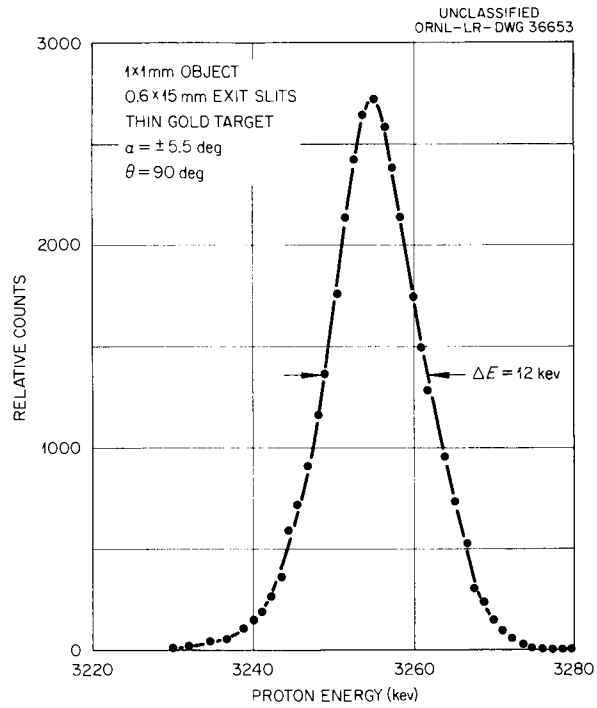

Fig. 5. Elastic Scattering Energy Resolution for a Thin Gold Target and the Full Magnet Solid Angle.

LARGE-OUTPUT TIME-TO-VOLTAGE CONVERTER FOR HIGH COUNTING RATES

D. G. Maeder

INTRODUCTION

One of the most flexible methods for measuring short time intervals consists in the linear charging of a capacitor, C, during the unknown time interval $T = t_2 - t_1$ (t_1 = "start" time, t_2 = "stop" time) and subsequent measurement of the voltage change across C. When applying this technique to measurements in the nanosecond (1 nsec = 10^{-9} sec) range, suitable switching signals for turning the charging current, i_1, on and off are available only from low impedance sources (~ 100 ohms) which barely develop enough voltage to cut off any tube. Most suitable among presently available long-life tubes appear to be the following:

E88CC (triode), 1 → 20 ma with 2.1-v grid swing

E180F (pentode), 1 → 20 ma with 1.7-v grid swing

Figure 1 depicts possible arrangements of switching tubes, including one based on double grid control (Fig. 1*b*) using a 6AS6 or 6BN6[1] tube, which requires larger grid swings (3 to 5 v) for efficient switching. Figure 1*a* shows the basic method used presently at ORNL,[2] where switching speed is limited mainly by the response of the coupling diodes. According to Figs. 1*a* and 1*b*, conversion linearity and stability would depend on tube characteristics, whereas the actual ORNL design[2] makes use of a "long tail" cathode circuit with a 1N34A clamping diode, in order to stabilize total

[1] W. Weber, C. W. Johnstone, and L. Cranberg, *Rev. Sci. Instr.* 27, 166–70 (1956).

[2] J. H. Neiler *et al.*, *Phys. Semiann. Prog. Rep. Sept. 10, 1955*, ORNL-1975, p 66.

UNCLASSIFIED
ORNL-LR-DWG 35643

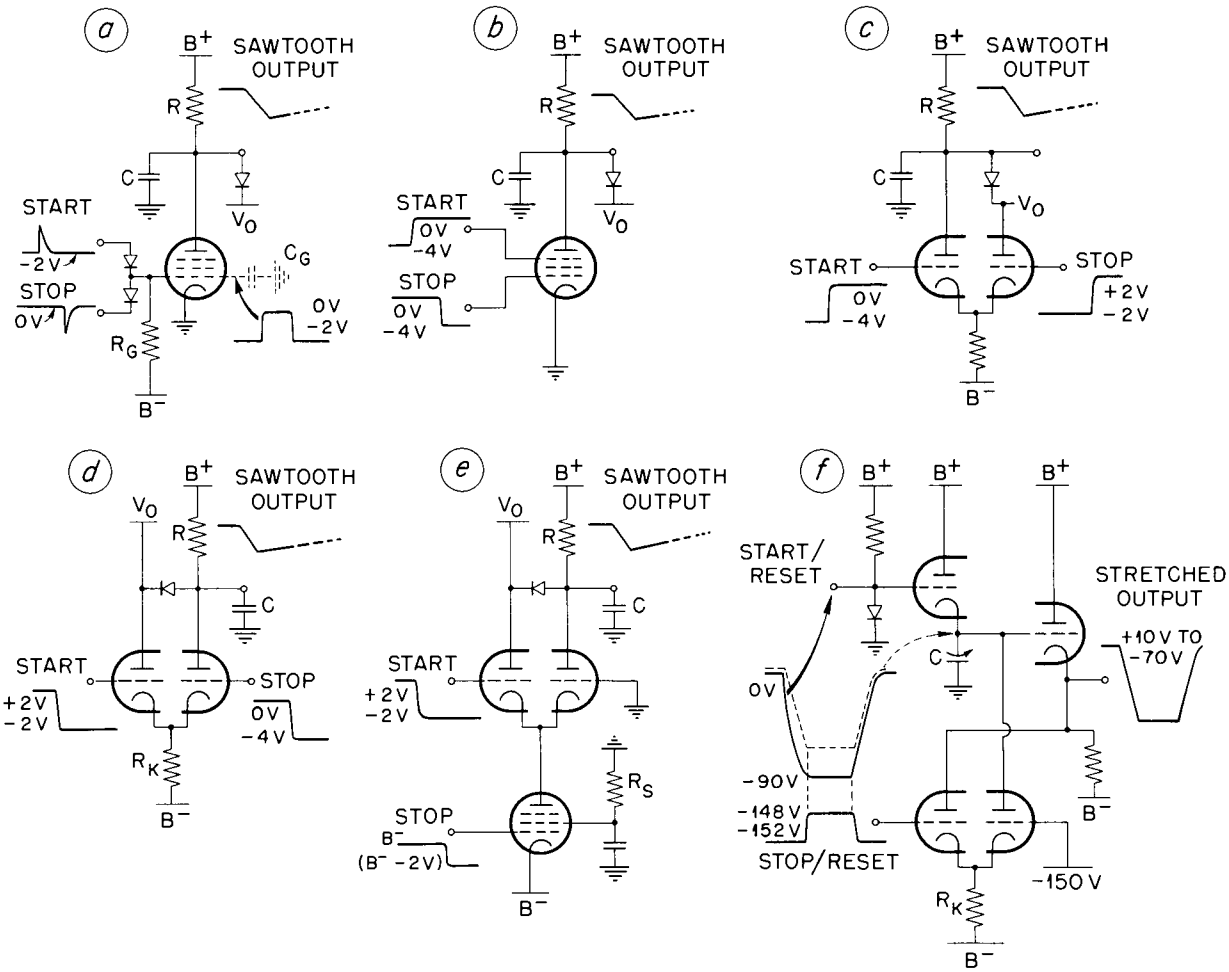

Fig. 1. Compilation of Basic Time-to-Pulse-Amplitude Converter Schemes.

cathode current. With this scheme the current flowing into C is still sensitive to the screen-to-plate current ratio of the particular tube. At the expense of requiring an increased switching signal (4 v, compared with about 3 v, ref 2), the cathode clamping diode may be replaced by a triode, as in Figs. 1*c* and 1*d*, so that all of the transferred current is used to charge C. In Fig. 1*e* the two switching operations (on/off) are assigned to two separate tubes, with the advantage that the triode grid facing the output does not have to carry any signal. Again, the stability of the lower tube plate current could be improved by "long tail" techniques as discussed above (requiring a 3- or 4-v "stop" signal instead of only 2 v).

LEVEL OF OUTPUT PULSES

Since $i_0 \ll i_1$ (i_0 denoting the quiescent current) is not compatible with extremely fast switching, the voltage drop i_0R in the circuits of Fig. 1 cannot in general be neglected. We must choose $R > T_{max}/\epsilon C$ (where T_{max} = longest interval $t_2 - t_1$ to be measured) if the time-to-amplitude conversion at low repetition rates is to be (differentially) linear within a relative error of $\pm\epsilon/2$. The output amplitude is thus limited to

$$\Delta V_{max} = \frac{T_{max}(i_1 - i_0)}{C} < \epsilon R(i_1 - i_0)$$

or, since the drop across R should be limited to

about half the plate supply voltage,

$$i_0 R < \frac{1}{2} B^+ ,$$

output amplitudes must be kept below

$$\Delta V_{max} < \frac{\epsilon}{2} \frac{i_1 - i_0}{i_0} B^+ \cong \frac{\epsilon}{2} \frac{i_1}{i_0} B^+ . \qquad (1)$$

Even with a high switching ratio (e.g., $i_1/i_0 = 10$) and ideally constant i_0 and i_1 values, a $\pm 1\%$ differential linearity can be expected only for output pulses smaller than one-tenth of B^+.

In addition, at a high counting rate ν, the average duty cycle $\nu\overline{T}$ determines the effective charging current, which then becomes

$$(i_1 - i_0)(1 - \nu\overline{T}) ,$$

while the average drop across R is increased to

$$[i_0 + \nu\overline{T}(i_1 - i_0)] R ,$$

which must be $< \frac{1}{2} B^+$. In order to keep rate-dependent variations of the time conversion factor within $\pm\delta/2$, the repetition rate is limited to

$$\nu_{max(RC)} < \frac{\delta}{\overline{T}} = \frac{\delta}{T_{max}} \cdot \frac{T_{max}}{\overline{T}} . \qquad (2)$$

Since the average of the time intervals between actual "start" and "stop" pulses may be much larger than T_{max}, the longest interval of interest for the conversion (even with pulsed accelerator experiments, in cases where a fast-particle spectrum is to be measured in the presence of a slow-particle group), and since δ should be small ($\lesssim 10^{-3}$) to preserve good time resolution with random pulses, the counting rates are seriously limited, with all schemes depending on a slow exponential decay of the output pulse. The plate circuit diodes indicated in Figs. 1*a* to 1*e* would improve this situation but are likely to introduce nonlinearities (considering the small amplitude of the output pulses), and therefore are usually omitted.

A design free of the limitations (1) and (2) results from the use of a tube-controlled fast resetting circuit to replace the leak resistor R ($R \to \infty$). If the reset signal is delayed, a period of constant output voltage is obtained after the "stop" signal, as shown in Fig. 1*f*, which is the basic circuit adopted for the new converter described below.

The large output amplitude capability and the stretching feature of this arrangement make it feasible to feed the converter output directly into a multichannel sorting device. Thus separate amplifiers, pulse clipping networks, and pulse stretchers between the time conversion and the voltage measurement are eliminated, which otherwise are potential sources of scale factor and scale zero drifts, nonlinearities, counting rate dependence, and overload effects. Since the previous history is wiped out by the resetting action, the converter can handle close to

$$\nu_{max(fast)} \cong \frac{1}{T_{max} + T_{stretch} + T_{reset}}$$

"start" pulses per second.

These advantages have to be paid for by the increased amplitude required at the "start" input. However, only the rapid traversal of the first 4 v has an effect on the time resolution of the converter, provided that the rest of the negative "start" wavefront proceeds somewhat faster than the linear saw tooth at the converting and stretching capacitor C. The "start" signal is produced by a fast flip-flop and finally reaches an amplitude of nearly 90 v. The maximum useful output signal is smaller than this value by the cutoff bias of the left upper triode in Fig. 1*f*.

OPERATION

The actual circuit diagrams of the "start" flip-flop (which is built into the phototube mounting, in order to keep the total capacitive load of the triggering input $\lesssim$ 15 pf, 1 picofarad = 10^{-12} f) and of the converter chassis (located about 150 cm away from the detector assembly; connecting cable ~33 pf) are shown in Figs. 2 and 3.

The logical operations of the complete arrangement can be summarized as follows:

1. Cut off a clamp tube (T_8, left half – Fig. 3) by a pulse from the "start" detector (T_2 – Fig. 2, flipped by phototube pulse). This initiates linear charging of the measuring capacitor C_1 and "arms" a gate circuit (T_2 – Fig. 3) to permit action (2) to take place.

2. Cut off a constant-current tube combination (T_5, T_6 – Fig. 3) by a pulse from the "stop" detector (via T_1, T_2, and the flip-flop $T_{3B} + T_{4A}$ – Fig. 3). This marks the beginning of the stretching period, subject to condition (4).

UNCLASSIFIED
ORNL-LR-DWG 37476

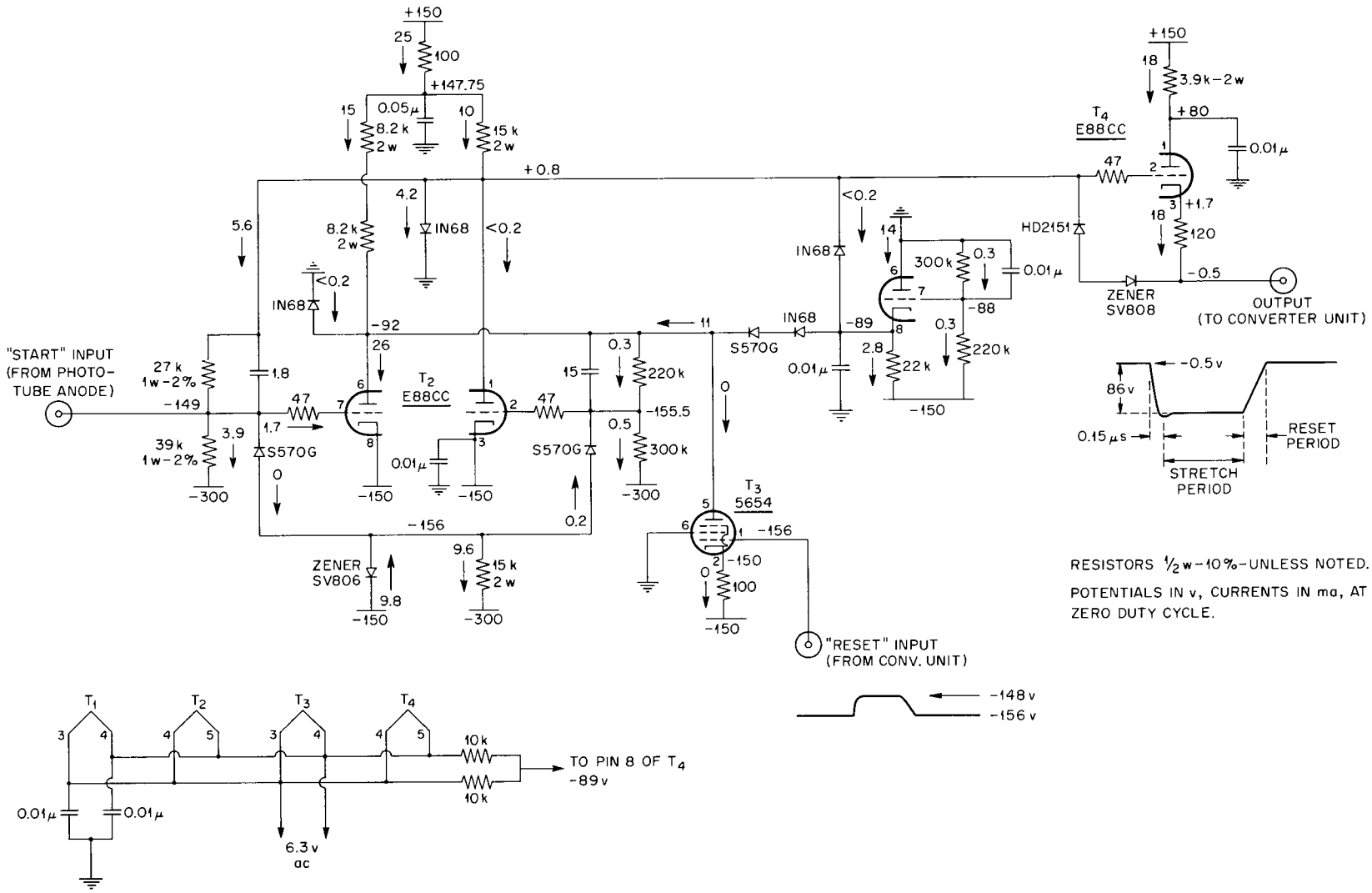

Fig. 2. Circuit Diagram of "Start" Detector Unit. Tube T_1 (5654), not shown here, is a cathode follower used for a linear signal which is picked from the tenth dynode of the phototube.

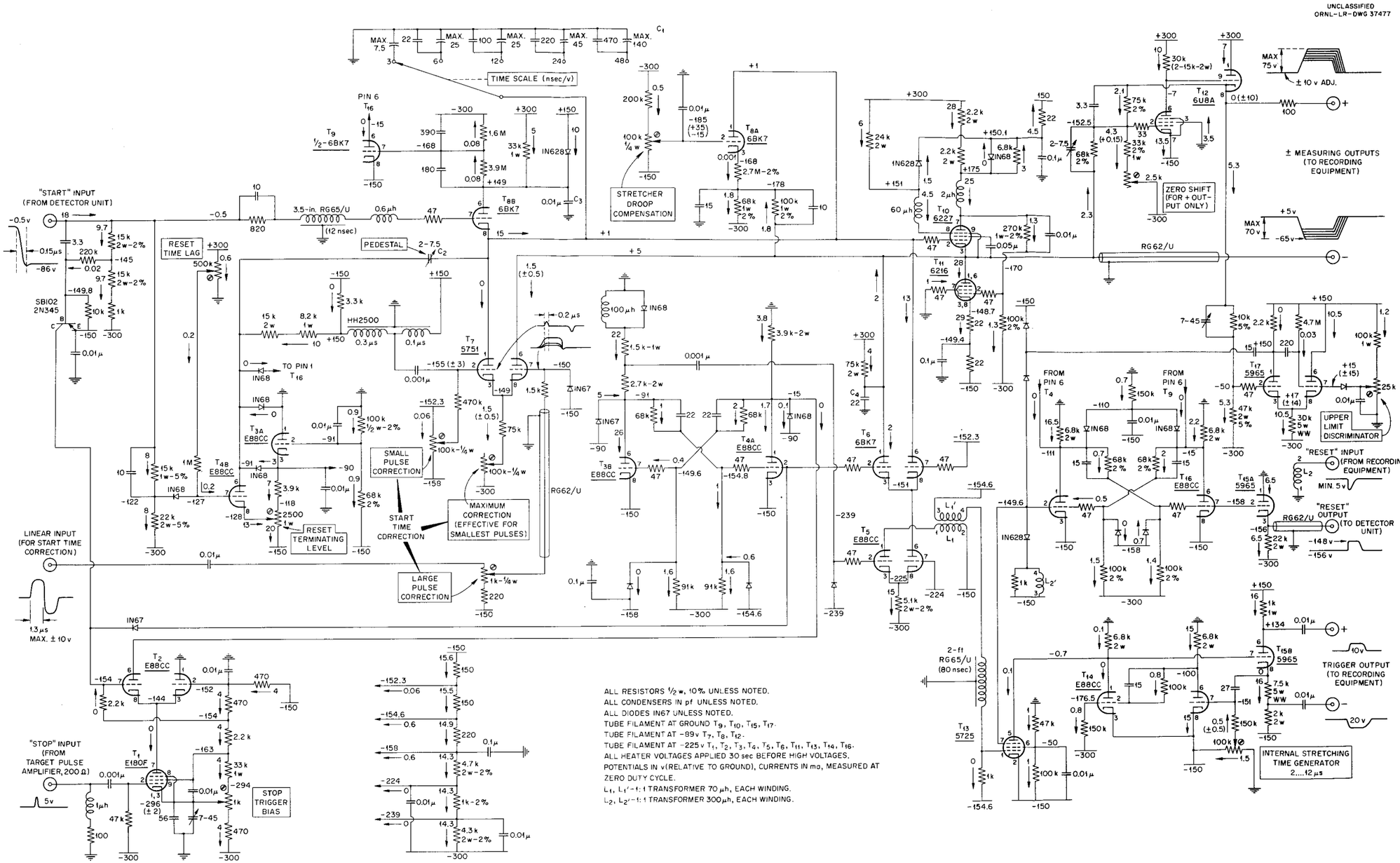

Fig. 3. Circuit Diagram of Converter Unit. Note: C_4, the diode-coupled plate load for T_{6A}, reduces the capacitive feedback signal on the grid of T_{6A}. Otherwise $T_{3B} + T_{4A}$ tend to retrigger when reset starts.

3. Discriminate, by means of a Schmitt circuit (T_{17}) receiving the inverted (T_{12}) (i.e., positive-going) output signal, against a "stop" delay exceeding the useful range. Lack of a useful "stop" signal thus leads to the generation of an "upper limit pulse" at time T_{max} after "start."

4. Produce a trigger output signal (T_{14}, T_{15}) upon occurrence of a useful "stop" signal [see (3)], as checked by the gate T_{13}. The trigger output is used to initiate the voltage measuring procedure, for example, in a multichannel sorter.

5. Turn on the clamp tube (T_{8B}) upon either (*a*) occurrence of an "upper limit pulse" [see (3)] (flipping T_{16}, right half, into conduction), (*b*) a "reset" pulse received from the voltage measuring (multichannel) equipment (flipping T_{16} as above), or (*c*) charging of a large auxiliary capacitor (C_3) to a certain level, turning on a "watchdog" circuit (T_9, will flip T_{16}) which takes care of the case that (*a*) or (*b*) might fail. Either of the events (*a*), (*b*), or (*c*) initiates the resetting period, defined by one state of the reset flip-flop circuit (T_{16}).

6. During the resetting of the "start" detector unit, action (1) is inhibited (by T_3 – Fig. 2).

7. Near the end of the reset (as checked by the 2N345 transistor), the constant-current tube is switched on again [see (2)] and the gate (T_2 – Fig. 3) disabled.

8. Terminate the resetting period by switching the reset flip-flop (T_{16}) back when the clamp tube grid potential reaches its quiescent value within a few volts (as checked by T_{4B} – Fig. 3).

Since practically all these operations are performed by d-c coupled logical circuitry, the time conversion factor and stretching period may be chosen arbitrarily in a wide range. With the minimum C_1 value set at 39 pf (including wiring and tubes) and a charging current of 13 ma, conversion factors of 3, 6, 12, 24, and 48 nsec/v are available at the negative-going output. When the upper limit is set at 67 v, the full time range can be selected between T_{max} = 200 nsec and 3.2 μsec.

LINEARITY AND COMPENSATING CIRCUITS

A constant (±1%) current of 15 ma is maintained by cathode degeneration in T_5 (Fig. 3); (87 ± 2)% of this current is drawn from C_1 during the conversion period. In order to keep the current ratio between the two halves of T_6 constant, regardless of the large amplitudes of converter output signal, essentially the same potential excursion is applied to both anodes of T_6 (by connecting the nonconducting anode to the cathode follower output of the converter).

When T_{4A} is flipped into conduction, most of the current in T_6 is rapidly transferred to its left section. Since the fast grid signal is limited to about 5 v, additional (somewhat slower) switching is applied to T_5, cutting off the cathode current in T_6. Total combined leak currents through T_7 (left), T_8 (right), and T_6 (right) can thus be kept <1 μa during the stretching period, giving a droop of <0.025 v/μsec for the T_{max} = 200 nsec conversion range, or <0.5 v during any stretching period which is 100 times longer than a particular conversion range selected.

Tube T_8 (left) is well enough cut off as long as the stretched pulse does not exceed a 50-v amplitude. To add another 20 v to the useful output range, T_8 (right) provides for a compensation of leakage currents, with two adjustable parameters (grid bias taken from 100-kilohm potentiometer; cathode resistor, 2.7 megohms, low-capacity mounting).

Tube T_7 compensates for a systematic dependence of the converter output on the "start" pulse amplitude, with three adjustable parameters. Such a dependence, sometimes called "walk" effect, is brought to evidence by two-dimensional records of pulse amplitude vs delay time such as shown in Fig. 4. In order to make this display available on a CR tube, a Tektronix type 511 A oscilloscope was modified to be triggered by a doubly clipped, flat-top proportional pulse from an A-8 amplifier only when a trigger output signal is received at the proper time from the time converter. The waveforms produced at the (*A*) measuring output, (*B*) trigger output, and (*C*) reset output of the converter are shown in Fig. 5, along with the (*D*) A-8 amplifier output and the (*E*) modified oscilloscope intensifier signal. These waveforms were observed when the "start" and "stop" signals originated from an NaI and a plastic scintillator, respectively, arranged on opposite sides of an Na^{22} source of annihilation rays. The phototubes (6810A) operated on the flip-flop circuit shown in Fig. 2 and on an E180F tube carrying 22 ma quiescent plate current, respectively. When the E180F tube was cut off, the grid was caught by an S570G diode at 3 v below cathode potential. The E180F plate line (200-ohm cable) was terminated with 390 ohms at the tube

UNCLASSIFIED
ORNL-LR-DWG. 37324

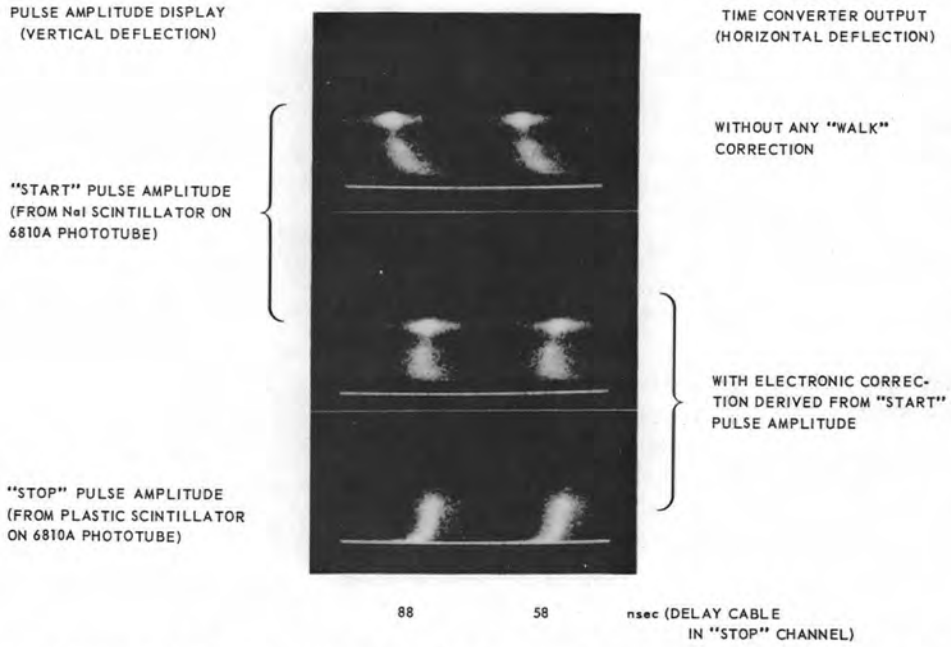

Fig. 4. Two-Dimensional Records of Pulse Amplitude vs Delay Time Distribution. Two groups have been obtained by using two different lengths of delay cable (200-ohm) for the display of annihilation coincidences from Na^{22}. The time axis was produced by uncorrelated random pulses.

UNCLASSIFIED
ORNL-LR-DWG. 37323

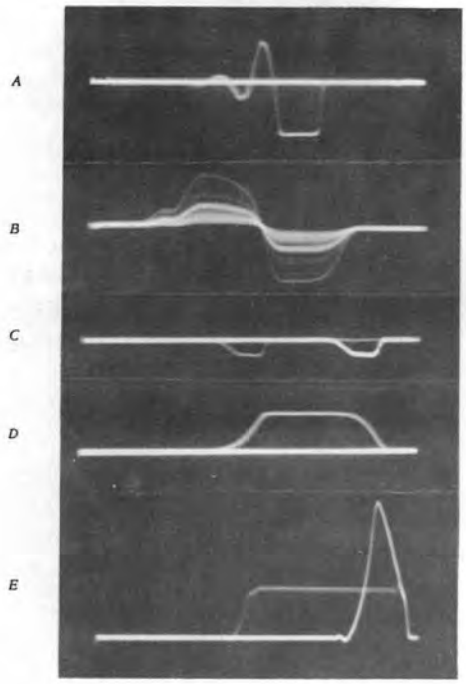

CONVERTER UNIT

(*A*) MEASURING OUTPUT, STRETCHED FOR 2 μsec WHENEVER A "STOP" PULSE IS RECEIVED BEFORE THE SWEEP VOLTAGE REACHES 70 v. OTHERWISE, THE SWEEP IS RESET IMMEDIATELY.

(*B*) TRIGGER OUTPUT, PRODUCING A PULSE ONLY IN THE CASE OF A USEFUL "STOP" SIGNAL.

(*C*) RESET OUTPUT, TO BE FED TO THE "START" DETECTOR UNIT. DELAYED RESET PULSES CORRESPOND TO USEFUL EVENTS.

DISPLAY UNIT

(*D*) PROPORTIONAL DETECTOR PULSE, FROM A-8 AMPLIFIER, DELAYED BY 0.9 μsec. THE AMPLITUDE DISTRIBUTION PRODUCED BY AN Na^{22} SOURCE CAN BE SEEN.

(*E*) UNBLANKING PULSE, TO BE FED TO CRT GRID, IS PRODUCED ONLY AFTER A USEFUL "STOP" SIGNAL. FITS INTO FLAT TOP OF (*D*).

Fig. 5. Waveforms in Time-of-Flight Measuring Equipment.

and 100 ohms + 1 μh at the converter input (see Fig. 3).

The "walk" effect is clearly seen in the upper part of Fig. 4; small "start" pulses (~100 kev) tend to fire the flip-flop (in Fig. 2) up to ~8 nsec later than do large ones (≧500 kev), thereby shortening the apparent $t_2 - t_1$ time interval. By feeding the linear signal to T_7, the slow output increment otherwise added through T_7 is canceled when a large linear signal occurs. The middle part of Fig. 4 shows that "walk" can even be overcompensated. The lower part of Fig. 4, which was obtained by displaying the "stop" pulses in the vertical direction, demonstrates the opposite sign of the "walk" associated with the "stop" pulse amplitude. In order not to lose part of the useful range of output voltage, the basic slow increment (and other undesirable increments) is balanced by a fixed-amplitude subtraction via a small capacitive coupling (C_2) to the positive wavefront occurring at the plate of T_{4B}. With the walk correction adjusted to give the smallest tail in the counting rate (positive-going converter output pulses per 0.3-v window), the full half width of the annihilation peak was measured as 4 nsec. When plastic scintillators were used for both "start" and "stop" detectors, the half width decreased to 3 nsec. A set of delay cables inserted in the "stop" channel, ranging from 30 nsec up to 180 nsec, gave a straight-line plot of peak locations (volts of output amplitude) within ±1 nsec on the T_{max} = 200 nsec range.

The behavior at variable counting rates is illustrated in Fig. 6. At 160,000 "starts"/sec (produced by a 1-mc Na^{22} source at ~9 cm from the center of each detector, using an NaI crystal in the "start" channel) the peak was shifted by 8.5 nsec, while at 50,000 "starts"/sec the shift was only 1.4 nsec. No appreciable rate-dependent widening of the peaks was observed below 50,000 "starts"/sec.

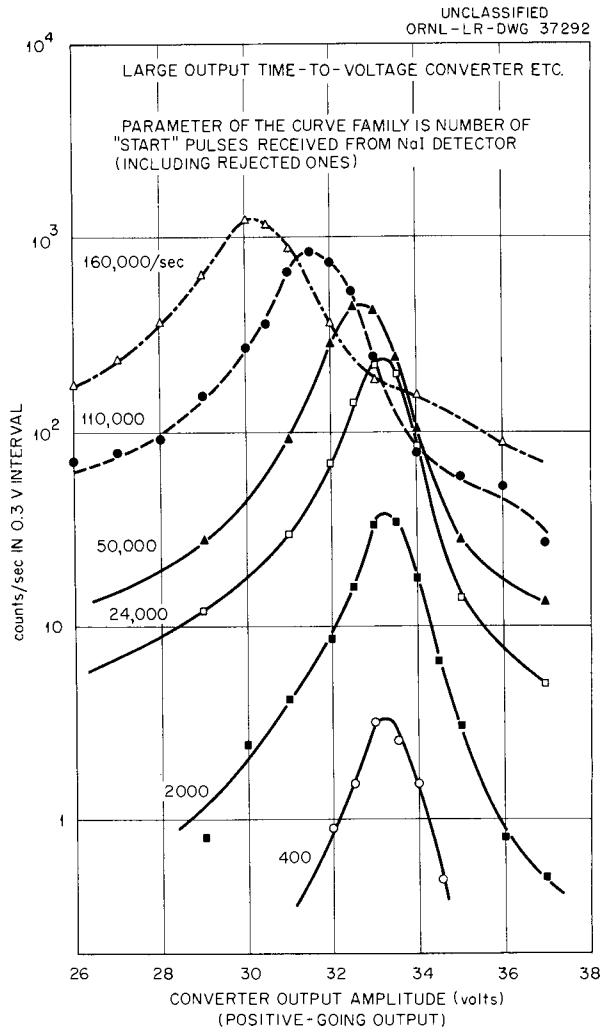

Fig. 6. Pulse Amplitude Spectra Obtained from Converter when Artificially Delayed Annihilation Coincidences Are Applied ("Start" Signal from an NaI Scintillator; "Stop" Signal from a Plastic Scintillator).

PUBLICATIONS

Becker, R. L., book review (*Nuclear Structure*, by L. Eisenbud and E. P. Wigner, 128 pp, Princeton University Press, 1958), *J. Franklin Inst.* **266,** 311 (1958).

Biedenharn, L. C., and H. B. Willard, "Eigenphaseshifts in Terms of Wigner's Nuclear Reaction Theory," *Proc. Phys. Soc. (London)* **72,** 874–79 (1958).

Block, R. C., "Angular Distribution of Neutrons Scattered by the 2.80-kev Resonance in Sodium," *Phys. Rev.* **109,** 1217 (1958).

Block, R. C., W. Haeberli, and H. W. Newson, "Neutron Resonances in the kev Region: Differential Scattering Cross Sections," *Phys. Rev.* **109,** 1620 (1958).

Blosser, H. G., R. E. Worsham, C. D. Goodman, R. S. Livingston, J. E. Mann, H. M. Moseley, G. T. Trammell, and T. A. Welton, "Four-Sector Azimuthally Varying Field Cyclotrons," *Rev. Sci. Instr.* **29,** 819–34 (1958).

Brysk, H., and M. E. Rose, "Theoretical Results on Orbital Capture," *Revs. Modern Phys.* **30,** 1169 (1958).

Busing, W. R., and H. W. Morgan, "The Infrared Spectrum of $Ca(OH)_2$," *J. Chem. Phys.* **28,** 998 (1958).

Charles, G. W., "On the Energy Levels of the Configuration $6p^2$ in Hg I," *J. Opt. Soc. Am.* **48,** 668 (1958).

Charles, G. W., "A Compilation of Data on Some Spectra of Thorium," *J. Opt. Soc. Am.* **48,** 859 (1958).

Church, E. L., M. E. Rose, and J. Weneser, "Electric Monopole Directional-Correlation Experiments," *Phys. Rev.* **109,** 1299 (1958).

Dabbs, J. W. T., L. D. Roberts, and G. W. Parker, "Alpha-Particle and Fission Anisotropies from Oriented Actinide Nuclei," *Physica* **XXIV,** S69–77 (1958).

Francis, J. E., P. R. Bell, and C. C. Harris, "Scintillation Spectrometry," chap. 4, p 32, in *External Collimation Detection of Intercranial Neoplasia with Unstable Nuclides*, Livingstone, London, 1958.

Gersch, H. A., and W. C. Koehler, "Types of Magnetically Ordered Configurations on Simple Lattices," *Phys. and Chem. Solids* **5,** 180–201 (1958).

Green, T. A., and M. E. Rose, "Nuclear Structure Effects in Internal Conversion," *Phys. Rev.* **110,** 105 (1958).

Harvey, J. A., and R. B. Schwartz, "Thermal and Resonance Neutron Cross Sections of Heavy Nuclei," *Progress in Nuclear Energy*, Series 1 – *Physics and Mathematics*, vol 2, p 51–90, Pergamon Press, New York, 1958.

Johnson, C. H., A. Galonsky, and J. P. Ulrich, "Proton Strength Functions from (p,n) Cross Sections," *Phys. Rev.* **109,** 1243 (1958).

Klema, E. D., "Angular Correlations of Gamma Rays in Cascade from Levels in Lu^{175} and Hf^{177}," *Phys. Rev.* **109,** 1652 (1958).

Koehler, W. C., E. O. Wollan, and M. K. Wilkinson, "Paramagnetic and Nuclear Scattering Cross Sections of Holmium Sesquioxide," *Phys. Rev.* **110,** 37 (1958).

Lazar, N. H., G. D. O'Kelley, J. H. Hamilton, L. M. Langer, and W. G. Smith, "Nuclear Structure of Zr^{90}," *Phys. Rev.* **110,** 513–19 (1958).

Lazar, N. H., "Analysis of Gamma Ray Scintillation Spectra for Quantitative Photon Intensities," *IRE Trans. on Nuclear Sci.* NS-5, No. 3, 138 (1958).

McNally, J. R., Jr., "High Resolution Spectroscopy. Part A – Principles and Practices in High Resolution Spectroscopy. Part B – Spectroscopic Research," *Eng. Prog. Univ. Florida* **XII**(11), 5, 15 (1958).

McNally, J. R., Jr., and K. L. Vander Sluis, "Preliminary Classification of the Spectrum of Singly-Ionized Erbium," *J. Opt. Soc. Am.* **49,** 200L (1959).

McNally, J. R., Jr., and P. M. Griffin, "Preliminary Classification of the Singly-Ionized Plutonium Atom (Pu II)," *J. Opt. Soc. Am.* **49,** 162 (1959).

Moak, C. D., A. Galonsky, R. L. Traughber, and C. M. Jones, "Energy Levels of Be^9, C^{12}, and C^{13}," *Phys. Rev.* **110,** 1369 (1958).

Norris, J. A., "Spectrographic Determination of Trace Elements in Metals," *Am. Soc. Testing Materials, Spec. Tech. Publ. No. 221,* p 23 (1958).

Rose, M. E., "Phenomena Affected by the Finite Size of the Nucleus," *Proceedings of the Rehovoth Conference on Nuclear Structure, Held at the Weizmann Institute of Science, Rehovoth, Sept. 8–14, 1957* (ed. by H. J. Lipkin), Interscience, New York, 1958.

Rose, M. E., and R. L. Becker, "Polarization of Conversion Electrons Following β-Decay," *Phys. Rev. Letters* **1,** 116 (1958).

Rose, M. E., "The Electrostatic Interaction of Two Arbitrary Charge Distributions," *J. Math. and Phys.* **37,** 215–22 (1958).

Rose, M. E., book review (*Quantum Mechanics, Non-Relativistic Theory,* by L. D. Landau and E. M. Lifshitz, trans. from Russian by J. B. Sykes and J. S. Bell, Addison-Wesley, Reading, Mass., 1958), *Phys. Today* **11**(12), 56–59 (1958).

Rose, M. E., book review (*The Physics of Elementary Particles,* by J. D. Jackson, 135 pp, Princeton University Press, 1958), *Phys. Today* **12,** 34 (1959).

Slaughter, G. G., E. M. Harth, and M. M. Block, "V-Particle Production by 1.9-Bev π^- Mesons," *Phys. Rev.* **109,** 2111 (1958).

Snell, A. H., and F. Pleasonton, "Charge Spectrometry for Xe^{133}-Cs^{133}," *Phys. Rev.* **111,** 1338 (1958).

Snell, A. H., and F. Pleasonton, "The Atomic and Molecular Consequences of Radioactive Decay," *J. Phys. Chem.* **62,** 1377 (1958).

Stelson, P. H., and F. K. McGowan, "Coulomb Excitation of Medium-Weight Even-Even Nuclei," *Phys. Rev.* **110,** 489 (1958).

Trammell, G. T., H. Zeldes, and R. Livingston, "Effect of Environmental Nuclei in Electron Spin Resonance Spectroscopy," *Phys. Rev.* **110,** 630 (1958).

Wollan, E. O., "Correlations Suggesting the *d*-Shell Configuration and a Magnetic Exchange Mechanism in Iron Group Metals," *Phys. Rev.* **110,** 1205 (1958).

Wollan, E. O., W. C. Koehler, and M. K. Wilkinson, "Neutron Diffraction Study of the Magnetic Properties of $MnBr_2$," *Phys. Rev.* **110,** 638 (1958).

Wollan, E. O., H. R. Child, W. C. Koehler, and M. K. Wilkinson, "Antiferromagnetic Properties of the Iron Group Trifluorides," *Phys. Rev.* **112,** 1132 (1958).

PAPERS PRESENTED AT SCIENTIFIC AND TECHNICAL MEETINGS

American Physical Society, Southeastern Section Meeting, Huntsville, Alabama, April 10–12, 1958

J. H. Gibbons (invited paper), "Cross Sections of kev Neutrons."

M. M. Gordon (invited paper), "Review of Beam Deflection Theoretical Studies."

P. M. Griffin (invited paper), "Application of the Echelle Spectrograph to Zeeman Spectroscopy."

K. L. Vander Sluis (invited paper), "An Application of Digital Computers to Zeeman Spectroscopy."

J. W. T. Dabbs, L. D. Roberts, and G. W. Parker, "Low Temperature Specific Heat Measurements on $U^{235}O_2Rb(NO_3)_3$."

J. L. Fowler and H. O. Cohn, "Differential Elastic Neutron Scattering from Beryllium."

A. Galonsky, H. B. Willard, A. R. Brosi, B. H. Ketelle, H. O. Cohn, and N. H. Lazar, "Spherical Electrostatic Spin-Rotator for Electron Polarization Measurements."

J. A. Harvey, R. C. Block, and G. G. Slaughter, "A High Intensity Time-of-Flight Neutron Spectrometer."

C. H. Johnson, A. Galonsky, and C. N. Inskeep, "Cross Sections for (p,n) Reactions in Intermediate Nuclei."

F. K. McGowan and P. H. Stelson, "Coulomb Excitation of States in Pt^{195}."

J. H. Neiler, J. H. Gibbons, and W. M. Good, "Application of Pulsed Beam Techniques to Nuclear Spectroscopy."

F. J. Walter, L. D. Roberts, and J. W. T. Dabbs, "Low Temperature Characteristics of Germanium *p-n* Junction Counters."

American Chemical Society Meeting, San Francisco, California, April 13–18, 1958

P. A. Staats, "Infrared Spectra of Deuterium Substituted Phosphine Molecules."

American Physical Society Meeting, Washington, D.C., May 1–3, 1958

R. C. Block, J. A. Harvey, and G. G. Slaughter, "Neutron Resonance Parameters of Pm^{147} and Am^{241}."

J. W. Cable, M. K. Wilkinson, E. O. Wollan, and W. C. Koehler, "Neutron Diffraction Investigations of the Antiferromagnetic Ordering in MnI_2."

J. A. Harvey, G. G. Slaughter, and R. C. Block, "Spin States for Resonances in W^{183}, Ag^{107}, and Ag^{109}."

F. K. McGowan and P. H. Stelson, "Coulomb Excitation of the Second 2^+ State in Isotopes of W, Os, and Pt."

R. L. Macklin and J. H. Gibbons, "Neutron Yields from Light Element (α,n) Reactions."

J. H. Neiler, J. H. Gibbons, and W. M. Good, "Total Cross Sections for 2- to 20-kev Neutrons."

L. D. Roberts, J. W. T. Dabbs, F. J. Walter, and G. W. Parker, "Anisotropy of Fission Fragments from Oriented U^{233} Nuclei."

G. G. Slaughter, R. C. Block, and J. A. Harvey, "Parameters of Neutron Resonances in Ag, I, and Au."

F. J. Walter, J. W. T. Dabbs, and L. D. Roberts, "Fission Fragment Counting with Germanium *n-p* Junction Counters."

Association for Computing Machinery, Annual Meeting, Urbana, Illinois, June 11-13, 1958

T. I. Arnette, "An Interpolation Procedure for Closed Curves."

Symposium on Molecular Structure and Spectroscopy, Ohio State University, Columbus, Ohio, June 16–20, 1958

H. W. Morgan and J. R. Lawson, "The Infrared Spectra of HNCS and DNCS."

Gordon Research Conference on Nuclear Chemistry, Meriden, New Hampshire, June 23–27, 1958

L. D. Roberts (invited paper), "Alpha Particle Emission from Oriented Actinide Nuclei."

P. H. Stelson (invited paper), "Some Recent Experimental Coulomb Excitation Results."

International Low Temperature Conference (Kamerlingh Onnes), Leiden, The Netherlands, June 23–28, 1958

J. W. T. Dabbs (invited paper), "Alpha-Particle and Fission Anisotropies from Oriented Actinide Nuclei."

W. C. Koehler, E. O. Wollan, M. K. Wilkinson, and J. W. Cable, "Neutron Diffraction Studies of Antiferromagnetic Rare Earth Compounds."

International Conference on Magnetism, University of Grenoble, Grenoble, France, July 2–5, 1958

W. C. Koehler, M. K. Wilkinson, J. W. Cable, and E. O. Wollan (invited paper), "Single Crystal Neutron Diffraction Studies of Antiferromagnets at Low Temperatures in Applied Magnetic Fields."

International Congress on Nuclear Physics, Paris, France, July 7–12, 1958

F. K. McGowan (invited paper), "Coulomb Excitation."

7th Annual Conference on Industrial Applications of X-Ray Analysis, Denver, Colorado, August 13–15, 1958

W. F. Peed (invited paper), "Wavelength Measurements of Radioactive Materials."

American Physical Society Meeting, Vancouver, British Columbia, August 26–28, 1958

M. E. Rose, "Depolarization of Mu Mesons in Bound States."

*2nd Geneva Conference on the Peaceful Uses of Atomic Energy, Geneva, Switzerland, September 1–13, 1958**

J. A. Harvey, R. C. Block, and G. G. Slaughter, "Low Energy Neutron Cross Sections of Radioactive Fission Product Nuclides."

R. L. Macklin, "Neutron Absorption at Intermediate Energies."

L. D. Roberts, J. W. T. Dabbs, and G. W. Parker, "Alpha Emission from Oriented Np^{237} and U^{233} Nuclei."

American Chemical Society Meeting, Chicago, Illinois, September 7–12, 1958

M. K. Wilkinson (invited paper), Neutron Diffraction Investigations of Antiferromagnetism at Low Temperatures."

Accelerator Conference, High Voltage Engineering Corporation, Burlington, Massachusetts, October 14–16, 1958

W. M. Good (invited paper), "Millimicrosecond Pulsing – Its Application and Technique."

H. B. Willard (invited paper), "Polarized Projectiles."

Conference on Weak Interactions, Gatlinburg, Tennessee, October 27–29, 1958 (Sponsored by the American Physical Society and the Oak Ridge National Laboratory)

R. L. Becker and M. E. Rose, "Polarization of Conversion Electrons Following Beta Decay."

B. H. Ketelle, A. R. Brosi, A. Galonsky, and H. B. Willard, "Measurement of the Longitudinal Polarization of Beta Particles from P^{32} Decay."

F. Pleasonton, C. H. Johnson, and A. H. Snell, "Recoil Momentum Spectrum for the β-Decay of He^6."

M. E. Rose, "Depolarization Processes for Negative Mu Mesons."

T. A. Welton, "A Universal Weak Interaction Between Bosons and Fermion Pairs."

---

*Papers to be included in the Geneva Conference Proceedings.

Conference on Magnetism and Magnetic Materials, Philadelphia, Pennsylvania, November 17–20, 1958

M. K. Wilkinson (invited paper), "Neutron Diffraction Investigations of Magnetic Phenomena in Crystalline Compounds."

American Physical Society Meeting, Chicago, Illinois, November 28–29, 1958

J. H. Gibbons and R. L. Macklin, "Total Cross Section for $T(p,n)He^3$."

J. A. Harvey, R. C. Block, and G. G. Slaughter, "Level Spacing of Heavy Odd-Odd Nuclei."

C. D. Moak, J. N. Thurston, H. E. Banta, and J. W. Johnson, "Some Performance Figures for the Duo-Plasmatron Ion Source for H_1^+, H_1^-, He^+, He^{++} and e^-."

R. B. Murray and H. W. Schmitt, "Cross Section of the $Li^6(n,\alpha)T$ Reaction from 1.2 to 8 Mev."

J. E. Sherwood, "Nuclear Spin of I^{130}."

G. G. Slaughter, J. A. Harvey, R. C. Block, and G. L. Jenkins, "Neutron Resonance Parameters of Np^{237} and Tc^{99}."

W. G. Smith, P. H. Stelson, and F. K. McGowan, "Decay of $I^{130} \rightarrow Xe^{130}$."

Tennessee Academy of Science Meeting, Oak Ridge, Tennessee, December 5–6, 1958

J. L. Fowler, "Co-op Students in Nuclear Research."

American Physical Society Meeting, New York, New York, January 28–31, 1959

R. C. Block, G. G. Slaughter, and J. A. Harvey, "Total Cross Section Measurements of Pu^{240}, Np^{237} and Radioactive Fission Products Near Thermal Energies."

S. H. Hanauer, J. W. T. Dabbs, and L. D. Roberts, "Low Temperature Helium Pulse Ionization Chamber."

J. A. Harvey, R. C. Block, and G. G. Slaughter, "Neutron Resonance Parameters of Am^{241}."

R. L. Macklin, J. H. Neiler, J. H. Gibbons, and P. D. Miller, "Gamma Detection of Kilovolt Neutron Capture – II."

P. D. Miller, W. M. Good, J. H. Neiler, and J. H. Gibbons, "Total Cross Sections in the Kilovolt Region by Time-of-Flight."

J. H. Neiler, R. L. Macklin, J. H. Gibbons, and P. D. Miller, "Gamma Detection of Kilovolt Neutron Capture – I."

H. W. Schmitt, J. H. Gibbons, and C. N. Inskeep, "Neutron Absorption Cross Sections at 27 kev."

A. H. Snell, F. Pleasonton, and J. L. Need, "Charge Spectrometry for Kr^{79}-Br^{79}."

Conference on Medium-Energy Cyclotrons, Sea Island, Georgia, February 2–4, 1959 (Sponsored by the National Research Council's Subcommittee on Instruments and Techniques and the American Physical Society)

T. A. Welton, "ORNL Computation Methods."

Symposium on Fast Pulse Techniques, Lawrence Radiation Laboratory, Berkeley, California, February 12–14, 1959

D. Maeder, "Multidimensional Pulse Recording."

J. H. Neiler, "Millimicrosecond Time Measurement."

Conference on Neutron Time-of-Flight Techniques, Northwestern University, Evanston, Illinois, February 16, 1959 (also sponsored by Radiation Counter Laboratories)

J. H. Neiler (invited paper), "Neutron Measurements with Pulsed Accelerators."

LECTURES

Visiting Scientist Lecture Program in Physics, Sponsored by the American Institute of Physics and the American Association of Physics Teachers

R. C. Block, "Research and the Government Laboratories" (Carson-Newman College, Jefferson City, Tennessee, April 25, 1958).

J. L. Fowler, "Fundamental Particles of Physics" (Kenyon College, Gambier, Ohio, May 7–8, 1958).

J. L. Fowler, "What's Ahead in Science and Technology"; "The Neutron as a Tool for Science" (Colorado College, Colorado Springs, Colorado, February 17–18, 1959).

J. H. Neiler, "The Work of a Nuclear Physicist" (Atlanta University Center, Atlanta, Georgia, April 23–25, 1958).

H. W. Schmitt, "Nuclear Reactors: Instruments of Research"; "Science, Education, and Thought" (Western Kentucky State College, Bowling Green, Kentucky, February 24–25, 1959).

ANNOUNCEMENTS

Additions to the Physics Division staff during this period were as follows: P. D. Miller (High Voltage Group); R. L. Robinson (Classification of Low-Lying Nuclear Energy Levels); and C. G. Gardner (High Energy Accelerator Studies).

J. Walter, formerly of the Reactor Experimental Engineering Division, has transferred to the Physics Division's Low Temperature Group, where he will work toward the Ph.D. degree in physics.

T. A. Carlson of the Chemistry Division is on loan to the Charge Spectrometry Group.

The appointment of D. G. Maeder (from the Physikalisches Institut in Zurich, Switzerland) has been extended for one year; he will continue work with the Scintillation Spectrometry and Instrument Development Group.

Co-op students assigned to the High Voltage Group during this period include D. O. Patterson, M. C. Taylor, and C. E. Hughey from the University of Tennessee (Martin Branch) and A. F. Nickle from the University of Tennessee (Knoxville).

R. A. Mann (University of Alabama) and C. P. Bhalla (University of Tennessee) have been granted Oak Ridge Institute of Nuclear Studies Graduate Fellowships. They will complete work toward the Ph.D. degree with the Theoretical Physics Group.

H. O. Cohn (High Voltage Laboratory) has returned to the Laboratory from a ten-month assignment to the University of California Radiation Laboratory at Berkeley, California, to perform an experiment with the Bevatron machine.

Summer personnel during 1958 included the following research participants and visitors: G. L. Jenkins (Head of the Physics Department at Stetson University), Neutron Velocity Selector Program; M. S. McCay (Head of the Physics Department at the University of Chattanooga) and J. H. Wise (summer visitor, Washington and Lee University), Spectroscopy Research; W. G. Smith (Assistant Professor of Physics at Purdue University), Classification of Low-Lying Nuclear Energy Levels; H. A. Gersch (summer visitor, Georgia Institute of Technology) and A. W. Saenz (summer visitor, on loan from the Naval Research Laboratory), Neutron Diffraction Group; F. S. Levin (summer visitor, University of Maryland), Theoretical Physics; J. N. Thurston (summer visitor, Clemson College), Scintillation Spectrometry and Instrument Development Group.

W. C. Koehler (Neutron Diffraction Group) is on a year's leave of absence to do research at the University of Grenoble in Grenoble, France, under a Guggenheim Foundation Fellowship and a Fulbright Scholarship. L. D. Roberts (Low Temperature Physics Group) is on a year's leave

of absence for study of low-temperature nuclear physics at the Clarendon Laboratory in Oxford, England, under a Guggenheim Foundation Fellowship and a Fulbright Scholarship.

M. M. Gordon (High Energy Accelerator Studies) returned to the University of Florida, having completed a one-year appointment with the Laboratory.

A Conference on Weak Interactions, sponsored by the American Physical Society and the Oak Ridge National Laboratory, was held in Gatlinburg, Tennessee, October 27–29, 1958. It is expected that the invited papers presented at this Conference will be published in the April 1, 1959, issue of *Reviews of Modern Physics*; the contributed papers have been published in the *Bulletin of the American Physical Society* for the New York meeting of 1959.

R. L. Becker (High Energy Accelerator Studies) presented at the Oak Ridge National Laboratory a series of nine lectures entitled "Fundamental Particles and Their Weak Interactions" during January and February of 1959.

Physics Division progress reports previously issued in this series are as follows:

ORNL-325 Supplement	December, January, and February, 1948-1949
ORNL-366	Period Ending June 15, 1949
ORNL-481	Period Ending September 25, 1949
ORNL-577	Period Ending December 15, 1949
ORNL-694	Period Ending March 15, 1950
ORNL-782	Period Ending June 15, 1950
ORNL-865	Period Ending September 20, 1950
ORNL-940	Period Ending December 20, 1950
ORNL-1005	Period Ending March 20, 1951
ORNL-1092	Period Ending June 20, 1951
ORNL-1164	Period Ending September 20, 1951
ORNL-1278	Period Ending December 20, 1951
ORNL-1289	Period Ending March 20, 1952
ORNL-1365	Period Ending June 20, 1952
ORNL-1415	Period Ending September 20, 1952
ORNL-1496	Period Ending December 20, 1952
ORNL-1620	Period Ending September 10, 1953
ORNL-1705	Period Ending March 10, 1954
ORNL-1798	Period Ending September 10, 1954
ORNL-1879	Period Ending March 20, 1955
ORNL-2076	Period Ending March 10, 1956
ORNL-2204	Period Ending September 10, 1956
ORNL-2302	Period Ending March 10, 1957
ORNL-2430	Period Ending September 10, 1957
ORNL-2501	Period Ending March 10, 1958
ORNL-2610	Period Ending September 20, 1958

INTERNAL DISTRIBUTION

1. C. E. Center
2. Biology Library
3. Health Physics Library
4–6. Central Research Library
7. Reactor Experimental Engineering Library
8–19. Laboratory Records Department
20. Laboratory Records, ORNL R.C.
21. A. M. Weinberg
22. L. B. Emlet (K-25)
23. J. P. Murray (Y-12)
24. J. A. Swartout
25. E. H. Taylor
26. E. D. Shipley
27–37. J. L. Fowler
38. M. L. Nelson
39. A. H. Snell
40. A. Hollaender
41. K. Z. Morgan
42. F. L. Culler
43. M. T. Kelley
44. D. Phillips
45. E. O. Wollan
46. H. E. Seagren
47. A. S. Householder
48. L. D. Roberts
49. R. B. Briggs
50. R. N. Lyon
51. W. C. Koehler
52. E. P. Blizard
53. M. E. Rose
54. G. E. Boyd
55. W. H Sullivan
56. R. W. Stoughton
57. C. E. Winters
58. W. H. Jordan
59. E. C. Campbell
60. D. S. Billington
61. M. A. Bredig
62. R. S. Livingston
63. C. P. Keim
64. F. C. Maienschein
65. C. E. Clifford
66. R. C. Block
67. C. D. Susano
68. C. J. Borkowski
69. M. J. Skinner
70. M. K. Wilkinson
71. J. W. Cable
72. P. M. Reyling
73. G. deSaussure
74. W. M. Good
75. G. C. Williams
76. F. K. McGowan
77. R. W. Johnson
78. J. R. McNally, Jr.
79. J. L. Gabbard
80. R. A. Charpie
81. G. G. Slaughter
82. Eugene Guth
83. R. W. Peelle
84. P. R. Bell
85. G. G. Kelley
86. C. C. Harris
87. H. G. MacPherson
88. P. H. Stelson
89. J. E. Sherwood
90. W. Zobel
91. R. B. Murray
92. H. B. Willard
93. J. Schenck
94. J. H. Neiler
95. J. A. Harvey
96. C. F. Barnett
97. N. H. Lazar
98. R. R. Dickison
99. A. Simon
100. J. H. Gibbons
101. J. J. Penajian
102. S. Bernstein
103. F. Pleasonton
104. C. A. Preskitt
105. H. R. Child
106. C. G. Gardner
107. C. J. McHargue
108. J. A. Lane
109. C. S. Harrill
110. A. J. Miller
111. S. C. Lind
112. K. L. Vander Sluis

113. R. L. Robinson
114. G. R. Satchler
115. H. W. Morgan
116. H. W. Schmitt
117. E. P. Wigner (consultant)
118. J. H. Van Vleck (consultant)
119. M. S. Livingston (consultant)
120. J. R. Richardson (consultant)
121. R. F. Christy (consultant)
122. M. Goldhaber (consultant)
123. W. A. Fowler (consultant)
124. J. A. Wheeler (consultant)
125. N. F. Ramsey (consultant)
126. H. Feshbach (consultant)
127. ORNL – Y-12 Technical Library, Document Reference Section

EXTERNAL DISTRIBUTION

128–222. Given external distribution
223–837. Given distribution as shown in TID-4500 (14th ed.) under Physics and Mathematics category (75 copies – OTS)